Università degli Studi di Napoli Federico II
DEPARTMENT OF CHEMICAL, MATERIALS AND PRODUCTION ENGINEERING
(DICMAPI)
PHD IN INDUSTRIAL PRODUCTS AND PROCESSES ENGINEERING
XXIX CYCLE

DEVELOPMENT OF VASCULARIZED PATHOLOGICAL AND PHYSIOLOGICAL ENGINEERED TISSUES

Supervisor
Prof. Dott. P.A. Netti

Coordinator
Prof. Dr G. Mensitieri

Advisors
Francesco Urciuolo, PhD
Giorgia Imparato, PhD
Costantino Casale, PhD

PhD Student Claudia Mazio

2014/2017

Table of contents

Acronyms list (alphabetic order)

Abbreviation	Expanded form
αSMA	α Smooth muscle actinin
µTPs	Micro-Tissues
2D	Two Dimensional
3D	Three Dimensional
BM	Basement Membrane
BPE	Bovine Pituitary Extract
BSA	Bovine Serum Albumin
CAD	Collagen Assembly Degree
CAFs	Cancer Associated Fibroblasts
Cf	Final Concentration
CLS	Capillary-Like Structures
CSCs	Cancer Stem Cells
CTCs	Circulating Tumor Cells
CTRL	Control
DAPI	4' 6-DiAmidino-2-PhenylIndole
DCIS	Ductal Carcinoma In Situ
ECM	ExtraCellular Matrix
ECs	Endothelial Cells
EDTA	EthyleneDiamineTetra-acetic Acid
EGF	Epidermal Growth Factor
EMT	Epithelial-Mesenchymal Transition
EtOH	Ethanol
FBS	Fetal Bovine Serum
GAL	Glyceraldehyde
GLCM	Gray-Level Co-Occurrence Matrix
GPMs	Gelatin porous microbeads

h	hour/hours
HDFs	Human Dermal Fibroblasts
HDFs-µTPs	Micro-tissue made up of Fibroblasts and ECM
HDMEC	Human microvascular Endothelial Cells
HUVECs	Human Umbilical Vein Endothelial cells
IBC	Inflammatory Breast Cancer
IDC	Invasive (or infiltrating) Ductal Carcinoma
ILC	Invasive (or infiltrating) Lobular Carcinoma
K14	CytoKeratin 14
K18	CytoKeratin 18
KGM	Keratinocyte growth medium
LSGS	Low Serum Growth Supplement (final concentrations: fetal bovine serum, 2% v/v; hydrocortisone, 1 µg/ml; human epidermal growth factor, 10 ng/ml; basic fibroblast growth factor, 3 ng/ml; and heparin, 10 µg/ml.
M200	Endothelial Cell Basal Medium
MCF10	Non-tumorigenic epithelial cell line
MCF10-µTPs	µTPs with MCF10 seeded on vascularized HDFs-µTPs
MCF7	Human Breast Adenocarcinoma Cells (ER+, PR+: Estrogen/Progesterone receptors +)
MCF7-µTPs	µTPs with MCF7 seeded on vascularized HDFs-µTPs
MDA MB-231	Human Breast Adenocarcinoma Cells (ER+, PR+, HER-2+: Estrogen/Progesterone Receptors + and Human Epidermal Growth Factor Receptor 2 +)
MEBM	Mammary Epithelial Basal Medium
MEGM	Mammary Epithelial Cell Growth Medium
MEM	Minimum Essential Medium
MLC	Myosin Light Chain
MLCK	Myosin Light Chain Kinase
MMP	Metalloproteinase

MPLSM	MultiPhoton Laser-Scanning Electron Microscopy
MPM	MultiPhoton Microscopy
n.a.	Numerical Aperture
NIH-3T3	Murine embryonic fibroblasts
O/W/O	Oil/Water/Oil
ON	Over Night
P	Cell passage
PBS	Phosphate buffered saline
PDGF	Platelet Derived Growth Factor
PDMS	PolyDimethylSiloxane
PEG	Poly-ethylene-Glycol
PLA	Poly-lactide-Acid
PLG	Poly-lactide-co-Glycolide
PTFE	PolyTetraFluoroEthylene
PVT	PreVascularized Tumor
ROI	Region of Interest
RPMI	Roswell Park Memorial Institute Medium
RT	Room Temperature
SHG	Second Harmonic Generation
TACS	Tumor Associated Fibroblasts
TEM	TransEndothelial Migration
TGFβ1	Transforming Growth Factor β1
TIME	Telomerase Immortalized Microvascular Endothelial Cells

Chapter 1

The importance to mimic micro-environment in Tissue Engineering

1 General Abstract

Vascularization is still a great challenge in Tissue Engineering. First this is important to avoid mass transfer limitation in engineered tissues but also for innovative *in vivo* and *in vitro* applications. A pre-vascularized tissue can accelerate the formation of functional anastomosis with host vasculature *in vivo* ensuring the sustenance of the implant, its integration and long term survival. In the same time, *in vitro*, it can be a suitable model in view of fundamental research about physiological and pathological angiogenesis and industrial applications like drugs screening.

In this work, we analyse the formation of capillary like networks into pathological and physiological tissues obtained by bottom up approach and strengthened by an endogenous extracellular matrix (ECM).

The introduction describes the fundamental role of vascularization in tissue engineering and the bottom up approach that we exploit in order to obtain stroma-rich tissues. Chapter 2 retraces interesting steps of the state of art regarding 3D engineered models of pathological and physiological conditions, specifically, analyzing human breast and skin tissues and underling the role of microenvironment in tissue functionality. Chapter 3 and 4 are dedicated to the description of our work with the aim to achieve and investigate the features of vascularized pathological and physiological engineered models suitable for pharmaceutical and clinical applications.

Notably, chapter 3 describes the development of vascularized breast cancer micro-tissues which are able to recapitulate tumor vascular pro-angiogenic and stromal desmoplastic reaction, and heterogeneity in cluster migration during interstitial invasion.

On the other hand, chapter 4 shows how healthy micro-tissues are assembled and cultured in order to obtain vascularized dermis/skin equivalents mirroring physiological angiogenesis.

Both models are featured by the presence of an active and organized stroma which is part of an interactive microenvironment and able to receive, store and release physio-pathological stimuli.

We speculate that the vascularized dermis/skin model could be useful for *in vivo* applications in order to repair and restore damaged tissues. Furthermore, both vascularized tumor and healthy tissues are suitable research models. Thus, allowing the study of tumor progression, physio-pathological angiogenesis and providing a platform for drug screening on multicomponent systems.

1.1 General Introduction

1.1.1 The fundamental role of vascularization and ECM in Tissue Engineering and main strategies

Tissue microenvironment consists of a dynamic population of cellular and non-cellular components which form a multifaceted regulatory network that helps to maintain tissue homeostasis. Fundamental elements of the microenvironment are the vascular network and the extracellular matrix (ECM) which features regulate tissue functionality. These normal cellular and non-cellular microenvironment components are not only essential for tissue normal, physiological and biological behavior, but are critical in opposing resistance to malignant cell growth [24].

Mimic vascularization is still a great challenge in Tissue Engineering. First this is important to avoid mass transfer limitation in engineered tissues but also for innovative *in vivo* and *in vitro* applications [1]. Most cells of human body are found no more than 100–200 μm from the nearest capillary, with this spacing providing sufficient diffusion of oxygen, nutrients, and waste products to support and maintain viable tissue [2]. Similarly, every reconstructed tissue or organ that exceeds 400 μm in any dimension must be vascularized in order to survive and to be able to fulfill their biological functions. This need for vascularization exists both at the stage when tissue-engineered constructs are grown and/or assembled *in vitro* and when they are implanted in patients [1].

A pre-vascularized tissue has a high potential for *in vivo* applications as it provides functional points of anastomosis with the host vascular system present in the implant site [2], promotes tissue functionalization and innervation because endothelial cells (ECs) are able to retrieve neural precursors through the release of neurotrophic factors [3]. In research a pre-vascularized tissue is a model to study angiogenesis, wound healing or vascular *phenomena* such as thrombosis or

metastatic events involving tumor-endothelial cells interaction. In view of industrial applications vascularized constructs represent a platform to study drugs or active principles such as anti-inflammatory, pro- and anti-angiogenic, vaso-constrictors/dilators [1]. In some recent works, it is emphasized the importance of the lymphatic vascular system, in addition to the blood one, for the maintenance of fluids homeostasis and for the transport of cells of the immune system [4].

The two processes through which neovascularization can take place in tissues are angiogenesis and vasculogenesis. Angiogenesis is the process through which new blood vessels are formed from preexisting ones, whereas vasculogenesis generates new vascularization in the absence of preexisting blood vessels. For the most part, normal vasculogenic formation of new capillaries takes place during embryologic development, although in some instances, such as wound healing and the menstrual cycle, neovascularization can be seen in adults. Pathological angiogenesis occurs in some disease states such as tumor growth or chronic inflammatory diseases [1].

Two distinct mechanisms of angiogenesis have been described: sprouting and intussusception. Intussusceptive angiogenesis is caused by the insertion of interstitial cellular columns into the lumen of preexisting vessels. The subsequent growth of these columns and their stabilization results in partitioning of the vessel and remodeling of the local vascular network. Sprouting angiogenesis entails two successive phases: neovessel growth and neovessel stabilization. During the initial phase, the following sequence of events usually occurs: dissolution of the basement membrane of the “mother” vessel and its surrounding interstitial matrix, migration of endothelial cells in this created space toward the angiogenic factor, proliferation of endothelial cells behind the front of migration, lumen formation within the endothelial sprout, and formation of loops by anastomoses of sprouts. The stabilization phase consists of arrest of endothelial cell proliferation, reconstruction of a basement membrane around the neocapillary, and investment and coverage of the immature capillary with pericytes.[5].

Vascular networks formed by vessel sprouting undergo extensive vascular remodeling to form a functional and mature vasculature. This ‘‘trimming’’ includes distinct processes of vascular pruning, the regression of selected vascular branches. In some situations complete vascular networks may undergo physiological regression. Vessel regression is an understudied yet emerging field of research. For example this happens during the regression of hyaloid vessels and in the adult during luteolysis (Fig.1). Luteolysis marks the rapid dissociation of the mature ovarian corpus luteum at the end of the ovarian cycle. Triggered by the downregulation of VEGF and the upregulation of ANG2, the extensive vascular network of the corpus luteum completely dissociates within a few days and gradually resolves into scar tissue over a period of weeks. This prominent example illustrates that nature has secured mechanisms and pathways for the controlled dissociation of established vascular networks. It also highlights that vessel regression may be triggered by the shut-off of ON signals (e.g., VEGF) as well as the active engagement of OFF signals (e.g., ANG2). [6].

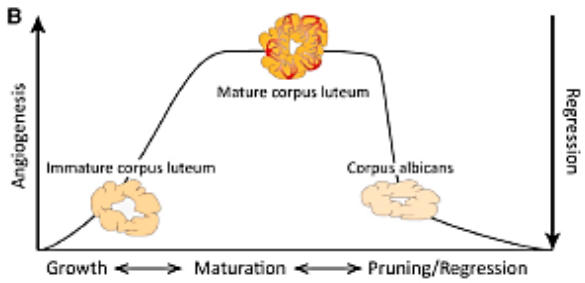

Fig.1 Concepts of Angiogenesis and Vessel Regression as Dynamic Processes. Mature vascular networks may undergo complete vascular regression. In the ovary, growth and regression of the cyclic corpus luteum is associated with distinct phases of angiogenesis, vessel maturation, and vessel regression. Luteolysis leads to the physiologically triggered massive destruction of the entire corpus luteum vasculature [6]**.**

Angiogenesis events are finely regulated at the molecular level by the expression of pro- and anti-angiogenic factors (Tab.1) [7].

There are several vascularization strategies in Tissue Engineering, some aim to promote host vessels invasion into the construct directly after *in vivo* implantation and others to the development of pre-vascularized tissues [2]. The main strategy of Tissue Engineering involves the use of cells, scaffolds and growth factors [8]. The scaffold is a structural support able to guide the reorganization and cell growth. It can be functionalized using pro-angiogenic growth factors such as VEGF (Vascular Endothelial Growth Factor), PDGF (Platelet-derived Growth Factor) and heparin. Despite the functionalization methods are very effective, the use of these scaffolds is limited by the difficulty to adjust the kinetics release of various pro-angiogenic factors over time *in vivo*. The scaffolds can also be functionalized physically increasing the porosity or with the presence of channels in the structure [2].

Table 1 List of proangiogenic and antiangiogenic factors. Adapted from [7]

Proangiogenic factors	Antiangiogenic factors
Vascular endothelial growth factor-A, -C	Thrombospondin-1
Fibroblast growth factor-2	Transforming growth factor β-1
Hepatocyte growth factor	Platelet factor-4
Angiopoietin-1	Hepatocyte growth factor-derived fragments
Platelet-derived growth factor	Plasminogen (precursor of angiostatin)
Epidermal growth factor	α2-antiplasmin
Insulin-like growth factor-1, -2	Plasminogen activator inhibitor-1
Insulin-like growth factor binding protein-3	Heparin binding fibronectin fragments
Vitronectin	Epidermal growth factor fragment
Fibronectin	Endostatin
Fibrinogen	High-molecular-weight kininogen (precursor of kininostatin)
Heparanase	Tissue inhibitor of metalloproteinase-1, 2
Thymidine phosphorylase	
Sphingosine 1-phosphate	

In many works the vascularization strategy is based on the co-culture of endothelial cells with other cell types. In fact when endothelial cells are cultured *in vitro* under permissive conditions, in particular when they are in 3 dimensional (3D) co-culture with other cell types and a relevant ECM, they are able to spontaneously form capillary networks [1]. Auger et al in 2006 have shown that fibroblasts promote endothelial cells proliferation, migration and angiogenesis. This is due to their ability to produce an organized ECM and growth factors that represent a suitable microenvironment to promote the organization of endothelial cells in 3D and the formation of capillary-like tubular structures [9]. Cells can be seeded into 3D hydrogel or natural/synthetic scaffolds able to provide a biocompatible support miming the role of the ECM [10].

As native tissues are finely organized, modulating scaffold micro-architecture can be a powerful way to get biomimetic tissues [11]. This type of functionalization often exploits a physical guidance (e.g. holes or channels) or chemistry to create cell patterns [12]. Tien et al in 2006 have described the construction of microvascular tubes of endothelial cells with final diameters ranging from 75 to 150 μm into Rat Tail Type I collagen. The endothelial cells tubes slightly increase in diameter after maturation, show a strong barrier function, resistance to leukocyte adhesion in normal condition and a quick responsiveness to inflammatory stimuli leading the increase in vascular permeability and leukocytes adhesion [13]. Bertassoni et al developed a channel network into hydrogel at different concentration using agarose fibers with a 3D defined architecture as mold. Channels can have different diameters, are totally covered by endothelial cells and perusable [14].

Using the 3D bio-printing technology, Lee et al have obtained functional and perfused vascular channels within a collagen scaffold. The channels have a lumen and the inner surface is covered by a confluent monolayer of endothelial cells. The perfused channel supports the vitality of the adjacent tissue and shows a barrier

function for the BSA (Bovine Serum Albumin) and dextran. The vascular channel maintains its integrity in long-term cultures in flow condition and the endothelial cells are aligned in the direction of flow. In static conditions, endothelial cells are able to proliferate and sprout, forming structures that branch off from the channel towards the outside and have a lumen. On the other hand, during flow condition endothelial cells proliferation is suppressed and the cells remain confined within the channel structure [15].

The geometric control of the vascular network is important for engineered tissues functionalization as well as for their *in vivo* integration [16]. Chen et al obtained cords of endothelial and mesenchymal cells in type I collagen within micro-channels in PDMS (polydimethylsiloxane). These cords were coated with fibrin from one side, detached from PDMS and then covered with fibrin on the other side. The obtained construct was sutured directly into the parametrial fat pad in the intraperitoneal space of nude mice. Analysis conducted at various days after implantation allowed detecting that endothelial cells cords perfectly anastomosed with host vessels and were perfused by blood. They showed that geometrically controlled constructs survive more effectively and were more functional than random ones [16].

Besides vascularization, the other fundamental micro-environmental component to mimic in engineered tissue is the ECM. It is a heterogeneous, connective network composed of fibrous glycoproteins that coordinate *in vivo* to provide the physical scaffolding, mechanical stability, and biochemical cues necessary for tissue morphogenesis and homeostasis [17].

In the classical tissue engineering approach, or top-down approach, cells are seeded into preformed, functionalized, porous, and biodegradable polymeric scaffolds acting as temporary template for new tissue growth and reorganization, replacing ECM functions. One of the limits of this traditional method is that it difficulty recreate the intricate microstructural features of 3D-tissue. For this reason, efforts

have been devoted to bottom-up approaches aimed at generating a larger tissue construct by assembling smaller building blocks that mimic the *in vivo* tissue structure of repeating functional units. These building blocks can be created in several ways, such as self-assembled cell aggregates, microfabrication of cell-laden microgel, creation of cell sheets, and microfabrication of cell seeded microbeads. Once obtained, these building blocks can be assembled in larger tissue through a number of methods including random packing, stacking of layers, or direct assembly [18]. By mimicking native microstructural functional units, bottom-up approaches aim to create more biomimetic engineered tissues. One of the major challenges by using this approach is to assemble modular tissues with specific micro architectures into macroscale biomimetic engineered tissues with robust mechanical properties [19][20].

To address this issue, we use a bottom-up method to fabricate micron-sized tissue of connective origin by coupling cells and micro-scaffold. Despite other bottom-up strategies are completely scaffold-free, we use a porous micron-sized scaffold as a temporary support that plays a crucial role in guiding the correct spatial organization of the *de novo* synthesized ECM. This way, the micro-tissue is more than a mere cell aggregate: it represents a more complex living structure in which the cell works as tissue builder. These micro-tissues are then used as building blocks to create 3D functional tissues [18].

In this work, we exploit dynamic cell seeding on porous gelatin micro-carriers using a spinner flask bioreactor. We use human fibroblasts extracted from the dermis and gelatin porous μspheres, crosslinked by 4% w/w glyceraldehyde, as scaffold. During the dynamic culture, cells adhere, proliferate and synthesize a thin layer of ECM in and around the beads, generating μTPs rich in type I collagen. The cells and ECM layer around the μTPs allow their biological sintering via cell–cell and cell–matrix interaction after only a few days of dynamic seeding. The assembling ability of μTPs is exploited by placing them into specific maturation

chamber, in order to obtain final macro-tissues. They have tunable shape and dimensions, depending on the shape of the mold used into the maturation chamber, are scaffold free after the maturation period of about 4 weeks and are enriched by a strong collagen rich matrix [21] [22] [23]. It was demonstrated that modulating the crosslinking density of the gelatin micro-scaffolds it is possible to guide the process of collagen deposition and assembly within the extracellular space and match the processes of scaffold degradation, cell traction and tissue maturation to obtain firmer collagen network able to withstand the effect of contraction. We use 4% w/w glyceraldehyde to obtain a massive deposition of immature collagen that is progressively assembled in mature collagen fibrils. The relationship between the degradation time of the scaffold and the synthesis of collagen is just below the unit by determining an intermediate tissue ability to resist contraction [24].

This process has been used to develop both 3D dermal equivalent and cardiac-muscle fabrication [18].

Human keratinocytes seeded on this dermis equivalent model are able to develop a mature and functional *epithelium*. In such physiologically relevant environment our group observed the development of appendage-like structures, which resemble the structure of the first step of hair follicle embryogenesis, without adding mesenchymal stem cells. Such results suggest a possible regulatory role of the dermis in the skin equivalent model, highlighting that it represents an instructive environment in which the inductive signals and the ability to maintain the germinative phenotypes of the basal keratinocytes can be preserved [22]

Chapter 2

3D pathological/physiological engineered models

2 State of the art

Here we describe the state of the art relative to stroma-rich tissues, namely breast and skin in pathological and physiological state, respectively. We underline the importance of reproducing micro-environmental conditions in order to obtain biomimetic 3D engineered tissues useful for *in vitro* and *in vivo* applications.

2.1 Pathological tissue: Breast Cancer

2.1.1 Breast Cancer: *In vivo* overview

Breast cancer is the second most common cancer in the world after lung cancer and the most frequent among women [25]. It is a malignant tumor that starts in the cells of the breast. It is found mostly in women, but men can get breast cancer, too. A woman's breast is made up of glands that can make breast milk (lobules), small tubes that carry milk from the lobules to the nipple (ducts), fatty and connective tissue, blood vessels, and lymph vessels (Fig.1).

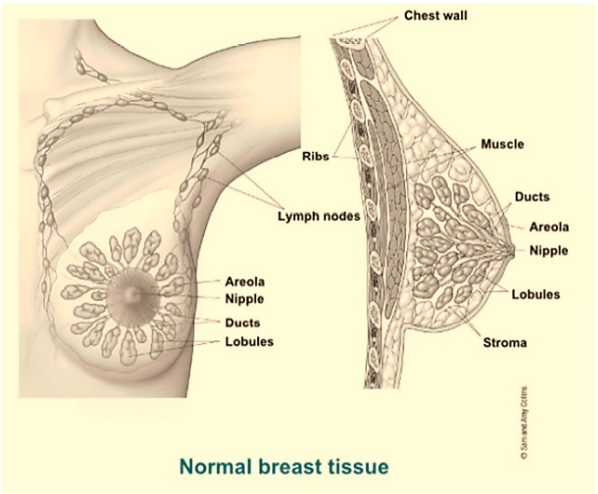

Fig. 1: Design of normal breast made up of lobules, ducts, fatty and connective tissue, blood vessels, and lymph vessels [26]**.**

Most breast cancers begin in the cells that line the ducts. Fewer breast cancers start in the cells lining the lobules [26]. Nearly all breast cancers are adenocarcinomas. It is a type of carcinoma that starts in gland tissue (that makes and secretes a substance). The ducts and lobules of the breast are gland tissues because they make breast milk, so cancers starting in these areas are often called adenocarcinomas[26]. The mature gland comprises a branching bilayered *epithelium* of inner luminal cells enveloping ducts positive for cytokeratin 18 (K18) and lobulo-alveolar structures surrounded by a thin myo*epithelium* which stain positively for cytokeratin 14 (K14) and smooth muscle actinin (α-SMA), enveloped within an adipose rich stroma (Fig.2). The mammary *epithelium* is highly dependent upon the composition of basement membrane (BM) proteins, specifically laminin species, for its apico-basal polarity and function [27].

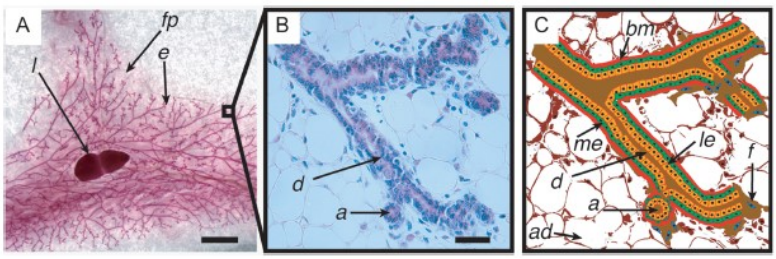

Fig. 2: Ultrastructure of the murine mammary gland. (A) Whole-mount and (B) higher power micrograph (10-day gestation) and (C) schematic showing a branched *epithelium* (e) composed of ducts (d) and acini (a) within an adipocyte-rich fat pad (fp) with a prominent lymph node (l). Bars = 1 mm and 50 µm [27].

Breast cancer starts as a local disease, but it can metastasize to the lymph nodes and distant organs [28]. Once disseminated, metastases from carcinoma of the breast are formed in various organs. The common sites for metastatic spread are bone, lung and liver [28] (Fig.3). Breast cancers are classified in:

- Ductal carcinoma in situ (DCIS): generally non-invasive;
- Invasive (or infiltrating) ductal carcinoma (IDC): the most common breast cancer. It starts in the cells lining a duct, and then the abnormal cells break

through the wall of the duct and grow into (invade) the tissue of the breast and can spread to nearby lymph nodes or other parts of the body;

- Invasive (infiltrating) lobular carcinoma (ILC): it starts in the cells lining the milk glands (the lobules). The cells grow through the wall of the lobules and then can spread to nearby lymph nodes or other parts of the body;
- Inflammatory breast cancer (IBC): a rare type of invasive breast cancer [26].

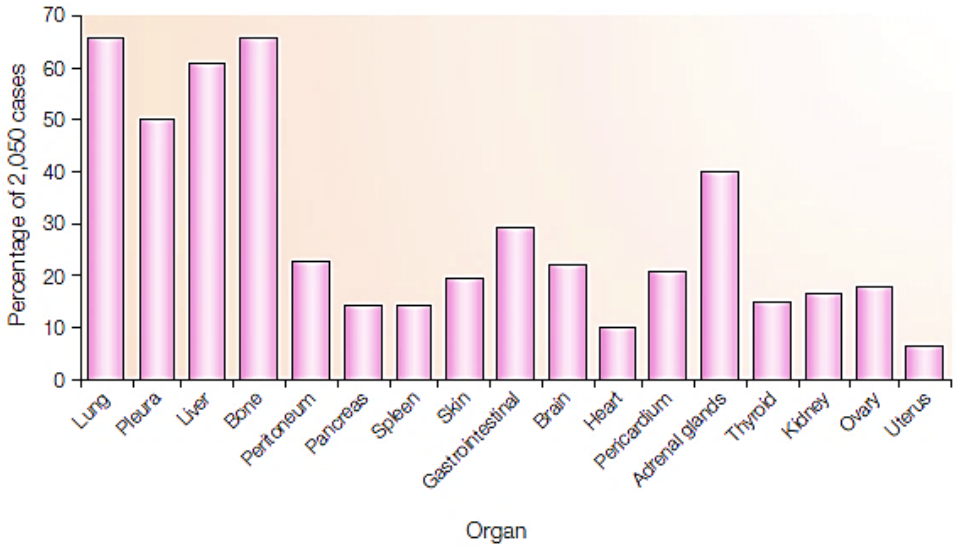

Fig. 3: Most common metastasis sites of breast cancer. Primary breast cancer cells metastasize through the blood vessels to various distant organs, preferentially, to the lung, liver and bones. Patients frequently develop metastases at multiple sites [28]**.**

At now, the main types of treatment for breast cancer are: surgery, radiation, chemotherapy, hormone therapy, targeted therapy or bone-directed therapy.

Because advanced breast cancers are often hard to treat, researchers are looking for newer, better drugs. A drug class has been developed that targets cancers caused by BRCA mutations. This class of drugs is called PARP inhibitors and they have shown promise in clinical trials treating breast, ovarian, and prostate cancers that

had spread and were resistant to other treatments. Further studies are being done to see if this drug can help patients without BRCA mutations.

Targeted therapies are a group of newer drugs that take advantage of gene changes in cells that cause cancer. Drugs that target the HER2 protein and anti-angiogenesis drugs are being tested in clinical trials [26].

Despite significant improvements in research and development in the cancer field, about 95% of oncology drugs in clinical trials fail to receive approval. Part of the issue is the lack of suitable preclinical models that take into account the complexity of the disease and accurately represent disease progression. A growing need exists for technologies in research that can recapitulate the *in vivo* environment [29]. Difficulties arise from the evidence that breast cancer is a heterogeneous disease [28]. There is a high degree of diversity between and within tumors as well as among cancer-bearing individuals, and all of these factors together determine the risk of disease progression and therapeutic resistance [30]. Furthermore, patients with breast cancer are at risk of experiencing metastasis for their entire lifetime. The heterogeneous nature of breast cancer metastasis makes it difficult not only to define cure for this disease, but also to assess risk factors for metastasis [28].

2.1.2 Cancer microenvironment

In recent years, it has been shown that breast cancer consists not only of neoplastic cells, but also of significant alterations in the surrounding stroma or tumor microenvironment. These alterations are now recognized as a critical element for breast cancer development and progression, as well as potential therapeutic targets [31]. Tumor microenvironment is a complex milieu comprising cancer and non-cancer cells embedded into the ECM (Fig.4) [32]. Tumors are a heterogeneous mixture of epithelial cells consisting of cancer stem cells (CSCs) that have mixed epithelial–mesenchymal phenotypes and non-stem cells that are epithelial. Non-

cancer cells are inflammatory/immune cells, vascular cells and cells of mesenchymal origin (e.g. fibroblasts, myofibroblasts, adipocytes or mesenchymal stem cells). The ECM can be subdivided into the more compact basement membrane — which is a specialized ECM that is rich in type IV collagen, laminin and fibronectin — and the interstitial matrix, which consists of fibrillar collagens, proteoglycans and glycoproteins [33]. The ECM provides structural support to the tissue and acts as a reservoir of growth factor and cytokines [32].

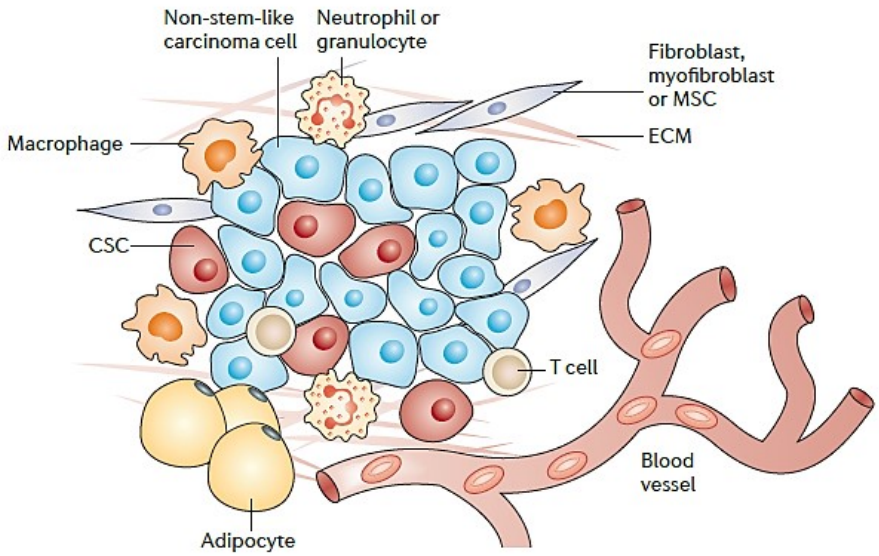

Fig. 4: Tumor microenvironment is a complex milieu comprising cancer cells, non-cancer cells as inflammatory/immune cells, vascular cells, cells of mesenchymal origin (e.g. fibroblasts, mesenchymal cells) and the ECM which provides tissue structural support and acts as reservoir of growth factors and cytokines [32][33]**.**

- **Angiogenic switch in cancer**

In order to understand tumor growth, it needs consider components of the stromal microenvironment, such as the vasculature.

Like normal tissues, tumors require an adequate supply of oxygen, metabolites and an effective way to remove waste products. Tissues beyond 1-2mm in diameter must recruit new blood vessels by vasculogenesis and angiogenesis to sustain growth. Physiologically these processes are regulated by a fine balance between pro- and antiangiogenic molecules which is altered in cancer. This process is called angiogenic switch and it depends on how heavily that balance tips in favor of pro-angiogenesis [34]. Pro-angiogenic gene expression is increased by physiological stimuli, such as hypoxia, which results from increased tissue mass, and also by oncogene activation or tumor-suppressor mutation. Hypoxia and acidosis are the most prominent consequences of deregulated vascular function and promote tumor progression and new vessel formation by activating a variety of transcriptional factors [35]. The angiogenic switch can occur at different stages of the tumor progression pathway, depending on tumor type and environment [34]. Without blood vessels, tumors cannot grow beyond a critical size or metastasize to another organ [36] and enter a dormant though viable state until they are able to secrete angiogenic factors and downregulate angiogenic suppressors (Fig.5) [37].

The fact that tumors are dependent on blood supply has inspired many researchers to search for anti-angiogenic molecules, and to design antiangiogenic strategies for cancer treatment [34]. Currently relevant anti-angiogenic agents are used in the clinic and target the vascular endothelial growth factor system such as bevacizumab, ramucirumab and sorafenib. The efficacy of anti-angiogenic drugs in adjuvant therapy or as neo-adjuvant treatment has been estimated in clinical trials of advanced breast cancer. To date, the overall observed clinical improvements are unconvincing, and further research is required to demonstrate the efficacy of anti-angiogenic drugs in breast cancer treatments. The outcomes of anti-angiogenic therapy have been highly variable in terms of tumor response [38]. This could be due to the fact that tumor heterogeneity leads to heterogeneity in the tumor vasculature [34]. Furthermore, it’s important consider that without an

homogeneous blood supply it become difficult to deliver anti-cancer drugs to all regions of a tumor in effective quantities [36].

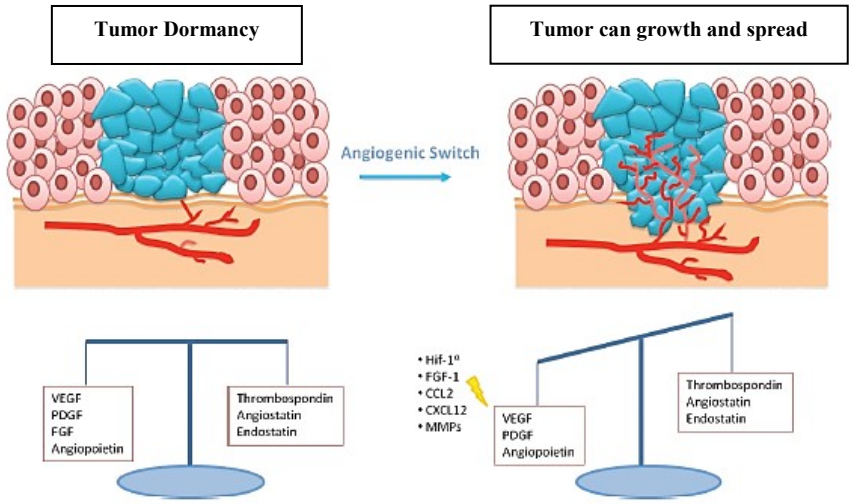

Fig.5: Angiogenic switch: In dormant tumors there is a balance between angiogenic and anti-angiogenic factors. When this equilibrium is destroyed by the prevalence of angiogenic factors, tumor can grow[37].

- **Tumor vessels characteristics**

Tumor vascular heterogeneity depends from the loss of the appropriate balances between positive and negative controls. Consequently, the vascular network develops unique characteristics and becomes quite distinct from the normal blood supply system. One feature of tumor blood vessels is that they fail to become quiescent, enabling the constant growth of new tumor blood vessels.[34]. Nevertheless, tumor blood vessels are more abundant at the tumor–host interface than in central regions. So, even if there are tumor areas richly vascularized, there are also some zones of ischemia and necrosis [39].

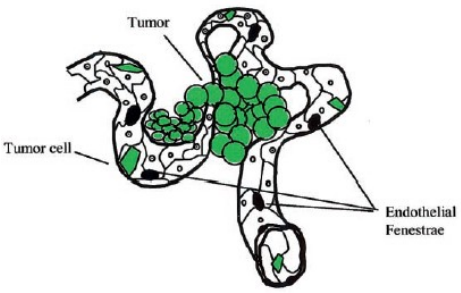

Fig. 6Schematic tumor blood vessel [40].

Tumor microvascular architecture has unique abnormal features. Tumor blood vessels have thin walls, tortuous shape, absence of pericytes, and variation in diameter. Numerous gaps or fenestrae are found between endothelial cells. The vessel wall is a mosaic and can consist of both tumor cells as well as endothelial cells (Fig.6) [40]. Tumors have an atypical branching pattern, they exhibit trifurcations, true and self-loop and polygonal structure of the capillary meshwork which cannot be classified by any preexisting branching scheme. (Fig. 7) [41].

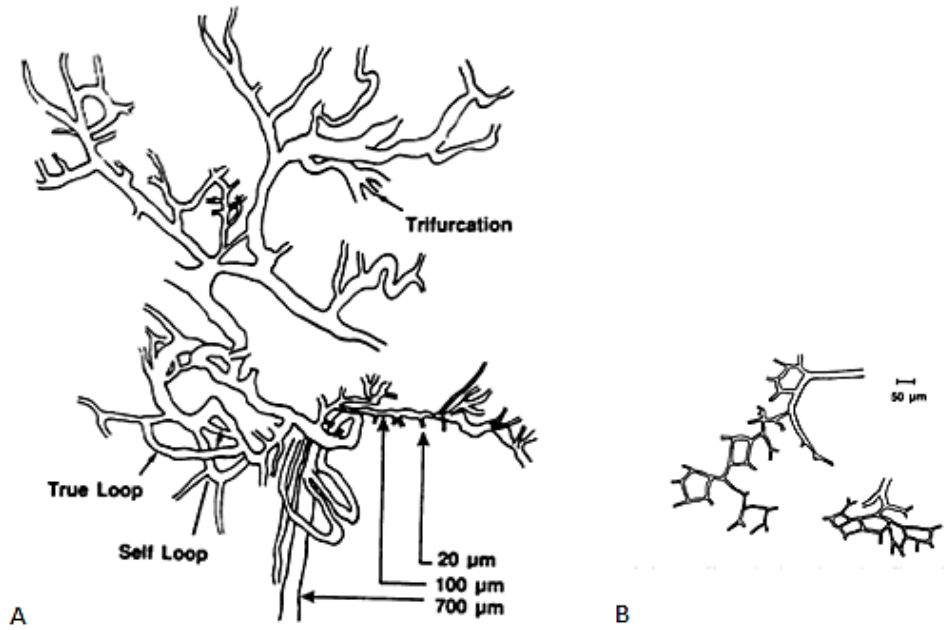

Fig. 7 Representation of some of tumor vasculature features: A) Trifurcation, presence of self/true loop and variation in the diameter. B) Capillary meshwork [41].

Because angiogenesis is essential for breast cancer, several groups have tried to find quantitative parameters correlated with its progression.

Young et al found that micro-vessel density correlated significantly with several prognostic factors, including lymph node metastasis [42].

Some interesting studies have shown that fractal geometry can be useful for describing the pathological architecture of tumors and for yielding insight into the

mechanism of tumor growth and angiogenesis. This because the fractal dimension can quantify the degree of randomness to the vascular distribution, a characteristic not easily captured by the vascular density (Fig.8) [43].

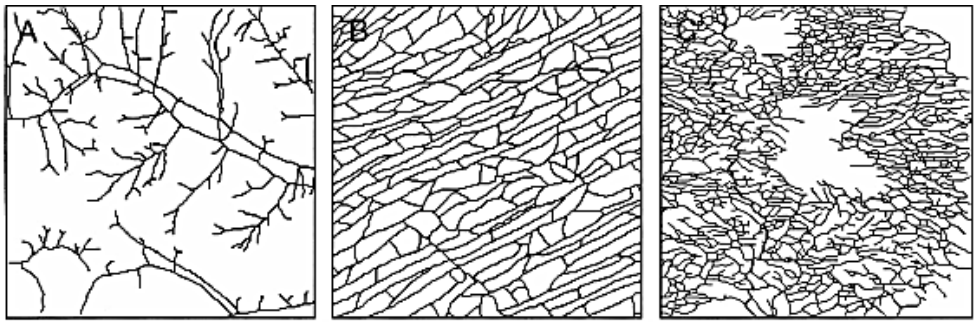

Fig. 8: Skeletonized images of vascular networks. A) Normal arteries and veins. B) Normal subcutaneous capillaries. C) Tumor vasculature [43]**.**

Saito et all showed that the number of branching point for unit area was significantly higher in tumor than normal tissues [44].

Jain et all introduced a tumor vessel classification and provide the first quantitative measurement of vessel branching patterns and the related vascular dimensions in a mammary carcinoma. They assigned a number, corresponding to an order, to each vessels of a vascular structure. The feeding or draining vessel is assigned to order 1. The angle of bifurcation determines the classification of the daughter vessels. If a vessel continues past the bifurcation at an angle of 160-180 degrees, then it retains the same order; otherwise, it is assigned to the next higher branching order. To enter a true loop, this angle determines the order of the vessels in the loop because all segments are assigned to the same order. In a self-loop, the two daughter vessels retain the same order as the parent, and when the daughters

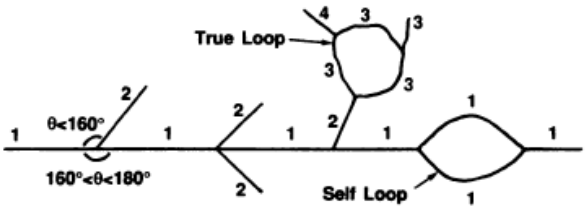

Fig. 9: Vessels branching pattern and relative orders [16].

converge they also retain the same order. At a trifurcation, the branch angle rules are applied to the two pairs of vessels, each of which includes the middle vessel (Fig.9). For each branching order, they measured vessels diameter and length. Furthermore they showed that heterogeneity in vascularization of tumors results in diverse local microenvironments for the tumor cells and could drastically affect the efficacy of cancer therapies [41]. An important variable is that blood flow through tumors does not follow a constant, unidirectional path. Not all open vessels are perfused continuously, and, over a few minutes, blood flow may follow different paths and even proceed in alternating directions through the same vessel [39].

- **Desmoplastic reaction in cancer**

Increased mammographic density is one of the greatest risk factors for the development of breast cancer, representing a two- to six-fold increase in tumor susceptibility among women with dense breasts. The increased density is due largely to an elevated collagen concentration, and is commonly identified in the mammogram as a general increase in X-ray absorbance throughout the entire breast [45]. Keely et al demonstrated that collagen density correlate positively with both tumorigenesis and tumor progression [46]. One of the features of breast cancer is the desmoplastic reaction, responsible for the clinical presentation of a tumor as a 'lump'[47]. The phenomenon is characterized by amplified collagen matrix deposition and stromal cell recruitment and activation (e.g. fibroblasts, myofibroblasts and macrophages) [45]. The stromal reaction occurs with the increase in dense fibrotic or connective tissue rich in collagen and other ECM macromolecules including specific species of proteoglycans and hyaluronic acid surrounding the tumor mass [48]. The reorganization of the stromal network is primarily mediated by stromal cells, most prominently fibroblasts. Cancer-associated fibroblasts (CAFs) reorganize the stroma by secreting ECM elements

and enzymes that covalently cross-link collagens fibers and by physically pulling on the collagen network. As a result, the stromal network becomes stiffer. In breast cancers, neoplastic tissue can be two- to ten-fold stiffer than normal tissue. This increase in tissue stiffness is thought to primarily reflect changes in the stroma, while tumor cells themselves appear to become softer [49].

The exact role of the desmoplastic reaction associated with cancer development is not known. However, it has been proposed to represent either a defense mechanism by normal host cells against invading cancer cells or to be a tumorigenesis promoting phenomenon induced by cancer cells to assist their propagation [48].

As collagen content, fiber structure, and organization are potentially key determinants of tumor cell behavior Keely et al employed nonlinear optical imaging of tumor-stromal interactions in intact live tumors by Multiphoton laser-scanning microscopy (MPLSM) in order to identify specific Tumor-Associated Collagen Signatures (TACS). They defined three signatures. Specifically:

- TACS-1, the presence of locally dense collagen within the globally increased collagen concentration surrounding tumors, indicated by increased signal intensity at a region near the tumor, which serves as a reliable hallmark for locating small tumor regions;
- TACS-2, straightened (taut) collagen fibers stretched around the tumor, constraining the tumor volume;
- TACS-3, identification of radially aligned collagen fibers that facilitate local invasion [46].

Furthermore, because of the strong statistical evidence for poor survival in patients with TACS, and because the assessment can be performed in routine histopathological samples imaged via second harmonic generation or using picrosirius, they proposed that quantifying collagen alignment could be a viable, novel paradigm for the prediction of human breast cancer survival [45].

However, the desmoplastic response is nearly an exclusively human occurrence, being quite rare among spontaneous and transplantable animal tumors and absent in most human tumoral xenografts in athymic `nude' mice. Difficulties in the study of the phenomenon arise from the lack of a good experimental model where the desmoplastic response occurs and can be successfully perturbed [47]. Barsky et al hypothesized two explanations for the absence of desmoplasia in human xenografts. The first was that the rapid growth of the tumor cells might overwhelm any host stromal response. The second was that breast carcinoma cell lines could lose their desmoplasia-inducing phenotype with increasing *in vitro* passage through the loss of critical gene products such as paracrine growth factors. Despite classical model fail to reproduce desmoplastic reaction, some transgenic models are effective for the study of the phenomenon. For their studies, Barsky et al used c-ras^{H} transfected Human Breast Adenocarcinoma cells (MCF-7) which overexpress ras p2l. Their results suggest that breast carcinoma-secreted PDGF is the major initiator of tumor desmoplasia [47].

Keely et al demonstrated that mammary tumor formation, invasion and metastasis are enhanced in collagen-dense stroma in a bi-transgenic mouse model with increased stromal collagen in mouse mammary tissue [46].

However, further studies are needed to better clarify the exact role of desmoplastic reaction in tumors before it is possible to fully assess whether desmoplastic reaction associated molecules might provide a target in the treatment of cancers. This could be of central interest also because the excessive ECM deposition due to fibrotic remodeling physically hinders diffusion of large anti-tumoral molecules through the interstitium [35].

Sainio and Järveläinen presented some examples of strategies how ECM macromolecules involved in desmoplastic reaction could be considered in the development of innovative oncological pharmacotherapies in the future [48].

2.1.3 Cancer cells metastasis

Metastasis is a hallmark of cancer and the leading cause of mortality among cancer patients. Cancer is not only a disease of uncontrolled cell growth, but also a disease of uncontrolled cell migration. The first step in metastasis is the migration of cancer cells away from the primary tumor, a process called tumor invasion. In solid epithelial tumors, invading cells must first cross the basement membrane (BM). It is a natural barrier between the *epithelium* and the stroma, a network of ECM populated by a number of other cell types that surround the tissue. Metastasizing cells migrate through the stroma to reach blood or lymph vessels, where they are able to enter and to be carried to other organs (Fig.10) [49].

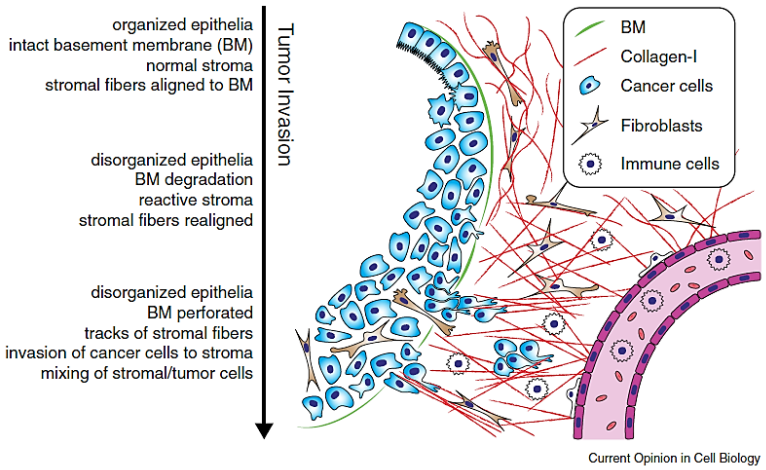

Fig. 10: Summary of tumor progression and invasion. In invasive tumors, cancer cells perforate the BM or migrate through regions of dysfunctional BM deposition, allowing the tumor cells to invade the stroma and migrate toward the blood stream [49] **.**

- **Interstitial cancer invasion**

In vitro and *in vivo* observations have shown that tumor cells infiltrate neighboring tissue matrices in diverse patterns. When cell-cell contact are absent, cells can disseminate as individual cells, referred to as ‘individual cell migration’, whereas

when cell-cell adhesions are retained, cells can expand in solid cell strands, sheets, files or clusters, called ‘collective migration’[50]. Cancer cells possess a unique ability to adapt to different environmental conditions, assuming different morphologies and migration characteristics in order to stay motile. In human cancer pathology studies, cancer cells from epithelial tumors primarily invade collectively. Intravital imaging studies show that cancer cells display a wide range of different migration modes and morphologies. *In vitro* studies have identified several intrinsic factors regulating migration mode and morphology. In cancer cells migrating individually, increased contractility, under control of the Rho-pathway, favors amoeboid-like migration, while lower contractility (and/or increased adhesion) favors more mesenchymal phenotypes. Increased cell-cell interactions via cadherins and cell- ECM binding via integrins can promote collective migration in cancer cells. In addition to intrinsic factors, the microenvironment plays a significant role in determining cancer cell migration mode and morphology [49]. Friedl and Alexander talk about cancer cell invasion like a heterogeneous and adaptive process in which “plasticity” in cell adhesion, cytoskeletal dynamics, and mechanotransduction perpetuates migration and dissemination under diverse structural, molecular, and even adverse microenvironmental conditions. Such heterogeneous tumor progression is mirrored by the ‘‘activation’’ response of stromal cells nearby the growing tumor, including fibroblasts, endothelial cells, and macrophages. These cells reorganize the structure and composition of the connective tissue by depositing ECM, cytokines, and growth factors. By remodeling the tissue structure, releasing growth factors, and imposing metabolic stress, the reactive tumor stroma, in turn, influences cancer cell functions, often enhancing tumor growth and invasion and aggravating cancer resistance during metabolic challenge and therapy. Thus, in a reciprocal manner, tumor cells influence the stroma and vice versa, jointly driving cancer progression. The mechanisms of tumor cells migration recapitulate those of normal, non-tumor cells

but neoplastic cells lack physiological “stop signals” immobilizing and anchoring the cells [51].

Individual-cell migration can be mesenchymal or amoeboid. Cells can move alone or in multicellular streaming when are one after each other following the same path. Collective invasion may adopt different morphologies. Groups of cells can form small clusters, solid strands, or files; if epithelial polarity is retained during migration, these structures can even form an inner lumen. In most cases of collective cancer invasion, one or several leader cells with mesenchymal characteristics form the tip of multicellular strands and generate forward traction and pericellular proteolysis

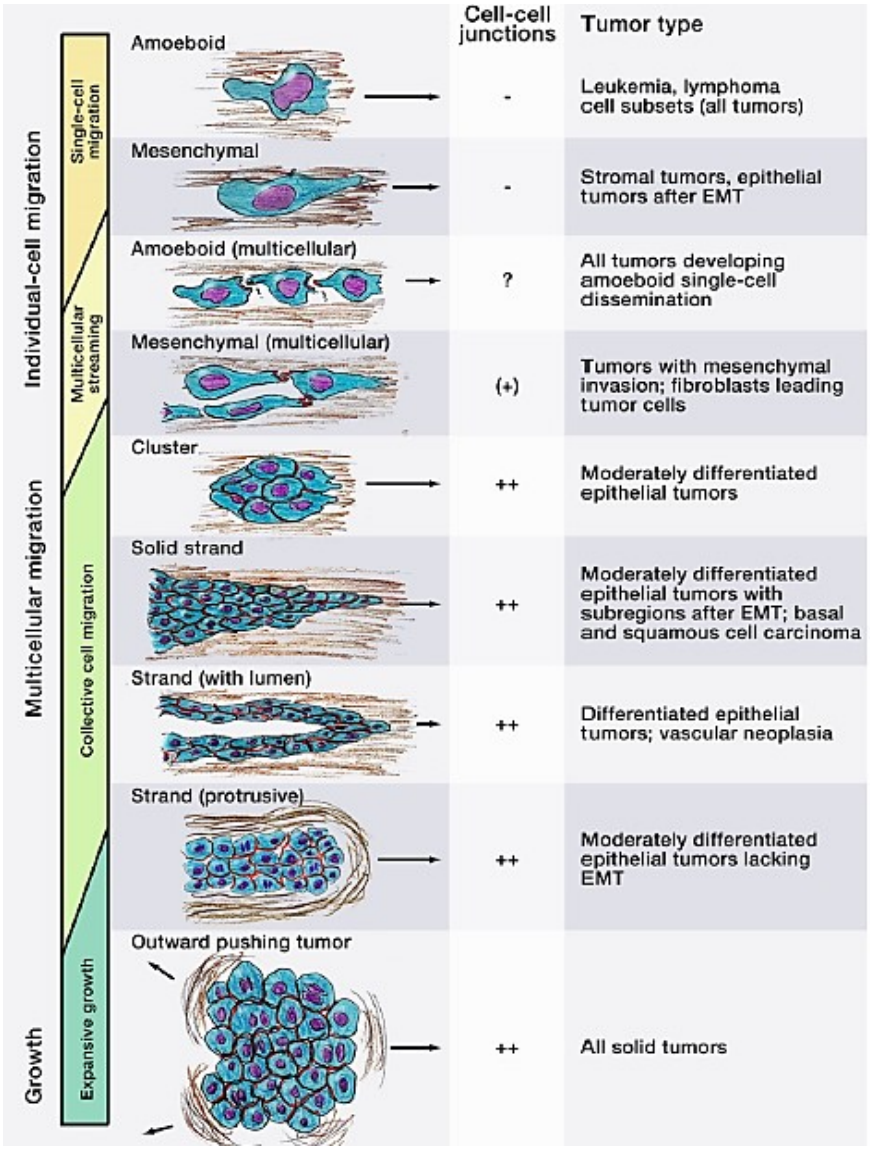

Fig.11 Modes of cell movement implicated in cancer invasion and metastasis [51]

toward the tissue structure. In a second type of collective invasion, a blunt bud-like tip protrudes along tissue space consisting of multiple cells that variably change position, lacking defined leader cells. The mechanism of expansive growth occurs when surrounding tissues impose little to no physical confinement on proliferating tumor cells and thus do not hinder the expansion of a cancerous lesion. When tumor cells grow in this way, the increase in volume leads to multicellular outward pushing with intact cell-cell junctions and no signs of active migration (Fig.11) [51]. Tumor cells can migrate assuming these different morphologies determined by the cell type but they can also switch migration mode depending on the microenvironment conditions or assume intermediate phenotypes.

The most well-established example of changes in cancer-cell pattern and function is termed the Epithelial–Mesenchymal Transition (EMT). Following tumor progression and dedifferentiation, epithelial cancer cells can undergo a transition from a collective invasion pattern towards a detached and disseminated cell migration mechanism. These cells move in a fibroblast-like fashion [50]. Complete EMT is defined by a metastable, fibroblastoid phenotype plus loss of E-cadherin and gain of vimentin and it was most closely correlated with local invasion and metastasis [52]. EMT is also thought to represent a program transiently controlled by the microenvironment, which locally downregulates epithelial characteristics and facilitates cell escape from the primary tumor. However, with local upstream signaling lost, cells can undergo mesenchymal-to-epithelial reversion after metastatic seeding in the secondary organ. Thus, EMT-dependent invasion and metastasis programs are strongly responsive to microenvironmental changes and adaptive in their signaling program and associated invasion dynamics [51].

The understanding of these mechanisms is fundamental to investigate the mechanisms of drug resistance and develop new therapies for the treatment of metastatic tumors.

- **Intravasation**

Tumor cells can penetrate blood or lymphatic vessels, circulate through the intravascular stream, and then proliferate at another site: metastasis [53]. So, after the interstitial migration, invading cancer cells enter the circulation by migrating directly through blood vessels walls (intravasation). If they survive the shear stress and the protective immune cells in the bloodstream, they can eventually attach to the *endothelium* that line the blood vessels. This process frequently involves leukocytes and platelets. Circulating cancer cells usually extravasate and then start to proliferate in the stroma. However, in some cases they initially proliferate in the blood vessels, then cross the *endothelium* and invade the underlying tissues as groups (micro-metastasis). Intravasation and extravasation of cancer cells both require the disruption of endothelial junctions for the cancer cells to cross the *endothelium* — a process that is known as transendothelial migration (TEM) — but intravasation and extravasation are fundamentally different because the cancer cells approach the *endothelium* from opposite sides. To intravasate, tumor cells need to invade through the tissues towards blood vessels. Otherwise tumors inducing local angiogenesis can enter the vasculature through new blood vessels generally having weak cell–cell junctions.

Tumor cells can cross the endothelial wall by paracellular intravasation or transcellular intravasation. Paracellular intravasation involves the disruption of endothelial junctions and in particular the cleavage of vascular endothelial cadherins (VE-cadherins) by metalloproteinases or their retraction. Tumor associated macrophages can attract cancer cells towards blood vessels by secreting epidermal growth factor (EGF) and can also secrete tumor necrosis factor 1α (TNF1α), which induces the retraction of endothelial junctions. Cancer cells can use Notch receptors to bind to Notch ligands on ECs and thereby transmigrate through the endothelial junctions; they can also secrete transforming growth factor

β1 (TGFβ1), which induces the retraction of endothelial junctions. During transcellular intravasation, the Ca2+ –calmodulin complex in an EC activates myosin light chain (MLC) kinase (MLCK) at the sites of cancer cell attachment, which leads to local phosphorylation (P) of MLC and to actomyosin contraction. In turn, this leads to rapid cytoskeletal and membrane remodeling, which creates a transitory pore-like structure for the cancer cell to cross the EC (Fig.12) [54].

Another paradigm for tumor intravasation suggested by Weider, citing Sugino et al, is that, in some tumor models, tumor cells can gain access into blood vessels by intravasation of tumor cell nests surrounded by vascular endothelial cells, followed by intravascular tumor growth without penetration of the vascular wall. This concept depends from the evidence that intratumor micro-vessel density correlate with aggressive tumor behavior and the greater number of tumor vessels increases the opportunity for tumor cells to enter the circulation. They suggested that high angiogenic activity and sinusoidal remodeling of tumor blood vessels around tumor cells are prerequisites for tumor metastasis [55].

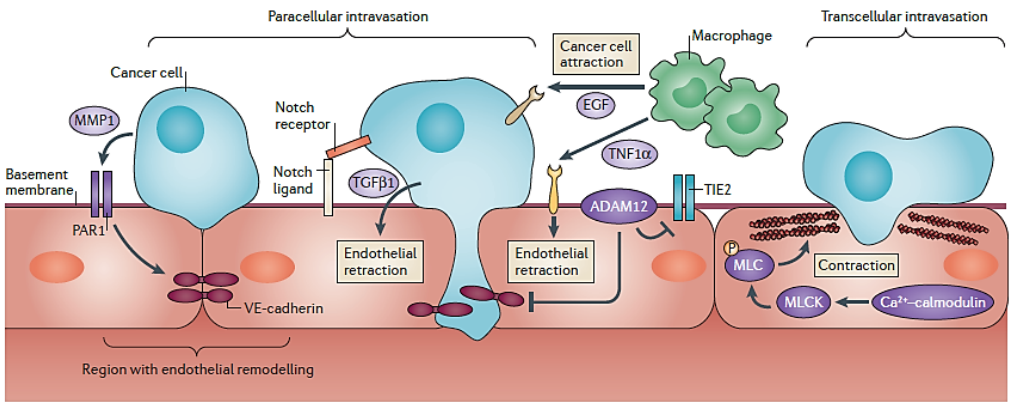

Fig. 12: Mechanisms of transendothelial migration: paracellular or transcellular intravasation [54].

In the bloodstream of patients with metastatic epithelial cancer both single and cluster circulating tumor cells (CTCs) are present. CTCs-clusters describe groups

of 2-50 cancer cells [56]. Using mouse models with tagged mammary tumors, Maheswaran et al demonstrated that CTCs-clusters arise from oligoclonal tumor cell groupings and not from intravascular aggregation events. Although rare in the circulation compared with single CTC, CTCs-clusters have 23-50-fold increased metastatic potential. In breast cancer patients, both abundance of CTCs clusters and high levels of the cell junction plakoglobin denote adverse outcomes [57]. Toner et al used engineered microfluidic constriction devices with dimensions mimicking human capillaries to study the behavior of CTCs clusters within constrictions under physiological temperature and pressures. They found that CTCs clusters successfully traversed 5- to 10-μm constrictions even in whole blood. Clusters rapidly and reversibly reorganized into single-file chain-like geometries that substantially reduced their hydrodynamic resistances. They performed also *in vivo* studies by xenotransplantation of human CTCs clusters into zebrafish and showed similar reorganization and transit through capillary-sized vessels. In their work, preliminary experiments demonstrated that clusters could be disrupted during transit using drugs that affected cellular interaction energies. Beyond their role in metastasis, CTCs clusters may also serve as biomarkers for early detection, as prognostic markers, may have utility for non-invasively tracking changing drug susceptibilities in patients undergoing treatment and for the development of new therapeutic approaches [58]. It is not clear whether CTCs clusters passively enter the bloodstream through compromised tumor vasculature or whether they actively traverse the endothelial cell barrier as observed in collective cell migration *phenomena* [59]. One possible entry way of CTCs cluster into the bloodstream could be the shedding from mosaic vessels [60].

2.1.4 Models for breast cancer research

Historically, cancer has been studied in two dimensional (2D) monolayer cultures and small animal models [61]. When cultured *in vitro*, cancer cells lose many of their *in vivo* features, because of the lack of environmental signals present in native tumors [32]. 2D cell culture models lack the structure for proper cell–cell and cell–matrix interactions and are not able to replicate the *in vivo* phenotype which is strongly influenced by the microenvironment [29]. Animal models also have limitations, as they often fail to represent the pathology of human tumors [32]. In fact, there exist major differences between cancer progression in humans and animals. Moreover, using animals can be very costly, laborious, and requires animal facilities as well as Institutional Animal Care and Use Committee approval.
Recently, there has been promising published work on three-dimensional (3D) cell culture models developed to study breast cancer tumor progression *in vitro* [29] [62]. Bissels and Nelson talk about not simply a culture model but a new paradigm, that tissue-specific functions can be recapitulated in the laboratory by providing cells with appropriate microenvironmental cues that allow the rebuilding of tissue-specific form. They have been one of the pioneers to use 3D to model the murine gland in both its normal and diseased state [63].

- ***In vitro* 3D models in cancer research**

3D *in vitro* culture systems to model tumors can be mainly classified into cells cultured as multicellular aggregates and cells embedded in construct made of natural or synthetic matrices (Fig.13).

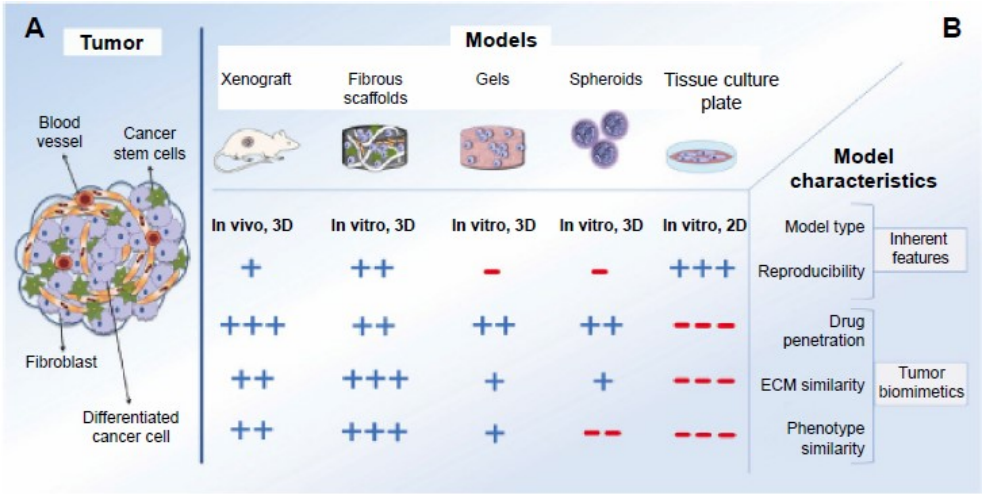

Fig.13: Schematic picture of A) a tumor and B) different tumor models [29].

In addition high-throughput technologies such as microfluidic devices have been developed to model tumors and the influence of the microenvironment [29]. Another culture system involve cells seeding on fibroblast derived 3D matrices with the aim to mimic the native 3D environment [64].

- ***Multicellular aggregates***

In 1966, Halpern et al cultured cancer cells in suspension using an Erlenmeyer on a shaker – the Moscona's technique – and showed that malignant cells have higher capacity to aggregate than normal cells. For a long time cancer biologists have modeled cancer in cell aggregates or spheroids, using Moscona's technique [32]. Spheroids have been widely used in the cancer field as a model system in several studies involving 3D cell culture for drug screening predominantly for high-throughput applications. Spheroids are 20–1000 μm diameter clusters of cells that self-aggregate when cultured in rotary wall vessels or spinner flasks. Spheroids have been shown to preserve the physiological shape of the tumor, respond to chemotherapy and radiation therapy, and maintain tissue-specific properties of the

primary tissue. Several techniques have been presented in the literature for culturing spheroids. The most widely used techniques involve growing cells on plates coated with low attachment substrates to prevent cell–substrate interaction, in hanging drops, or in a continually rotated suspension such as a spinner flask. However, these techniques are time consuming and hard to standardize [29]. Moreover, it was demonstrated that spheroids contain few or no stromal elements [65]. In 2011, a new method to culture spheroids from primary cancer cells was developed by Kondo et al. Tumors were dissociated mechanically and enzymatically to isolate cancer cells and make cancer tissue originated spheroids also known as 'tumor organoids'. Tumor organoids are important for displaying the typical histological characteristics of the original tumor and for their ability for seemingly indefinite expansion *in vitro* [32]. Ewald et al developed three-dimensional organoid assay to identify the most invasive cancer cells in primary breast tumor. Tumor organoids in Collagen I hydrogel were used as experimental model. They found that basal epithelial markers, including Keratin14 (K14) and p63, are expressed in the invasive leader cells leading collective invasion and that the knockdown of either K14 or p63 was sufficient to block cells migration into collagen [66].

- ***Cells embedded in construct made of natural or synthetic matrices***

The 3D culture techniques usually include adding cell suspension to matrices or culturing cells on biomaterial scaffolds that can be fabricated into various desired architectures from different materials. Hydrogel matrices, such as Matrigel and type I collagen, and synthetic matrices have been widely used to investigate how the physical properties of the ECM modulate tumor cell invasion [29]. Matrigel is a basement membrane formulation derived from the Engelbreth-Holm-Swarm mouse sarcoma. In some works, Matrigel and collagen are used in combination. Sonnenschein et al have underlined the role of both the ECM composition and the

presence of fibroblasts in determining the fate of the epithelial cells and their phenotype [67]. Beebe et al incorporated human mammary fibroblasts and breast cancer cells in a 3D co-culture model based on collagen and Matrigel, modeling the progression from ductal carcinoma in situ to invasive ductal carcinoma [68]. Matrigel has been long used for invasion assay but several studies have identified batch-to-batch variations that cannot be controlled and can be problematic when interpreting results from studies [29].

Overall, native scaffold effectively promoted cell adhesion and growth [32]. Using porous collagen I scaffolds breast cancer cells recapitulate many of the tumor features: morphology, proliferation, overexpression of pro-angiogenic factors, and MMP transcriptions [69]. However, most of the 3D *in vitro* models fail to reproduce tumor complexity and plasticity, because they use homogeneous and passive scaffold [70] whose properties cannot be altered easily to interrogate the contributions of specific environmental cues to tumor assembly [71]. Another shortcoming of classical model is the lack of vascularization limiting diffusion properties of nutrient and oxygen, the size of engineered tumors, and cancer cell viability and function. Vascularization is also required for tumor metastasis. A number of approaches have sought to co-culture cancer cells, endothelial cells and supporting cells in order to create vascularized tumor models [32]. Rylader et al showed that paracrine signaling between telomerase-immortalized human microvascular endothelial (TIME) cells cultured as an *endothelium* on the surface of an acellular collagen I hydrogel and MDA-MB-231 cells cultured beneath in a separate collagen I hydrogel led to augmented angiogenic activity; specifically a significant increase in TIME cell number, the development of an elongated and aligned TIME morphology, and invasive angiogenic sprouting [72]. A particularly interesting tumor model was developed by tumor cells (breast and colon), human fibroblasts and endothelial cells cultured in fibrin matrix, resulting in a network of sprouting vessels, and cancer cells invasion of the surrounding matrix. In detail

George et al introduced the Pre-Vascularized Tumor (PVT) model to investigate early events of solid tumor progression. PVT spheroids were composed of endothelial and tumor cells, and were embedded in a fibrin matrix containing fibroblasts. The PVT model allowed robust sprouting angiogenesis into the matrix, and contiguous vascularization within the spheroid. Furthermore, the PVT model enabled the intravasation of tumor cells that was enhanced under low oxygen conditions and was also dependent on the key EMT transcription factor Slug [73].

Also synthetic materials have been widely used by cancer biologists and engineers. Synthetic biomaterials can be fabricated in a reproducible manner and in large quantities. Some of the commonly used synthetic biomaterials to generate breast cancer models include poly (lactide-co-glycolide) (PLG), poly (lactic acid) (PLA), and poly (ethylene glycol) (PEG). Paszek et al found that combining polyacrylamide gels with ECM components and changing the elastic moduli can disrupt epithelial tissue homeostasis, potentially leading to malignant behavior. Fischbach et al, Cross et al, and Szot have engineered 3D *in vitro* tumor models using both natural and synthetic polymeric scaffolds, respectively, showing that endothelial cells can remodel dense type I collagen matrices in response to angiogenic factors from cancer cells, and the different effects of these angiogenic factors on drug responsiveness [29].

Recent advances in microfluidic technology have made it possible to develop innovative assays that enable accurate control of the cellular microenvironment. Microfluidic assays are highly beneficial toward clinical applications since they are high throughput and automated, thus requiring minimal manual operations during measurements. Recently our group proposed a new model of breast cancer featuring both epithelial and stromal tissues arranged on a microfluidic chip. The model recapitulate the fibroblasts activation and ECM remodeling following tumor invasion into a microfluidic system which allows to quantify in real time the switch between a healthy to a pathologic status *in vitro* at ECM level [74].

Several 3D models have been established using microfluidic devices to study metastatic events. Polacheck et al exploited a microfluidic cell culture system to investigate the effects of interstitial flow on tumor cell migration and found that breast cancer cells migrated in an organized fashion with interstitial flow as compared to control devices without flow where cells migrated randomly.

Moreover, several investigators have applied microfabrication technologies to obtain engineered biomimetic vasculature in order to simulate physiological transport *phenomena*. The main objective of these studies was to characterize the processes activated by cancer cells under shear stress conditions: adhesion with endothelial cells and degradation of the basement membrane to undergo metastatic growth [29].

Kamm et al presented a unique approach using a microfluidic-based *in vitro* assay that enables real-time visualization and quantification of the interactions between tumor cells and an endothelial monolayer in the context of tumor cell invasion and intravasation. They showed that the *endothelium* poses a barrier to tumor cell intravasation that can be regulated by factors present in the tumor microenvironment [75].

Hughes et al developed a microfluidic micro-physiological system that incorporates human tumor and stromal cells in a 3D ECM, supported by perfused human micro-vessels. Through this microfluidic device they were able to deliver anti-angiogenic drugs and evaluate their effect on vasculature supporting tumor growth [76]. Their platform was constructed using standard photolithography from PDMS and consists of two outer microfluidic channels that act as arteriole (high pressure) and venule (low pressure), connected by three tissue chambers, into which it was injected a slurry of ECM and cells. Over the course of 5–7 days ECs self-assemble into an interconnected network that anastomoses with the outer channels resulting in the passage from interstitial to intraluminal flow [77] [78] [76].

- ***Cells seeded on fibroblasts 3D derived matrices***

Because *in vitro* collagen matrices, Matrigel, and other synthetic support systems do not closely resemble the mesenchymal microenvironment that is typically associated with advanced carcinomas *in vivo*, several groups have evaluated the ability of fibroblast derived 3D matrix to regulate the growth and invasion skills of human tumor epithelial cell lines. Cukierman et al proposed the use of decellularized NIH-3T3 derived matrices as *in vitro* drug screening platforms [79]. Another work showed that harvested primary stromal fibroblasts, obtained from different stages of tumor development, did not retain *in vivo* stromagenic characteristics when cultured on traditional 2D substrates but they were capable of effectively maintaining the tumor-associated stromal characteristics within 3D cultures. They demonstrated that *in vivo*-like 3D matrices appear to have the necessary topographical and molecular information sufficient to induce the activation normal fibroblasts [80].Moreover, they compared early and late 3D matrices respectively produced by NIH-3T3 and tumor-associated murine fibroblasts. After removing fibroblasts, extracted matrices were re-cultured with breast epithelial cells of assorted characteristics: MCF-10A (non-tumorigenic), MCF-7 and MDA-MB-231 (tumorigenic). They observed that assorted breast epithelial cells reacted differently to 2D vs 3D matrices. MCF-10A had a proliferative advantage on 2D substrates while MCF-7 and MDA-MB-231 showed no difference. MCF-10A and MCF-7 formed morphologically distinguishable aggregates within 3D matrices, while MDA-MB-231 exhibited increased spindle-shape morphologies and directional movements within three-dimensional matrices. Furthermore, MDA-MB-231 acquired a pattern of parallel oriented organization within tumor-associated, but not control matrices .[81]

Based on the idea that stroma and stromal fibroblasts have a fundamental role in both physiological and pathological tissuegenesis, our group, Netti et al, developed a new strategy to produce pieces of viable 3D tissue-equivalent to resemble and capture the major features of native tissue. In particular, micro-tissues (µTPs) were obtained by means of dynamic cell seeding of fibroblasts on porous gelatin micro-carriers using a spinner flask bioreactor. With this approach, it is possible to guide the process of collagen deposition and assembly within the extracellular space and match it with scaffold degradation, cell traction and tissue maturation in order to obtain firmer collagen network. In this way, it could be possible develop tumor micro-tissue with controlled microarchitecture and significant ECM components. The presence of the micro-scaffold in this micro-tissue induces collagen synthesis and sustains its assembly reproducing the tumor architecture found *in vivo*. By following the dynamic seeding approach cancer associated fibroblasts-µTPs were produced showing a strong second harmonic generation signaling (SHG) compared to spheroid demonstrating the production of collagen (Fig.14). This is extremely important in the effort of mimicking the behavior of some tumor types featured by a dense desmoplastic stromal reaction [65].

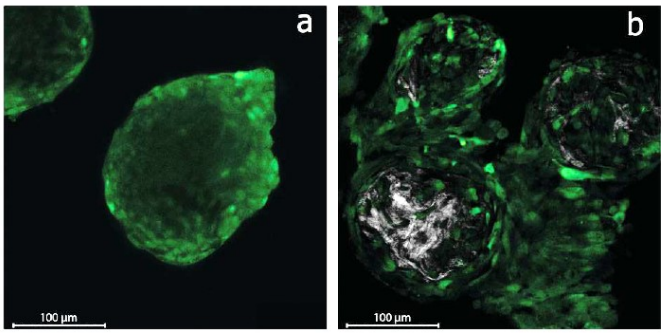

Fig. 14: A)CAF spheroids and B) CAF µTPs [65].

2.2 Physiological tissue: Human skin

2.2.1 Human skin: *In vivo* overview

The skin consists of a highly differentiated stratified *epithelium*, the epidermis, and a scaffold of connective tissue which is rich in neurovascular structures, the dermis. The latter is based on a fatty tissue arranged in lobules, the hypodermis. Also epithelial structures, which together are referred to as skin appendages, are part of the skin: the pilosebaceous units, the sweat glands and nails (Fig.1). The skin is a complex organ with specific functions and activities such as: thermoregulatory and sensory activity, barrier, deposit, metabolic, endocrine and secretory functions and it is involved in the maintenance of the homeostasis pressure [82].

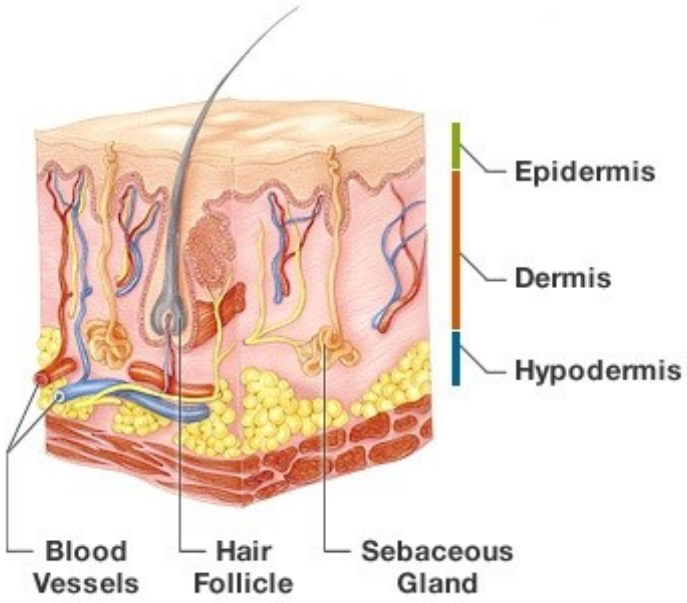

Fig. 1: Schematic representation of the skin.

The epidermis is a keratinized stratified *epithelium* without blood vessels. The epidermal cells are especially keratinocytes. It is composed by 5 layers and it is

connected to the dermis by a basement membrane. The deepest layer or basal consists of proliferating cells (germinal layer) which divide by mitosis to produce the majority of the epidermal cells and differentiate toward the external layer. The 5 layers of the *epithelium* are: basal *stratum*, *spinosum*, *granulosum*, *lucidum* and *corneum*. During development of epidermal layers, keratinocytes became anucleate, change shape and become highly organized, forming cellular junctions (desmosomes) between each other and secreting keratins [83].

The dermis is a dense irregular connective tissue populated by fibroblasts and other cells residing in an Extracellular Matrix composed of collagen (mainly types I and III), elastic fibers, glycosaminoglycans (GAGs), proteoglycans (PGs), and other minor components [84]. The dermis comprises 2 distinct layers: The layer that is closest to the epidermis, known as the papillary (or upper) dermis, has thin collagen fibers, below that lies the reticular (or deep) dermis, which has dense collagen fibers, and overlies the subcutaneous fat layer [85].

2.2.2 Skin microenvironment

The basal layer of the epidermis is attached to a basement membrane [85] mainly consisting of collagen IV, laminin, nidogen/entactin, and perlecan [86]. The underlying dermis is a thick layer of connective tissues (until 3.0 mm on the back) that consists mainly of ECM or structural components (predominantly collagen and elastin) which give mechanical strength and elasticity and a vascular plexus for skin nourishment. Cells interspersed within the ECM include fibroblasts, endothelial cells, smooth muscle cells and mast cells [87].The ECM is produced by stromal fibroblasts and provides structural scaffolding for cells, as well as contextual information [88].Research on the structure and composition of the ECM strongly indicates that the major role of this matrix is in regulating cell/cell communication rather than in passively supporting cells. A wealth of structural

data on the ECM suggests that there are specific arrangements of sequences within these proteins which profoundly influence the behavior of the cells moving in that area, with respect to attachment, migration, differentiation and proliferation. In the skin, the ECM can be argued to promote 'appropriate' communication between the keratinocyte and the fibroblast [89]. So, ECM constituents are essential for providing tissue structural integrity and regulate cellular functions cell-cell and cell-matrix interactions, and serve as a reservoir and modulator of cytokines and growth factors' action [90].

- **Vascularization of the skin**

The cutaneous microvasculature is composed by arterioles and venules forming two important plexuses in the dermis: an upper horizontal network in the papillary dermis from which the nutritive capillary loops of the dermal papillae arise and a lower horizontal plexus at the dermal-subcutaneous interface. The lower plexus, formed by perforating vessels from the underlying muscles and subcutaneous fat, gives rise to arterioles and venules that directly connect with the upper horizontal plexus and also provide lateral tributaries that supply the hair bulbs and sweat glands. The micro-vessels in the papillary dermis vary in diameter from 10 to 35 μm whereas in the lower dermis diameters are wider, of about 50 μm Some

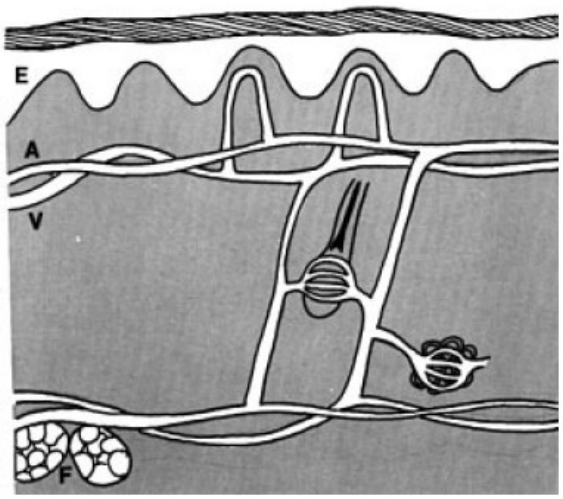

Fig. 2 Representation of the microvascular organization in human skin. E, epidermis; A, arteriole; V, venule; F, subcutaneous fat

interconnections are present among the ascending arterioles and descending venules within the dermis (Fig 2) [91]. Arteriovenous anastomoses (AVAs) are special feature of human skin microcirculation [92]. The arteriolar wall is formed by three layers: the 'adventitia', with collagen and elastic fibers, the 'media' with smooth muscle cells, and the 'with collagen fibers and *endothelium*. When the arterioles become smaller, the layer of smooth muscle cells becomes discontinuous (meta-arterioles) and it is replaced by pericytes at the capillary level. Capillaries are formed by a basal lamina, pericytes and endothelial cells. The post-capillary venules initially have the same structure of the meta-arterioles, but the basal lamina surrounding the *endothelium* is multilayered and sometimes collagen bundles are observed between the basal lamina and smooth muscle cells. Venules of greater caliber have a thicker 'media' and an 'adventitia' with an elastic basement membrane [82].

2.2.3 *In vitro* skin models

Over the past 30 years Tissue Engineering has made numerous efforts to get substitutes that mimic the structure and function of human skin.

The first stage of the general strategy for obtaining the skin-equivalent models involves fibroblasts and keratinocytes extraction from skin biopsies and their amplification in 2D cultures *in vitro*. Fibroblasts are seeded within a scaffold able to mimic the functions of the extracellular matrix and kept in 3D cultures for the realization of the dermal component of the skin. Following keratinocytes are seeded on the surface of the scaffold and maintained in culture in order to obtain a stratified and differentiated *epithelium* (Fig.3).

Dermo-epidermal substitutes have many applications both *in vivo* and *in vitro*. In fact they may be used for clinical applications and as platform for drug or cosmetic screening [93].

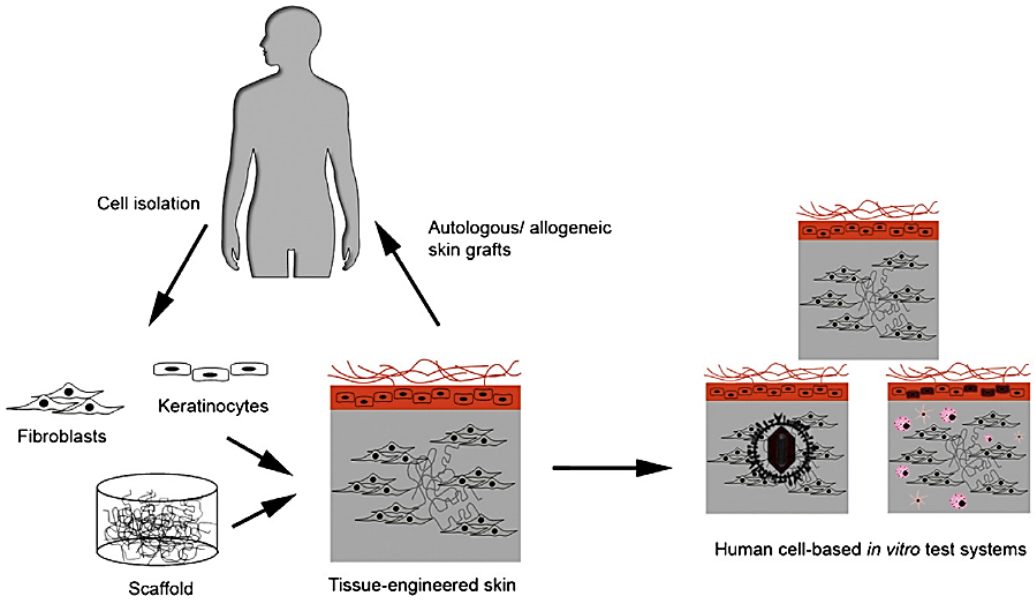

Fig. 3 Schematic illustration of principles of skin tissue engineering. Primary keratinocytes and fibroblasts are isolated from human donor tissues. For a full-thickness skin equivalent, the fibroblasts and the matrix are initially used to establish the dermal part. The keratinocytes are seeded afterwards on the top of the dermis to ultimately form the epidermal part of the skin substitute. The *in vitro*-engineered skin can serve as skin graft or can be used as human-cell based *in vitro* test system [93].

Recently our group showed the importance of an endogenous dermis compartment in tissue formation and function *in vitro*. The dermis was obtained using a bottom up approach. The strategy for the construction of biohybrid dermis equivalent was described in a paper published by Palmiero et al in 2010 and it is based on the principle that most of the tissues *in vivo* are composed by repeating units of dimensions in the order of µm, consisting of different cell types and with a µ-architecture and tissue-specific functions. The bottom up approach allowed to obtain thick and viable 3D tissues starting from the assembly of µ-Tissue-Precursors (µTPs) obtained via dynamic seeding and culture of fibroblasts on porous gelatin micro-spheres. Fibroblasts from human skin biopsies were dynamically seeded and cultured on gelatin porous µscaffolds into Spinner Flask. Cells were able to adhere on the surface and into the pores of the scaffold and here to proliferate and produce elements of the extracellular matrix (ECM) and in

particular collagen I. Thanks to cell-cell and cell-matrix interactions, adjacent µTPs were able to increase their size and coalesce, forming larger tissue precursors. To get the biohybrid dermis- equivalent, µTPs were assembled into specific maturation chambers and kept in dynamic culture regime (Fig.4).

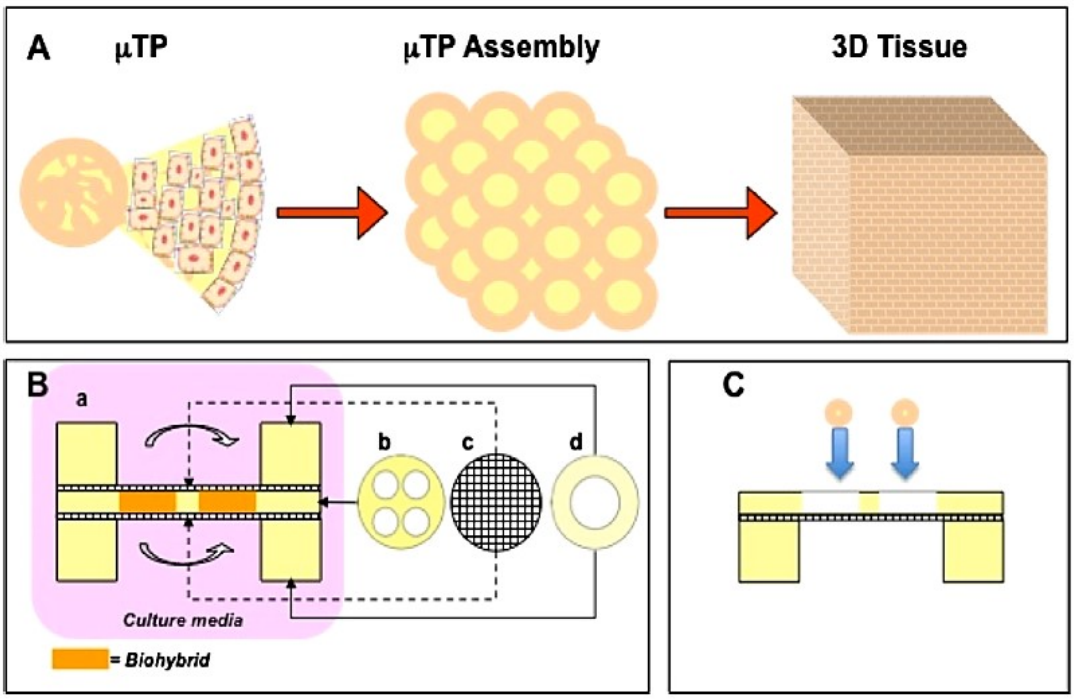

Fig. 3 Scheme of the bottom-up process (A); assembling chamber drawing (B), showing the configuration of the assembling chamber during the µTPs assembling process (a), the silicon mold with four empty spaces (b), the rigid mesh with 18 lm pore size (c) and the PTFE ring (d); µTPs loading (C) [21].

In a following work, Imparato et al demonstrated that the mechanical properties and the degradation rate of the scaffold impact on the organization and maturation of the *de novo* synthesized collagen. In particular, they showed that modulating the density of crosslinking is possible to drive the processes of collagen deposition and assembly as well as to balance the degradation rate of the scaffold with tissue maturation and cell traction. The use of micro-scaffolds crosslinked with 4% of glyceraldehyde allowed to obtain a massive deposition of immature collagen progressively assembled in mature collagen fibrils. The relationship between the

degradation time of the scaffold and the synthesis of collagen was just below the unit by determining an intermediate tissue ability to resist contraction [94].
Seeding human keratinocytes on this kind of matrix allowed obtaining a functional skin equivalent model in which it is possible to generate follicle-like structures *in vitro* resembling what occurs *in vivo* in the fetal skin. Thus, supporting the importance of the repository and regulatory role of the endogenous extra cellular matrix in guiding tissue morphogenesis [22].

- **Skin substitutes for clinical application**

Research in skin tissue engineering was initially prompted by the need to obtain substitutes for the care of patients with extensive damaged tissue area. There are multiple reasons for skin damage including genetic disorders, acute trauma, chronic wounds (e.g. lower extremity ulcers, decubitus ulcers, chronic venous or diabetic foot ulcers) or surgical interventions. One of the most common causes for major skin injury is thermal trauma (e.g. burns). In many cases, it is not possible to carry out the autograft because of the extension of the damaged are (> 50% -60% of the total body surface area, TBSA) and for the possibility of infection at the implant or graft site. The tissue engineering challenge is to obtain a skin model transplantable quickly, in large quantities, possibly during a single surgical intervention and without production of significant scarring [93] [95] [87].
Currently clinically available models are represented by epidermal, dermal or dermo-epidermal substitutes. These models can be used alone or in combination in order to repair damaged skin tissue.
The first step in skin tissue engineering was the *in vitro* culture of keratinocytes after enzymatic separation of the epidermis from the dermis [96]
Rheinwald and Green managed to grow human primary epidermal cells in serial culture on a layer of lethally irradiated 3T3 murine fibroblasts demonstrating the

importance of the crosstalk between keratinocytes and fibroblasts [97]. O'Connor et al. reported the world's first grafting of extensive burns with sheets of cultured *epithelium* expanded from autologous epidermal cells (CEA).

Burke et al. reported afterwards the successful use of an artificial dermis in the treatment of extensive burn injuries. This artificial dermis is now known as Integra and it is made up of bovine collagen and chondroitin 6-sulfate [87]. Another dermis substitutes is Matriderm which is an acellular lyophilized collagen and elastin based biomatrix [98]. In addition to these acellular matrices, there are some cellular substitutes such as Apligraft It is constructed by culturing human foreskin-derived neonatal fibroblasts in a bovine type I collagen matrix over which human foreskin-derived neonatal epidermal keratinocytes are then cultured and allowed to stratify [99]. Others commercially available skin substitutes are presented in Table 1.

Table 1 Tissue-engineered skin substitutes. Adapted from [87]

	Skin substitutes	Structure
EPIDERMAL	Cultured epithelial autograft (CEA)	Confluent autologous keratinocytes
DERMAL	Integra	Cross-linked bovine tendon collagen-based dermal matrix linked with glicosaminoglycan (GAG)
	Matriderm	Bovine non cross-linked lyophilized dermis, coated with alpha-elastin hydrolisate
	Matriderm Composite skin	Matriderm as template, seeded with expanded autologous skin fibroblasts and keratinocytes
Artificial biological materials	Biobrane	Silicone membrane and nylon mesh impregnated with porcine dermal collagen
	AlloDerm	Human acellular lyophilized dermis
Natural biological materials	Permacol	Porcine acellular lyophilized dermis
	Transcyte	Porcine collagen-coated nylon mesh seeded with allogenic neonatal human foreskin fibroblasts
Synthetic materials	Dermagraft	Bioabsorbable poliglactin mesh scaffold seeded with cryopreserved allogenic neonatal human foreskin fibroblasts
DERMO-EPIDERMAL	PermaDerm	Collagen-glycosamino-glycan substrates containing autologous fibroblasts and keratinocytes
	DenovoSkin	Plastically compressed collagen tipel hydrogels engineered with human keratinocytes and fibroblasts

These models shown success in clinical trials and are used in the clinic. However, they are still fraught of limitations. Sometimes patients have to undergo multiples surgical interventions because of the impossibility to transplant full-thickness construct owing the difficulty of diffusion of nutrients in thick tissues before host vessels invasion and vascularization. Moreover some of these models are very fragile, deformable, not able to withstand shear forces *in vivo* and hardly handled by surgeons [95].

- **Skin models for *in vitro* applications**

Besides the use of skin models as *in vivo* grafts, as, recently, other applications have emerged for skin substitutes as *in vitro* test systems. In this context, they enable not only the investigation of fundamental processes in the skin, but also the hazard assessment of various chemical compounds that are topically applied on the skin without the need to use animal models which can present significant differences with humans and whose use has been limited by ethical guidelines [100]. For several years, two dimensional (2D) *in vitro* monolayer cultures of human cells were use but these platforms are low relevance due to the lack of complex cell–cell and cell–ECM interactions [101]. To date, many types of skin substitutes, with or without a dermal component, have been developed and commercially available by different groups. Some of these were already developed in the early 1990's including the EpiSkin™ model (L'Oréal, Lyon, France) and EpiDerm™ model (MatTek Corporation, MA, USA). Subsequently, additional human skin models were introduced to the commercial market, including the RHE or Reconstructed Human Epidermis (SkinEthic, Lyon, France), the EST1000® skin model (CellSystems, Troisdorf, Germany), the Phenion® Full-Thickness Skin Model and OS-REp (Open Source Reconstructed Epidermis) model (Henkel, Düsseldorf, Germany), the Straticell model (Straticell, Les Isnes, Belgium), the

StrataTest® model (Stratatech, Madison, WI, USA) and the more recently introduced Labcyte model (Gamagori, Japan) and Vitrolife-Skin™ model (Kyoto, Japan) [102]. Mainly models are described in Table 2.

Table 2 Commercially available *in vitro* epidermal and full-thickness skin substitutes. Adapted from [94]

	Brand name/manufacturer	Scaffold	Cell source
EPIDERMAL	Episkin™/L'Oreal Nice, France	Collagen	Keratinocytes (mammary/abdominal samples obtained from healthy consenting donors during plastic surgery)
	Skinethic™ RHE/L'Oreal Nice, France	Polycarbonate membrane	Keratinocytes (neonatal foreskin tissue or adult breast tissue)
	Epiderm™/MatTek Corporation, Ashland MA, USA	Collagen-coated, polycarbonate membrane	Human keratinocytes (neonatal foreskin, adult breast skin)
	EST-1000/CellSystems, Troisdorf, Germany	Polycarbonate membrane	Keratinocytes (neonatal foreskin)
DERMO-EPIDERMAL	EpiDermFT™/MatTek Corporation, Ashland MA, USA	Collagen	Human keratinocytes (neonatal foreskin, adult breast skin), human fibroblasts (neonatal skin, adult skin)
	AST-2000/CellSystems, Troisdorf, Germany	Collagen	Human keratinocytes Human fibroblasts
	Phenion® FT Model/Henkel AG&Co.KGaA Duesseldorf, Germany	Bovine, cross linked, lyophilized collagen	Primary human keratinocytes (neonatal foreskin), human fibroblasts (neonatal foreskin)
	StrataTest®/Stratatech Corporation Madison WI, USA	Collagen I	Immortalized, human NIKS® keratinocytes dermal fibroblasts

- **Vascularized skin equivalent models**

Several studies show that endothelial cells within a 3D matrix, in presence of fibroblasts, are able to sprout and develop a capillary network. After graft, capillaries of pre-vascularized constructs are able to anastomose with host vessels at the site of implant [1]. Anastomosis of the pre-vascularized constructs requires about 4 days while the *de novo* vascularization of not vascularized skin/dermis substitutes occurs in approximately 2 weeks (Fig.4) [103]. Thus, ensuring adequate

oxygen and nutrients supply to all the cells of the construct in a relatively short time. This is very important in case of full thickness skin graft and it allow to solve some important limits of classical skin substitutes.

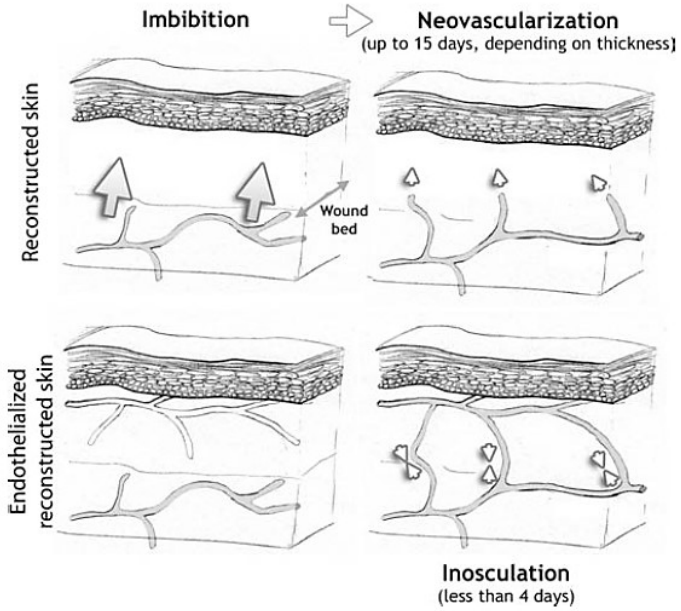

Fig. 4 Different times of neovascularization and inosculation. Neovascularization requires the migration of new blood vessels originating from the wound bed by angiogenesis and it is a slow process, which depends on the graft thickness. Inosculation is the connection of the blood vessel-like network of the graft with the host's vasculature. It is a rapid process (less than 4 days) and should be independent of the graft thickness.

The first vascularized skin-equivalent model *in vitro* is to Auger et al in 1998. The tissue was obtained through a co-culture of three types of human cells: fibroblasts, endothelial and epithelial cells within chitosan / collagen scaffolds. In the skin-equivalent model endothelial cells are capable of spontaneously forming, after 31 days, capillary structures in a highly differentiated extracellular matrix showing positivity for von Willebrand factor, the bodies of Weibel-Palade, the Laminin and Collagen IV, typical of the microcirculation *in vivo* vessels [10]. Endothelial cells were Human Umbilical Vein Endothelial Cells (HUVECs). Another work show that HUVECs can also grow and differentiate within artificial dermis obtained by

seeding fibroblasts on scaffold of hyaluronic acid and the best ratio for the co-culture, in terms of viability and metabolic activity, is of 1: 1 [18].

Besides HUVECs, several works demonstrated the ability of primary human dermal microvascular endothelial cells (HDMECs) to form capillary like structures both in presence or in absence of fibroblasts [104]. Pouliot et al developed a vascularized skin substitute the self-assembly method. They seeded HDMECs on fibroblasts sheets obtained culturing fibroblasts with ascorbic acid for 3 weeks in order to produce collagen. Endothelialized fibroblasts sheets were overlapped and cultured for 1 week as vascularized dermis on which Keratinocytes were seeded for the development of the vascularized skin model (Fig.5).

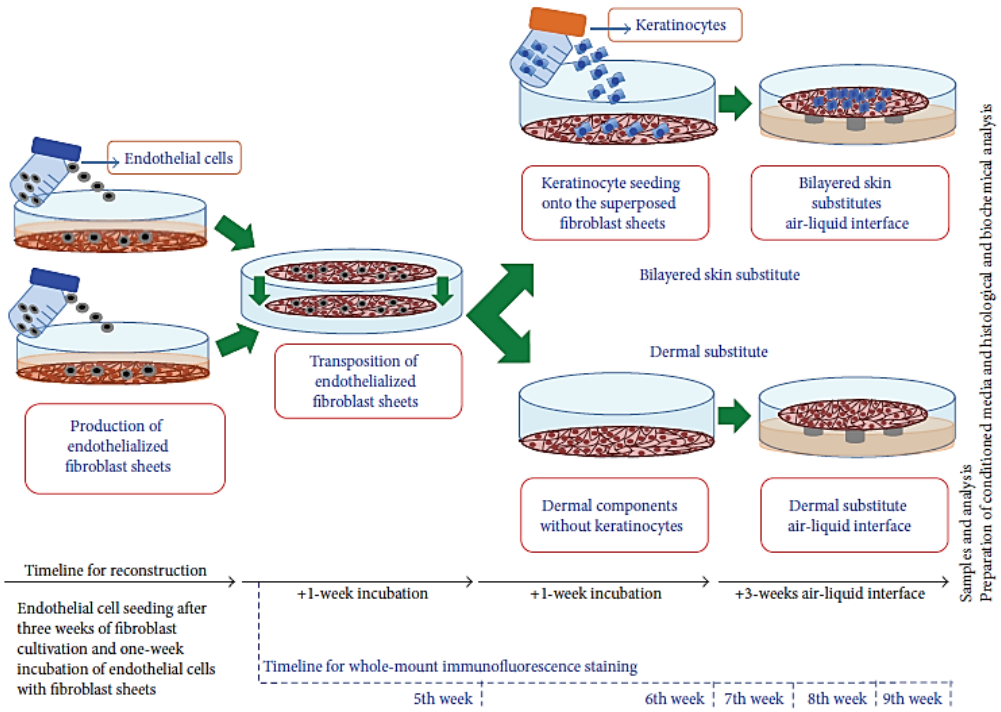

Fig. 5 Self-assembly method and experimental timelines [105].

They showed that the epidermal component of the substitutes can promote network expansion and density in the right culture condition [105].

Recent studies show that HDMECs can develop both blood and lymphatic vessels *in vitro*. Reichmann et al used a co-culture of endothelial cells and fibroblasts in hydrogel of pressed collagen I or fibrin. They cultured HDMECs from foreskin biopsies which include a mixed population of endothelial cells of both blood and lymph. After 3 weeks of 3D *in vitro* co-culture HDMECs organize themselves into blood and lymphatic capillaries structures as demonstrated by the positivity for CD31 marker (pan-endothelial) and Prox-1/Lyve-1 and podoplanin (lymphatic marker). Lymphatic vessels, unlike blood ones, possessed incomplete or absent basement membrane and lack of mural cells. Interestingly, the blood vessels and the lymphatic never anastomosed between them *in vitro* (Fig.6).

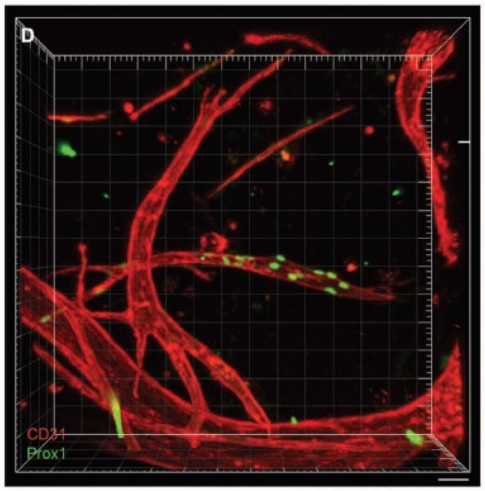

Fig. 6 CD31 in red shows all the endothelial cells. Prox1 in green mark the nuclei of lymphatic cells. Blood and lymph vessels don't anastomose between them *in vitro*. Scale bar 50µm [4].

Keratinocytes were seeded on the surface of this vascularized dermis model after 2 weeks of HDMECs and fibroblasts co-culture. After another week, the complete model was transplanted on the back of nu / nu immunosuppressed rats. 2 weeks after implantation the tissue was surgically removed and subjected to analysis which showed the successful anastomosis between the lymphatic vessels of the construct with the host ones as well as for blood vessels. In addition, the functionality of lymphatic vessels was evaluated by Evans Blue dye injection. The study showed that the hydrogel containing only the fibroblasts (negative control) restrained a five times higher amount of dye than the sample with lymphatic capillary network indicating the effective drainage function [4].

Besides the development of vascularized skin models for *in vivo* applications, several works underline the importance of vascularized models for drug screening.

In fact these complex models can be used for the study of molecules or active principles such as anti-inflammatory, pro/anti- angiogenic acting via topical or systemic administration [1]. Some works suggest innovative techniques for *in vitro* blood vessels perfusion which could be recapitulated for the development of perfusable vascularized skin models.

Okano et al overlaid triple layer of cardiac cell sheets, co-cultured with endothelial cells, on a resected tissue with a connectable artery and vein as vascular bed. The construct was supported by media perfused in a bioreactor. They showed that endothelial cells were able to connect to capillaries in the vascular bed and form tubular lumens, creating *in vitro* perfusable blood vessels in the cardiac cell sheets. Thicker engineered tissues can be produced *in vitro* by overlaying additional triple layer cell sheets (Fig.7) [106].

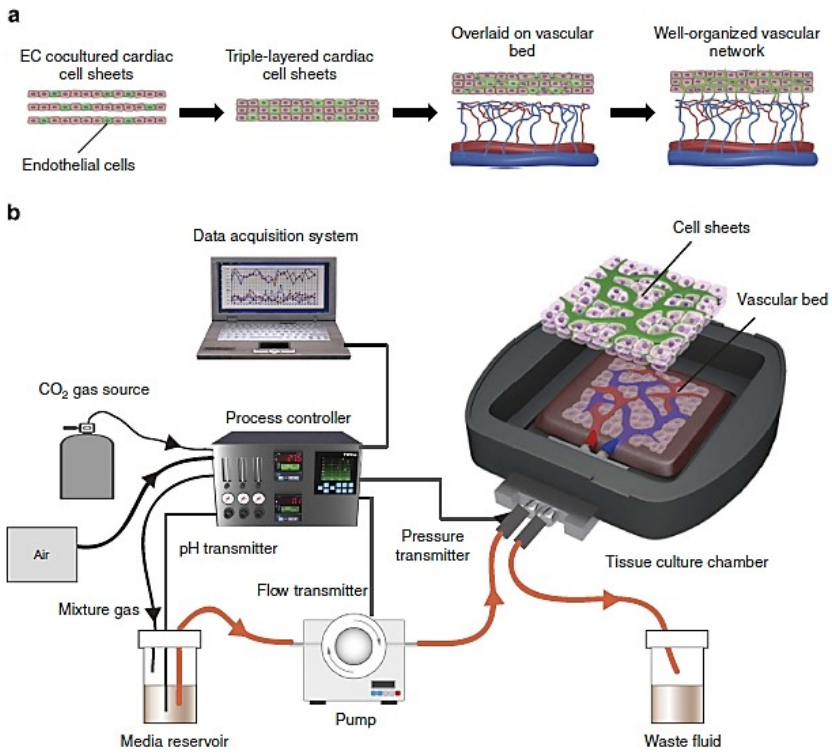

Fig. 7 *In vitro* engineering of functional 3-D tissue with perfusable blood vessels [22].

George et al combined tissue engineering and microfluidic technology to create an *in vitro* 3D metabolically active containing a perfused, living, dynamic, interconnected human capillary network. The platform is constructed using standard photolithography from polydimethylsiloxane siloxane (PDMS) and consists of two outer microfluidic channels that act as arteriole (high pressure) and venule (low pressure), connected by three tissue chambers, into which is injected a slurry of fibrin, fibroblasts and endothelial cells. Over the course of 5–7 days endothelial cells self-assemble into an interconnected network that anastomoses with the outer channels [77]. Endothelial cells were able to migrate into the outer channels, forming a tight seal, and over time, line the surface of the channel. At this point flow through the device switched from interstitial to intraluminal [76] (Fig.8).

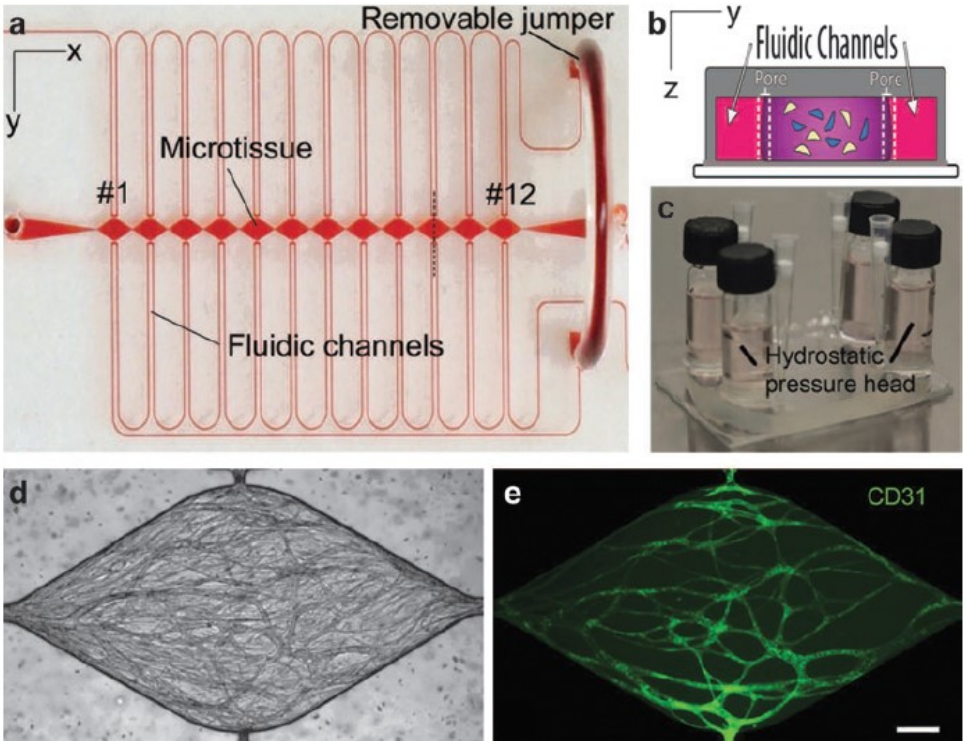

Fig. 8 Microfluidic platform for the development of a perfused capillary network. Endothelial cells are seeded within a fibroblast rich fibrin matrix into chambers connected to fluidic channels by pores. Endothelial cells (marked in green by CD31) are able to anastomose with l channels [77]**.**

Chapter 3

Heterogeneous invasive tumor mammary model featured by vascular and desmoplastic reaction

3 Abstract

Breast cancer is one of the most common cancers and the most frequent cause of mortality in patients is metastasis. Today researchers are still looking for new strategies of treatment. Difficulties arise from lack of an effective model able to recapitulate tumor heterogeneity and microenvironment. This is a complex milieu in which cancer cells and non-cancer cells are in mutual interaction into an activated stroma. The increase in pro-angiogenic signals by tumor cells induces the formation of a discontinuous and intricate vascular network with mosaic wall and variation in vessel diameter. Capillary density correlates positively with tumor malignancy. The activation of stromal cells by cancer cells induces the desmoplastic reaction with the increase in dense and aligned collagen and other molecules of the connective tissue such as hyaluronic acid. The entity of the desmoplastic reaction correlates positively with tumor invasiveness. Cancer cells during metastasis move across the ECM toward blood and lymphatic vessels adopting different shapes in order to stay always motile. Here we show a new breast cancer model able to recapitulate these critical features of tumor microenvironment and metastasis. We develop MCF7-μTPs in which pro-angiogenic signals lead the increase in capillary-like structures (CLS) volume fraction, n° of junctions/μm^3 and vessel diameter which wall is a mosaic of tumor and endothelial cells. The desmoplastic reaction occurs in the model with increase in collagen fraction, assembly and correlation and decrease in entropy. The model reiterates also the different morphologies of tumor cluster migration into the ECM recapitulating tumor heterogeneity in space and time. We speculate that MCF7-μTPs are suitable composite models for the study of tumor progression into an activated microenvironment and for drug screening assays.

3.1 Introduction

Breast cancer is one of the most common cancer in woman [25]. The most frequent breast cancer is the invasive ductal carcinoma (IDC) which starts in the epithelial cells lining the ducts of the mammary gland and invade the breast tissue moving toward blood or lymphatic vessels [26]. Metastasis is a hallmark of breast cancer leading cause of mortality among patients [49].

Despite significant improvements in cancer field, researchers are still working to find new and effective therapies against tumor. Part of the issue is the lack of suitable preclinical models able to recapitulate the complexity of cancer disease [29]. It is not only a pathology interesting neoplastic cells but the entire environment in which they are and move and with which they active interact by direct and indirect signals [31] .Tumor microenvironment is a complex milieu comprising cancer and non-cancer cells embedded into the ECM [32]. Cancer cells are mainly epithelial cells, while non-cancer cells are inflammatory/immune cells, vascular cells and stromal cells (e.g. fibroblasts). The interstitial matrix of the ECM consists of fibrillary collagens, proteoglycans and glycoproteins [33]. All these elements of the microenvironments are influenced by cancer cells and in turn influence tumor genesis and progression [35] [46]. So, in order to understand tumor growth and to develop new therapies it needs to consider all the components of tumor environment [31].

In particular, model of invasive breast cancer must take into account the fundamental role of tumor angiogenesis [36] and of the desmoplastic stromal reaction [46] which are key elements for metastatic events.

It was demonstrated that without blood vessels, tumors cannot grow beyond a critical size (1-2mm in diameter) or metastasize to other organs [36]. In this case tumors enter a dormant though viable state until they are able to secrete angiogenic factors and downregulate angiogenic suppressors [37]. Cancers recruit new blood

vessels by vasculogenesis and angiogenesis, by activating the so called ‘angiogenic switch’ that impairs the balance between pro and anti-angiogenic factors in favor of the pro-angiogenic ones [34]. The overall vascular density in tumors is increased but, nevertheless blood vessels are abundant in certain regions of the tissue, there are also some zones of ischemia and necrosis [39]. The vascular architecture has abnormal features such as thin walls, tortuous shape, absence of pericytes and variation in diameter. Numerous gaps or fenestrae are found between endothelial cells and the vessel wall is like a mosaic consisting of both endothelial and tumor cells [40] The desmoplastic reaction is characterized by amplified collagen deposition and stromal cells recruitment and activation (e.g. fibroblasts, macrophages) [45]. It consists in the increase in dense and fibrotic connective tissue rich in collagen and other ECM molecules such as hyaluronic acid, surrounding the tumor mass. The role of the desmoplastic reaction is object of interesting studies and it has been proposed as phenomenon induced by cancer cells to assist their propagation [48]. In fact it was demonstrated that the presence of a dense and aligned collagen enhances mammary tumor invasion and metastasis [45] [46]. The first step of tumor metastasis is the migration into the interstitial matrix toward blood or lymphatic vessels. Cells can move as single cells or in cluster (collective migration). They possess a unique ability to adapt to different environmental conditions, assuming different morphologies and migration characteristics in order to stay motile. In human cancer pathology studies, cancer cells from epithelial tumors primarily invade collectively. In intravital imaging studies, cancer cells display a wide range of different migration modes which are determined by both intrinsic factors and the microenvironment [49]. Friedl and Alexander talk about cancer cell invasion like a heterogeneous and adaptive process in which “plasticity” in cell adhesion, cytoskeletal dynamics, and mechanotransduction perpetuate migration and dissemination under diverse structural, molecular, and even adverse microenvironmental conditions, thus

inducing tumor cells resistance [51]. After interstitial invasion, tumor cells cross the discontinuous endothelial wall and enter the bloodstream. Here they circulate as single cells or clusters [56] [57] toward secondary sites of metastasis [53]. All of these analyzed elements, namely tumor angiogenesis, tumor desmoplastic reaction, tumor migration and invasion, could be target of cancer therapies because annoying each of them, the entire equilibrium leading tumor progression and metastasis could be altered.

Because *in vivo* animal model often fail to represent the pathology of human tumors, several *in vitro* models have been developed [32]. Whereas 2D cell cultures are not able to replicate the *in vivo* phenotype, which is strongly influenced by the microenvironment, there have been promising published works on 3D cell culture models [29] [62]. Bissels and Nelson have been one of the pioneers to use 3D to model the murine gland in both its normal and diseased state [63]. *In vitro* 3D breast cancer model include cells cultured as multicellular aggregates (spheroids) and cells embedded into natural (such as Matrigel, Fibrin or Collagen) or synthetic matrices (such as PLG, PLA, PEG) generally cultured in multiwell or into microfluidic devices [29]. Although these models have been used for the study of breast cancer and development of drugs, none of them recapitulates the actual environment in which cancer cells are found *in vivo*. In fact spheroids are characterized by shortage of collagen [65] and natural or synthetic matrices do not represent the complexity of the microenvironment typically associated with advanced carcinoma *in vivo*. Another recent culture system involve cell seeding on fibroblasts 3D matrices but these are commonly murine [79] [80] [81]. This could be a limit for the study of desmoplastic events which seems to be nearly an exclusively human occurrence, being quite rare among spontaneous and transplantable animal tumors and absent in most human tumoral xenografts in athymic nude mice [47].

In vitro models have the potential to explore mechanistically the individual contributions of various components of the microenvironment on tumor cell behavior, and the ability to modulate the biophysical and biomechanical aspects but they cannot recapitulate every aspect of the tumor microenvironment. For example, while a 3D culture of tumor cells in a collagen gel under interstitial flow might be used to explore direct effects of interstitial flow on tumor cell invasion it ignores other factors present at an invasive edge of the tumor such as the architecture and composition of the ECM (which is highly heterogeneous), the diversity of cell types present in the tumor stroma and their interaction [107].

Moreover, nevertheless cancer cell invasion is described as a heterogeneous and adaptive process [51], most of the 3D *in vitro* models fail to reproduce tumor complexity and plasticity, because they use homogeneous and passive scaffold [70] whose properties cannot be altered easily to interrogate the contributions of specific environmental cues to tumor assembly [71].

Here we present MCF7-µTP as new invasive breast cancer model featured by vascular and stromal reaction and able to recapitulate tumor cells plasticity and heterogeneity into an active microenvironment. MCF7 seeded on mammary HDFs-µTPs are able to induce the increase of the angiogenesis and the activation of the desmoplastic stromal reaction. Cluster of tumor cells take different morphologies of migration into the stroma recapitulating the heterogeneous shapes of collective interstitial invasion. The model replay the phenomenon of mosaic vessel formation by metastatic and endothelial cells which could be a preliminary state of tumor cluster shed into the circulation for aggressive metastasis [60].

Moreover, in several works MCF7 have been described as a tumor cell line without pro angiogenic potential and low invasive [72] [108] [109], while being a breast cancer cell line from pleural effusion. Interestingly, here we show that MCF7 into a human mammary fibroblast assembled collagen, are able to show pro angiogenic

and invasive features, underlining the fundamental role of the right *in vitro* microenvironment in the determination of cell phenotype [67].

Because MCF7-µTPs are representative of crucial events featuring tumor progression *in vivo* and they are easy to produce and in large quantity, we speculate that they depict a suitable model for drug screening.

3.2 Materials and Methods

3.2.1 Cell culture

Human dermal fibroblasts (HDFs) were extracted from healthy breast biopsies (protocol described in Chapter 5) and cultured in enriched MEM: MEM (Microtech L0440-500) with 20% of FBS (Sigma Aldrich F7524), 2% of Non-Essential Aminoacids (EuroClone ECB3054D), 1% of L-Glutamine (Lonza 17-605E) and 1% of penicillin/streptomycin (Microtech L0022-100), until passage 4/7.
HUVECs (GIBCO C0035C) were cultured in enriched M200: M200 (GIBCO Invitrogen Cell Culture M-200-500) supplemented with LSGS Kit (GIBCO Invitrogen Cell Culture S-003-K) until passage 3.
Human breast adenocarcinoma cells (MCF7) were kindly donated by Daidone's group (IRCCS, Istituto Nazionale dei Tumori, Milano, Italy) and cultured in enriched RPMI: RPMI-1640 (Microtech) medium supplemented with 10% FBS, 1% L-glutamine, 1% penicillin / streptomycin. MCF7 cells were transfected with pLVX-ZsGreen1-N1 (λex 493nm, λem 505 nm) viral vector purchased from Clontech, USA.
Human non-tumorigenic epithelial cell lines MCF10 (ATCC CRL-10317) were cultured in enriched MEBM: MEGM BulletKit (Lonza CC-3151 & CC-4136).
Cells were maintained at 37 °C in humidified atmosphere containing 5% CO2.

3.2.2 Micro-scaffold production

Gelatin porous microbeads (GPMs) were prepared according to a modified double emulsion protocol (O/W/O) [110]. GPMs were stabilized by crosslink reaction with glyceraldehyde (GAL) (SIGMA-G5001), in order to make them stable in aqueous environment at 37 °C, as previously described [94]. GAL at 4% w/w of the microbeads was used to perform all the experiments.

3.2.3 Micro-tissues production

All cells were cultured into spinner flask bioreactor (Integra) in continuous agitation (30 rpm) after 6 hours of intermitting stirring regime in order to promote cell seeding (30 min at 0 rpm, 5 min at 30 rpm).
Firstly $3,5*10^6$ HDFs P5/8 were seeded on 64mg of porous gelatin microspheres in order to have about 11 cells for bead. The culture medium was enriched MEM plus Ascorbic Acid (2-O-α-D-Glucopyranosiyl-L-Ascorbic-Acid TCI; Cf: 0.5mM). After 7-9 days $1*10^6$ HUVECs were seeded on HDFs micro-tissues (HDFs μTPs). Specifically, about 500 cells were seeded for μTP into spinner flask in agitation and cultured in a medium composed by 1/3 of enriched M200 and 2/3 of enriched MEM plus Ascorbic Acid, in order to obtain vascularized HDFs μTPs. After 7-9 days of culture μTPs were splitted from 1 to 3 spinner flasks and $7*10^6$ MCF10 and MCF7 were seeded separately into 2 bioreactors to produce MCF10-μTPs and MCF7-μTPs. About 30.000 epithelial cells (MCF10 or MCF7) were seeded for μTP. The media used for the tri-culture were: 1/3 of enriched MEM + 1/3 of enriched M200 + 1/3 of enriched MEBM plus Ascorbic Acid for MCF10-μTPs and 1/3 of enriched MEM + 1/3 of enriched M200 + 1/3 of enriched RPMI plus Ascorbic Acid for MCF7-μTPs. The third spinner flask without epithelial cells was used as control (CTRL) and cultured in a medium with 1/3 of enriched M200 and 2/3 of enriched MEM plus Ascorbic Acid. Cells were cultured for 10 days into spinner flask in agitation. Samples were harvested 6 hours, 3 and 10 days after the seeding of MCF10 and MCF7.

3.2.4 Histological analysis

Samples were fixed in Formalin 10% (HT501320 Sigma) for 1h at Room Temperature (RT) and washed in PBS1X (P4417-100TAB Sigma). They were dehydrated in Ethanol from 75% to 100% and treated with Xylene (A9982

ROMIL) before the inclusion in Paraffin. Tissue slices thick 7µm were cut using a microtome (Thermo Scientific HM 355S) and then deparaffinized using xylene. Sections were hydrated in ethanol from 100% to 75%, washed in water and stained using Masson's trichrome (HT15-1KT Sigma-Aldrich) in order to distinguish cell cytoplasm and muscle fibers in pink to red thanks to fucsin, collagen in blue thanks to anilin and nuclei in dark brown to black thanks to hematoxylin. The sections were mounted with Histomount Mounting Solution (Bio Mount HM 05-BMHM500 Bio-Optica) on coverslips and the morphological features of µTPs were observed with a light microscope (Olympus, BX53).

3.2.5 Immunofluorescence analysis

- **Immunofluorescence on the whole sample**

Sample were fixed in 4% Paraformaldehyde (P61148-500g Sigma Aldrich) for 30' at RT and washed in PBS1X. They were permeabilized using 0,1% Triton (Triton® X-100 T9284-100ML Sigma) in PBS1X for 5' at RT, washed in PBS1X and blocked in 3%BSA (A9418-100G Sigma), 3%FBS (F7524 Sigma), 0,01%Triton in PBS1X for 1h at RT. For the detection of the epithelial cells MCF10- µTPs were incubated in presence of the primary antibody against K14 (PRB-155P-100 Covance, Rabbit Polyclonal) diluted 1:300 in blocking solution. All the µTPs (CTRL, MCF10-µTPs and MCF7-µTPs) were stained with Rhodamine Ulex Europaeus Agglutinin I (UEAI Vector Laboratories RL-1062) at a final concentration of 20µg/ml in blocking solution in order to mark the *endothelium*. Samples were left in the solution with the antibodies overnight (ON) at 4°C in the dark. The morning after a Goat Anti-Rabbit IgG (H+L) Secondary Antibody Alexa Fluor 488 (A11008 diluted 1:500 in PBS1X), was used in order to mark K14 on MCF10- µTPs for 1h and half at RT. The nuclei of all the cells were stained with 4',6-diamidino-2-phenylindole (DAPI Sigma-Aldrich D9542) diluted 1:10.000 in

PBS1X for 20’ at RT. Samples were investigated by Confocal Leica TCS SP5 II. Images and z stack were analyzed using *Image J*.

- **Immunofluorescence on tissue sections**

Samples were fixed in Formalin 10% (HT501320 Sigma) for 1h at Room Temperature (RT) and washed in PBS1X (P4417-100TAB Sigma). They were dehydrated in Ethanol from 75% to 100% and treated with Xylene (A9982 ROMIL) before the inclusion in Paraffin. Tissue slices thick 7µm were cut using a microtome (Thermo Scientific HM 355S) and then deparaffinized using xylene. The sections were hydrated in ethanol from 100% to 75% and washed in water, Triton 0,2% and PBS1X. In order to release the epitopes from paraffin, heat mediated citrate buffer (pH=6, Thermo scientific TA-125-PM1X) unmasking was performed before the immunofluorence for keratin 14 (K14), whereas for K14 and hyaluronic acid an enzymatic unmasking was performed rinsing the slices in a solution with $CaCl_2$ (1.02378.0500 Merck) and Trypsin (215240 Difco^{TM} Trypsin 250) at a final concentration of 0,01% in PBS1X (pH 7.8) for 20’ at 37°C. Sections were washed in PBS1X and blocked using BSA6%, FBS 5%, $MgCl_2$ 20Mm and Tween20 0,02% in PBS1X for 2h at RT. Primary antibodies were diluted in blocking solution and they were: anti-Hyaluronic acid polyclonal antibody (dilution 1:50, Abcam ab53842) and anti-Keratin 14 polyclonal antibody (dilution 1:500, Covance PRB-155P). Sections were incubated with the primary antibodies ON at 4°C in a wet environment. The morning after samples were washed in PBS1X and the secondary antibodies 546 Donkey Anti-Sheep IgG H&L (dilution 1:500, Alexa Fluor® 546 A21098) and Goat Anti-Rabbit IgG (H+L) Secondary Antibody Alexa Fluor 488 (1:500, A11008) in PBS1X were added for 1h and half at RT. Nuclei were stained with DAPI and samples were investigated by Confocal Leica TCS SP5 II.

3.2.6 Quantitative MCF7 analysis

After immunofluorescence, whole samples and tissue sections were investigated by Confocal Leica TCS SP5 II performing at least 21 images in different random points of different µTPs. Samples were observed using λex = 488 nm/ λem=500/530 nm to detect Rhodamine and λex=700 nm (two photons)/ λem=400/450 nm to detect DAPI. Images were acquired with a resolution of 12 bit, 512x512 pixels by using a 25X water immersion objective (HCX IRAPO L 25.0X0.95 Water, n.a. 0.95). For each image (acquired unit) the number of MCF10/MCF7 was manually counted.

3.2.7 Quantitative Capillary-like structures (CLS) analysis

Whole samples were investigated by Confocal Leica TCS SP5 II performing 5 z-stacks in different random points of different µTPs. Samples were observed using λex = 543 nm/ λem=550/560 nm to detect Rhodamine and λex=700 nm (two photons)/ λem=400/450 nm to detect DAPI. The stacks were acquired with a resolution of 12 bit, 512x512 pixels by using a 25X water immersion objective (HCX IRAPO L 25.0X0.95 Water, n.a. 0.95). Each stack was composed by 16 sequential images with a z-slice-space of 1,98 µm.

- **CLS volume fraction**

The capillary like structures (CLS) volume fraction was calculated as percentage of the ratio between the thresholded red volume of the *endothelium* marked by Rhodamine-UEAI and the total volume of the sample acquired for each stack. The volume values were obtained applying the *ImageJ* plugin *Measure Stack* to the red thresholded channel and on the total µTP acquired volume.

$$\text{CLS Volume fraction} = \frac{\text{acquired CLS volume}}{\text{acquired sample volume}} * 100$$

- **Analysis of the junctions**

The number of junctions for each stack was calculated using the plugin *Skeletonize 3D* of *ImageJ*. Before the analysis, the red channel of the stacks was thresholded and smoothed in order to avoid the identification of false positive junctions by the plugin. The number of junctions for μm^3 was calculated as ratio between the number of junctions for stack and the total acquired volume obtained by *Measure Stack*.

$$\text{Junctions}/\mu m^3 = \frac{\text{n° of junctions for stack}}{\text{acquired sample volume}}$$

- **CLS diameter analysis**

The diameter of the capillary like structures was calculated tracing at least 3 adjacent lines joining the opposite major sides of capillaries using *ImageJ*. For each sample the diameter was calculated at least three times for each image of the z stack and then the mean and the standard deviation were represented in the graphic.

3.2.8 Second harmonic generation signal (SHG)

For SHG imaging samples were investigated by confocal microscopy (TCS SP5 II Leica) combined with a MPM where the NIR femtosecond laser beam was derived from a tunable compact mode-locked titanium: sapphire laser (Chamaleon Compact OPO-Vis, Coherent). Two-photon excited fluorescence was used to induce SHG and obtain high-resolution images of unstained collagen structures. The samples were observed by using λex = 840 nm (two photons) and λem=415-

425 nm. The SHG images were acquired with a resolution of 12 bit, 512x512 pixel by using a 25X water immersion objective (HCX IRAPO L 25.0X0.95 Water, n.a. 0.95).

3.2.9 Quantitative matrix analysis

- **Gray-level co-occurrence matrix analysis: Correlation and entropy**

To quantitatively assess the collagen-related changes, gray-level co-occurrence matrix (GLCM) texture analysis was performed using the *ImageJ* plugin *Texture* on SHG as previously described by Walker and collaborators [111]. The features correlation and entropy were evaluated. The correlation of the images reflects the similarity on a direction of the image texture area and it is the linear correlation measure of the local gray level in the image. This correlation is a measure of the dependence between two different pixel values. In particular, the correlation feature indicates a relation of intensity measure as a function of pixel distance, which is used to assess the similarity of matrix pixel horizontally and vertically. Entropy is the complexity feature of an image matrix and it mainly reflects the texture grayscale randomness distribution of the image. When the image has many fine textures the value of entropy is larger, and vice versa when the image has less number of fine textures the entropy value is smaller [112]. Here the correlation and entropy curves were calculated for distances ranging from 1 to 100 pixels in the horizontal and vertical direction of each optical section. In such spatial windows the distance at which the correlation functions fall off represents the correlation length of the texture. Correlation length was obtained by fitting data with an exponential low [113] [114].

- **Collagen amount quantification**

SHG images were analyzed using *ImageJ* software. Image from each z-stack were thresholded and for each one at least 3 ROIs of the same dimension were chosen in order to avoid the beads signal. The selected areas were analyzed by measuring the percentage of the ratio between the black pixels representative of the gray collagen signal respect to the total pixels. The % area was calculated by the software. The final value was calculated as mean of the % area of each ROI selected for sample and time.

- **Collagen assembly degree**

SHG images were analyzed by using *ImageJ* software. The degree of Collagen assembly degree (CAD) was evaluated by analyzing the Histogram of the SHG images in order to calculate the average intensity, as described by the equation:

$$CAD = \frac{\sum_{i=1}^{255} Iipi}{\sum_{i=1}^{255} pi}$$

Where I is the average intensity and Ii is the intensity corresponding to the pixel pi, which runs in the gray value interval from 1 to 255. The intensity I of collagen network is known to be proportional to the degree of assembly of the newly synthesized collagen.

- **Hyaluronic Acid quantification**

The fluorescent images were analyzed for semi-quantitative evaluation with *ImageJ*. After threshold, the RED area relative to hyaluronic acid was divided by the total number of cells obtained by analyzing the blue channel of DAPI with *Analyze particle*.

- **Collagen fibers and tumor clusters orientation**

Collagen fibers orientations were calculated by using the plugin *OrientationJ* of *ImageJ*. The plugin evaluates the local orientation and isotropic properties (coherency and energy) of every pixel of the image [115]. We specified the following parameters: Gaussian window σ 1 pixel, Min Coherency 20%, Min Energy 2%. The plugin outputs a hue-saturation-brightness (HSB) color-coded map which shows the angles of the oriented structures in the image, i.e. turquoise corresponds to 0° and red corresponds to ±90° [115]. The plugin also outputs a distribution of the fibers alignment directions. These distributions were normalized in order to obtain a normal distribution and compare fibers alignment in different point of the same sample.
Tumor orientation in degree was calculated by using *Orientationj Measure* on selected ROI around each cluster.

3.2.10 Statistics

Experiments were performed in triplicate. Data are expressed as mean ± SD. Differences between groups were determined using the statistic test ANOVA Tukey HSD test. Significance between groups was established for p value<0.01 or p value<0,05.

3.3 Results

3.3.1 Development of vascularized tumor µTPs

In this work, metastatic breast cancer cells (MCF7) and breast epithelial non-tumorigenic cells (MCF10) were seeded on vascularized HDFs-µTPs in order to obtain MCF7-µTPs and MCF10-µTPs.

Vascularized HDFs-µTPs were obtained seeding endothelial cells on HDFs-µTPs. HUVECs were able to seed and spread into HDFs-µTPs forming capillary-like structures (CLS) into the collagen rich matrix produced by mammary fibroblasts. CLS were growing up to 28 days after seeding without morphological signs of regression (Fig.1). Vascularized HDFs-µTPs were used as control (CTRL) in this work.

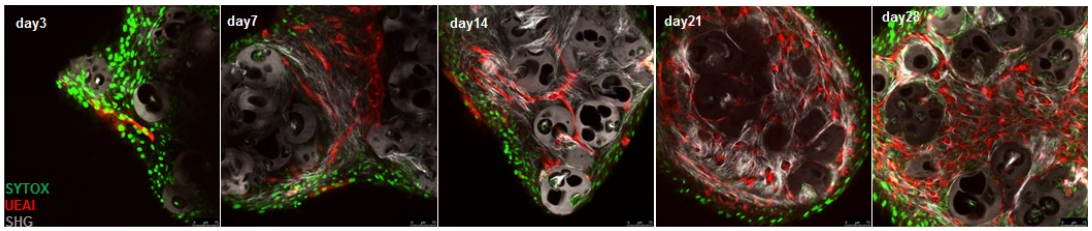

Fig. 1 Vascularized HDF-µTPs: In green the nuclei of all the cells marked by Sytox green; in red the HUVECs marked by UEAI and in gray the second harmonic generation signal of collagen. The endothelia cells start to spread from day 3 after seeding and form CLSs growing up until 28 days after seeding without morphological signs of regression. Dimensional bar: 75µm.

MCF7 and MCF10 arranged themselves differently once seeded on vascularized HDFs-µTPs. MCF10 adhered on the surface of the samples and then entered the matrix and localized around the perimeter of the beads. After 10 days, they polarized forming acinar structures as typical of exocrine glands like the mammary one.

MCF7 adhered on the surface of the sample and penetrated the matrix as well as MCF10 but they assumed heterogeneous morphologies in clusters. The number of cells for acquired unit was significantly increasing from the start to the end of the culture period for both MCF10 and MCF7. Nevertheless, the number of MCF7 was always greater than MCF10 excluding the time 6 hours that was the initial condition in which cells were seeded in equal number. From the image analysis of the number of cells for acquired unit, it is possible deduce that the proliferation rate of MCF7 was faster than MCF0 as expected by tumoral vs non-tumoral cells (Fig.2).

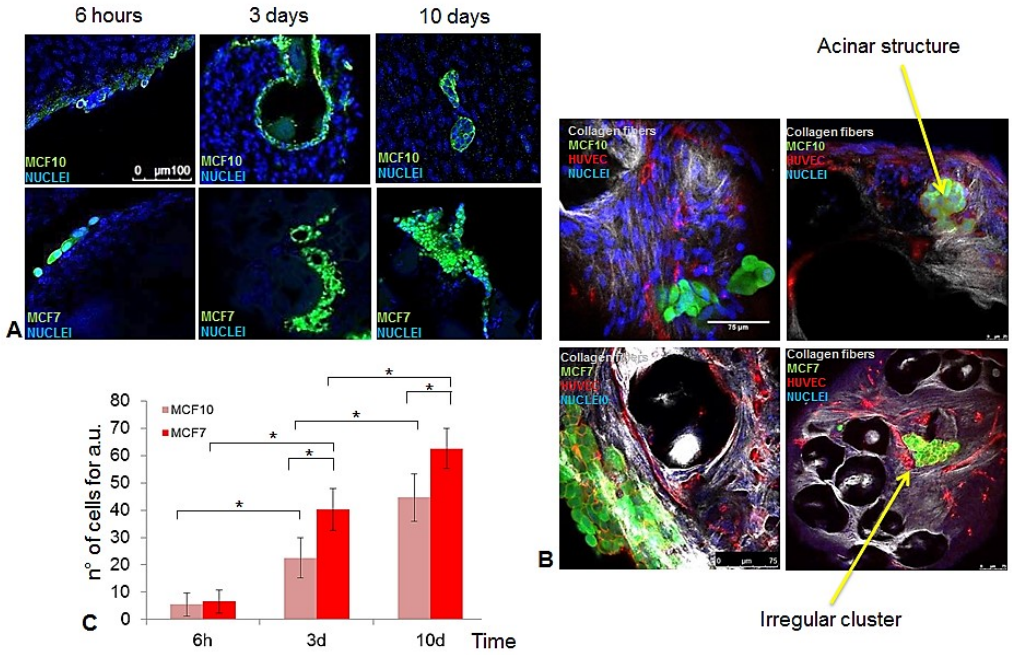

Fig. 2: Non-tumoral vs tumoral cells organization and proliferation: A+B) MCF10 are marked in green by indirect immunofluorescence for K14. The MCF7 are ZsGreen1+. The nuclei of all the cells are marked in blue by DAPI. Scale bar 100 µm; B) the HUVECs are marked in red by UEAI. MCF10 preferentially localize around the surface of the sample, around the beads and forming acinar structure. MCF7 form irregular cluster on the surface of the sample and into the matrix. Scale bar in B: 75 µm. C) Graphic of the number of cells per acquired unit. * p value< 0.05.

3.3.2 Tumor increases angiogenesis in the tissue model

- **CLS volume fraction and n° of junctions/µm^3**

The z-stacks analysis of acquired samples volumes demonstrated that tumor cells were able to secrete pro-angiogenic stimuli as indicated by the increase in CLS volume fraction and in the number of junctions/µm^3. The images and graphics show the CLS volume fraction and the number of junctions/µm^3 of MCF7-µTPs compared with MCF10-µTPs and vascularized HDFs-µTPs, used as control (CTRL). Both parameters were increasing for all three types of tissues from 3 to 10 days of culture but MCF7-µTPs values were always higher than the others, especially 10 days after seeding (Fig.3).

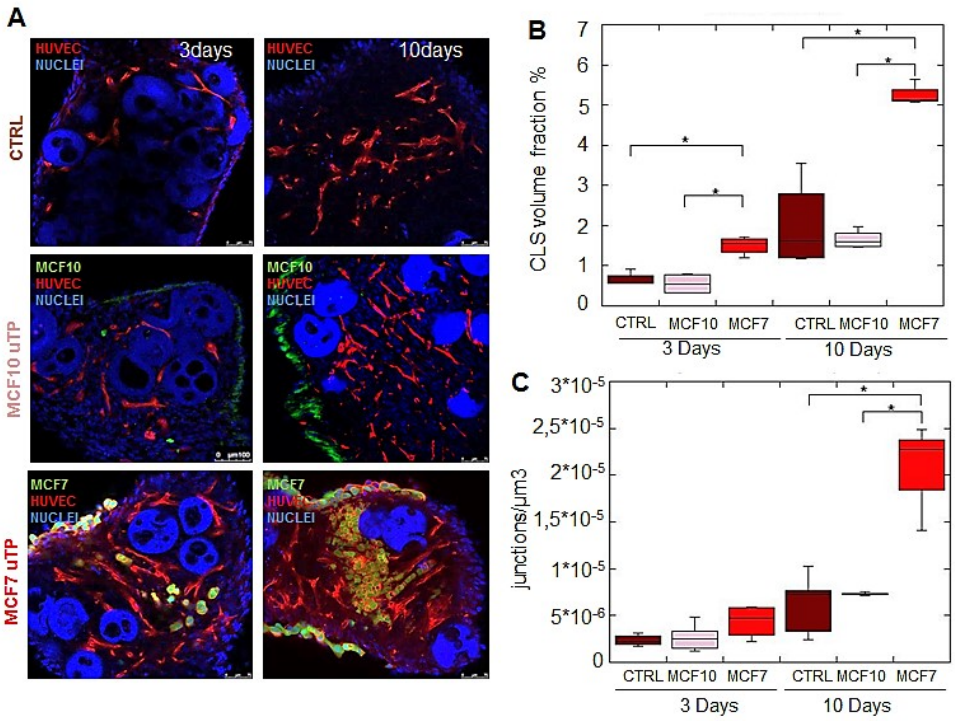

Fig. 3 Tumor increases CLS volume fraction and of the number of junctions/µm^3: A) in blue the nuclei of all the cells marked by DAPI, in red the HUVEC marked by UEAI, in green the MCF10/MCF7 marked by K14 and ZsGreen1 respectively. Scale bar 100µm; B+C) Graphics of the CLS volume fraction and of the number of junctions/µm^3. * p value< 0.05

- **CLS diameter**

The CLS average diameter was compared among CTRL, MCF10-µTPs and MCF7-µTPs. Data show that CLS average diameter was significantly higher for MCF7-µTPs both 3 and 10 days after seeding. From 3 to 10 days the average diameter dimension remained almost unchanged for all three types of tissues (Fig.4).

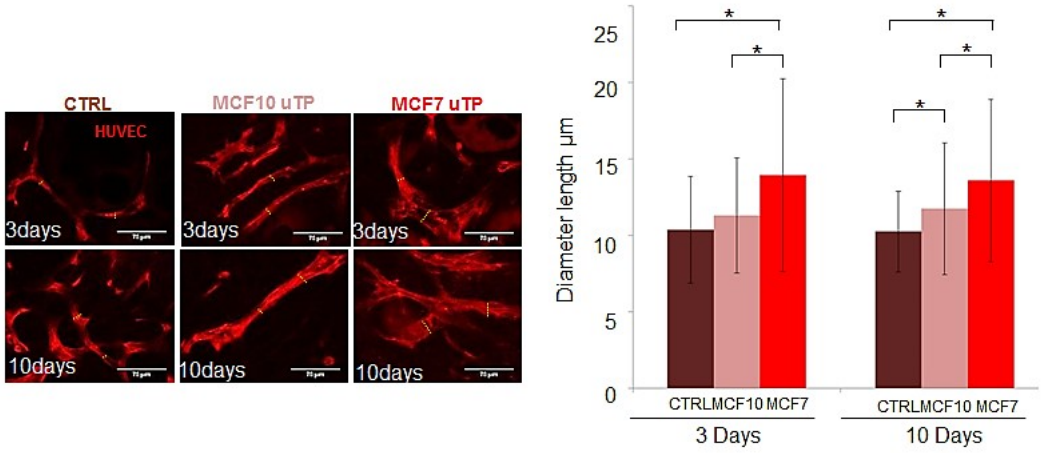

Fig. 4 Tumor increases capillaries diameters dimension: A) CLS marked in red by UEAI, the yellow lines connecting the two major sides of capillaries represents some of the length used for the image analysis. Scale bar 75 µm; B) Graphics of the diameter lengths. * p value< 0.05.

- **Close tumor vessels interactions**

We found a very fine interaction between tumor and capillary structures into MCF7-µTPs.

Frequently tumor clusters were localized as files of multiple or single cells parallel aligned to CLS. The morphology of tumor cells in single file remind that featuring cluster of circulating tumor cells in capillaries [58] but outside vessels (Fig.5 A/B)

3D views show a direct contact between MCF7 and HUVECs which together formed a tangled tumor mass surrounded and crossed by a discontinuous vascular network (Fig.5 C). In some cases, the interaction was so close to induce the

formation of mosaic vessels in which endothelial and tumor cells alternated in the capillary wall (Fig.5 D/E).

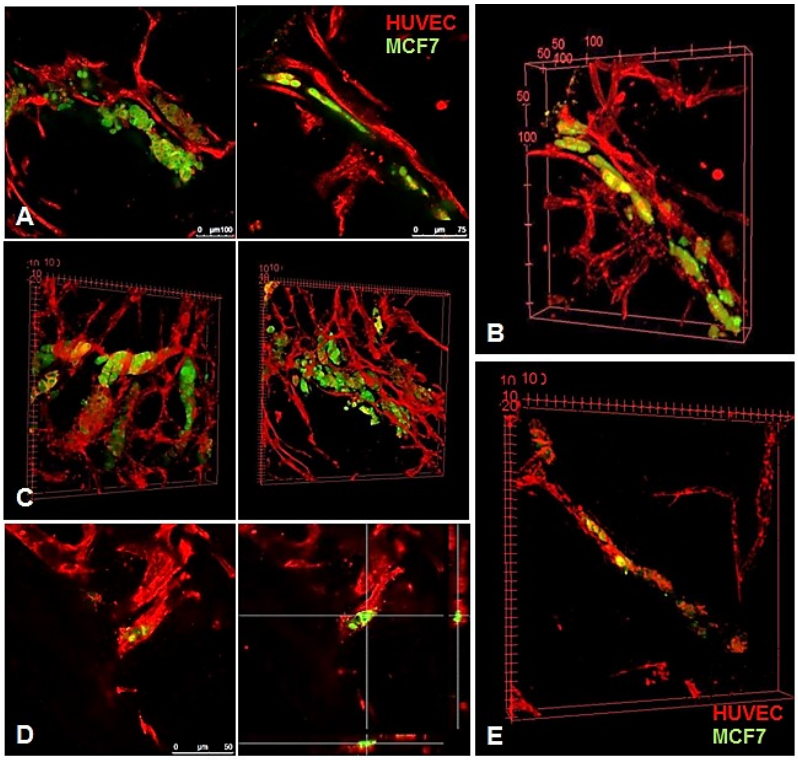

Fig. 5 Tumor cells guide and follow CLS: A/B/C/D/E) In red the HUVECs marked by UEAI, in green MCF7 ZsGreen1+. A/B) tumor clusters align parallel to CLS forming files of multiple or single cells. Scale bar on the left 100µm. Scale bar on the right 75µm; C) Tumor cells in close contact with the *endothelium*; D/E) Mosaic vessels. Scale bar 75µm.

3.3.3 Desmoplastic stromal reaction

- **Quantitative collagen analysis**

Thanks to multiphoton technology and second harmonic generation signal (SHG) we acquired collagen images from vascularized HDFs-µTPs (CTRL), MCF10-µTPs and MCF7-µTPs (Fig.6A).

Collagen fraction was increasing from 3 to 10 days after seeding and in particular, after 10 days, the tumor associated collagen fraction was significantly higher than

CTRL and MCF10-µTPs (Fig.6B). Also the collagen assembly degree was increasing from day 3 to day 10 for all three types of tissue but always higher in MCF7-µTPs (Fig.6C). The Gray-Level Co-Occurrence Matrix (GLCM) revealed that the normalized correlation curves of CTRL, MCF10-µTPs and MCF7-µTPs decreased almost together after 3 days. Otherwise, at day 10, the normalized correlation curve of tumor tissue decreased slower than the healthy and control and the correlation length was significantly higher (Fig.6 D/E/F). The curves of the collagen entropy show an inversion from day 3 to 10. In fact, after 3 days the curve of MCF7-µTPs was higher than MCF10-µTPs and CTRL. Whereas, after 10 days, the curve of MCF7-µTPs was lower than CTRL and MCF10-µTPs (Fig.6 G/H).

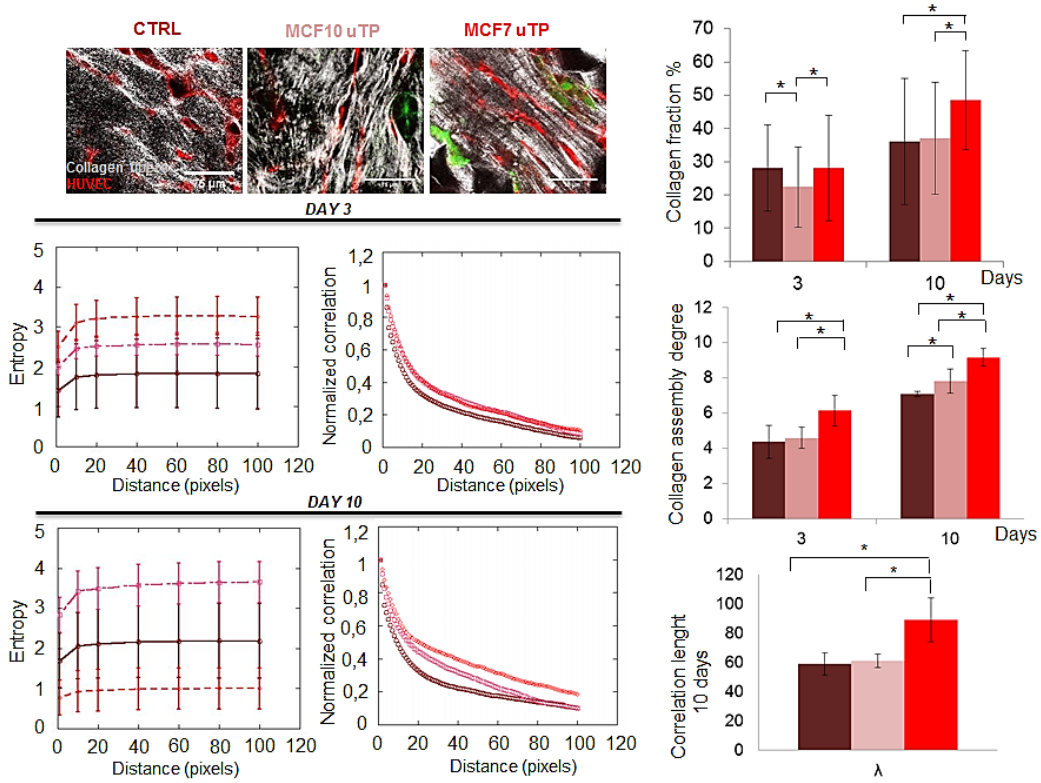

Fig. 6 The tumor associated extracellular matrix recapitulates events of the desmoplastic reaction: A) In gray the SHG collagen signal, in red the HUVECs marked by UEAI and in green the MCF10/MCF7 marked by K14 and ZsGreen1. Scale bar 75 µm; B) Graphic of the collagen fraction %; C) Graphic of the collagen assembly degree; D/E/F) GLCM analysis of collagen fibers correlation; G/H) GLCM analysis of collagen Entropy (Red MCF7-µTPs, Pink MCF10-µTPs, Brown CTRL). * p value< 0.05.

- **Quantitative Hyaluronic acid analysis**

The quantitative image analysis after indirect immunofluorescence revealed an increase in hyaluronic acid in tumor tissues compared to the control and healthy ones (Fig.7). This parameter is in accordance with the data about collagen confirming the activation of the stromal desmoplastic reaction after 10 days (Tab 1)

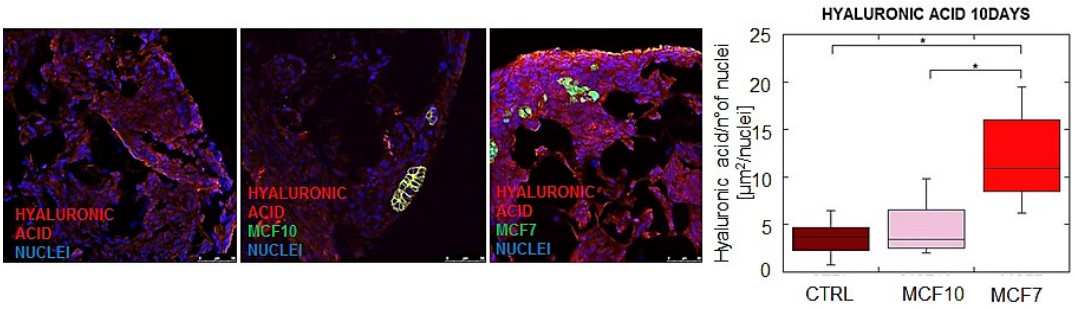

Fig. 7 Increase in hyaluronic acid in tumor: Indirect immunofluorence for Hyaluronic acid in red. The nuclei of all the cells are marked in blue by DAPI, the MCF10 are marked in green by K14 and the MCF7 in green by ZsGreen1. Scale bar 75µm. The graphic is representative of the quantitative image analysis for hyaluronic acid in CTRL, MCF10-µTPs and MCF7-µTPs. * p value< 0.05.

Table 1 Summary of the desmoplastic reaction in and MCF7-µTPs

Desmoplasic reaction of the tumor model after 10 days	
Collagen fraction%	Increase
Collagen assembly degree	Increase
Correlation lenght	Increase
Entropy	Decrease
Hyaluronic Acid	Increase

3.3.4 Spatiotemporal heterogeneity

MCF7 seeded on the surface of µTPs were able to penetrate the collagen matrix (Fig.8). After 3 days, tumor cells moved both as individual cells and clusters, whereas after 10 days they were only in the conformation of compact clusters (Fig.9).

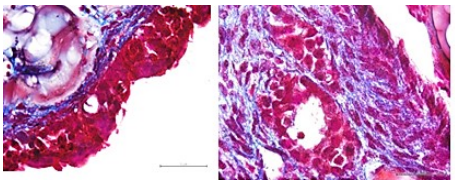

Fig. 8: MCF7 penetrate the collagen matrix: Masson's trichrome of MCF7 µTPs after 10 days. On the left MCF7 on the surface of the sample. On the right MCF7 clusters into the tissue matrix. Scale bar 50µm.

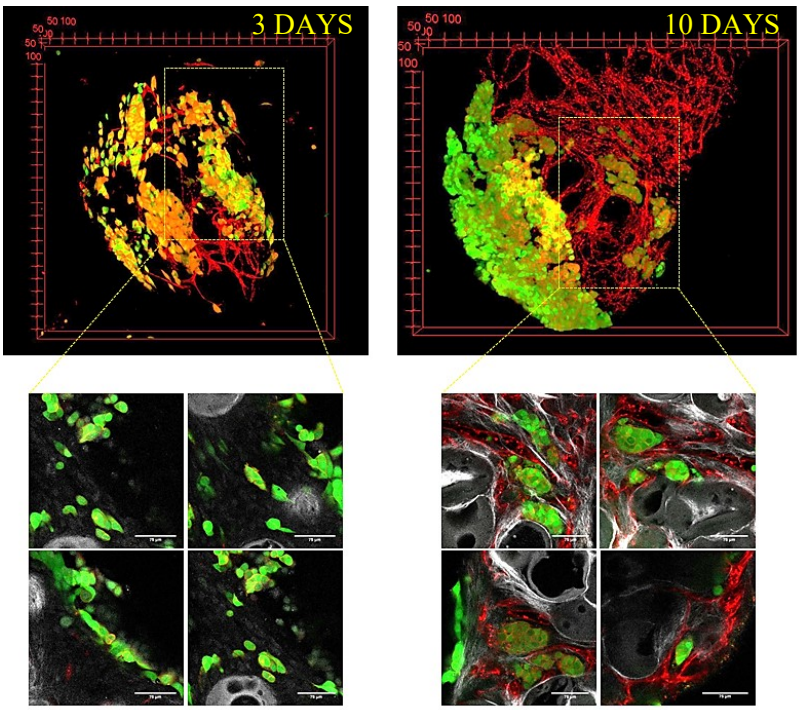

Fig. 9 MCF7 move as individual cells or clusters after 3 days and as compact clusters after 10 days: In green the MCF7 ZsGreen1+, in red the UEAI for endothelial cells detection and in gray the SHG signal of collagen. Up) 3D view of a tile scan and z stack on tumor tissue after 3 (on the left) and 10 (on the right) days. Down) images on tumor cells and cluster moving into the collagen matrix. Scale bar 75µm.

On the external surface of MCF7-µTPs, tumor cells grew by expansive growth without physical confinement on proliferation (Fig.10A on the left). Both 3 and 10 days after seeding, MCF7 clusters showed different morphologies. MCF7 invaded

the tissue in form of single files, multicellular strands with a blunt extremity (protrusive strand) or with leader cells on a tip (solid strand) and round clusters (Fig.10A), appointed on the basis of literature [51]. These movements are typical of metastatic cells invading the matrix toward blood and lymphatic vessels. Single files of cells were often parallel to capillaries and multicellular strand with leader cells on a tip seemed to point endothelial structures.

Tumor structures were simultaneously present in a single tissue and at different time points. Thus, demonstrating that MCF7-µTPs environment preserved spatiotemporal tumor heterogeneity. The number of cells for cluster was significantly increasing from 3 to 10 days, revealing that tumor cells in cluster were able to perpetuate their differences while proliferating (Fig.10B).

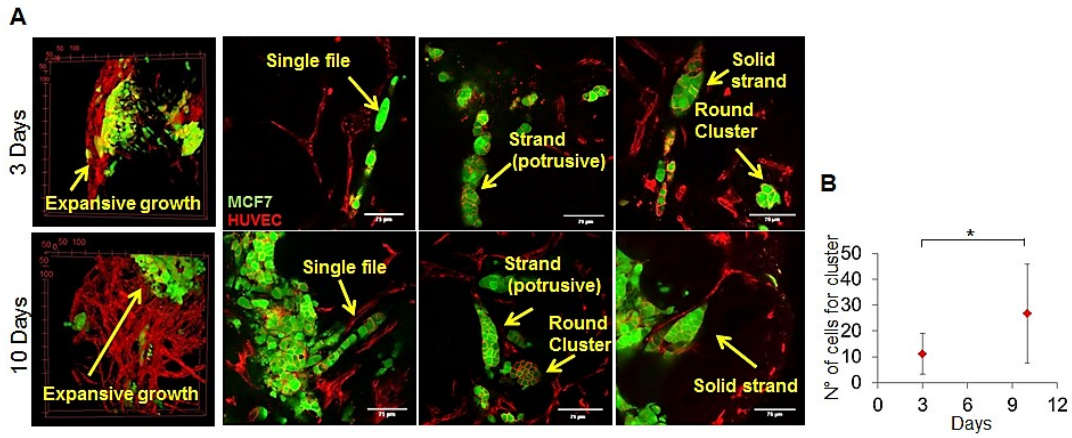

Fig. 10 MCF7-µTPs recapitulate tumor heterogeneity: A) In green the MCF7 ZsGreen1+ signal and in red the UEAI for endothelial cells. Arrows point to different tumor morphologies, named on the basis of the literature [51]. Scale bar: 75µm; B) Graphic of the number of cell for cluster (mean values ±SD). * p value< 0.05.

We supposed that the array of tumor morphologies in MCF7-µTPs could be linked to different environmental micro-heterogeneities. To this aim, we investigated collagen folding around tumor cluster. In the same tissue, despite the overall desmoplastic reaction, there were both random oriented collagen fibers, close to clusters with undefined form, and straightened collagen fibers stretched around

tumor cluster arranged in specific morphologies such as solid strand. These differences were visible after 10 day of culture when collagen was more mature (Fig.11A). Collagen images after 10 days were analyzed in order to obtain a distribution of collagen fibers orientations. In Fig.11B on the left it was indicated the color map of orientation of the plugin *OrientationJ*. The image on the top (Orange perimeter) didn't show a preferential collagen orientation whereas in the image on the bottom (Blue perimeter) most of the collagen fibers stained yellow-green and had a preferential orientation at -60°/-30°. On the right it is shown the graphic the normalized distribution of orientations. The orange curve is related to the image on the top (Orange perimeter) and the blue one to the image on the bottom (Blue perimeter). Tumor cluster surrounded by aligned collagen fibers had an orientation at about -50°/-30° (Fig.11C), within the range of preferential collagen orientation, indicating that the tumor masses were surrounded by collagen fibers aligned thereto.

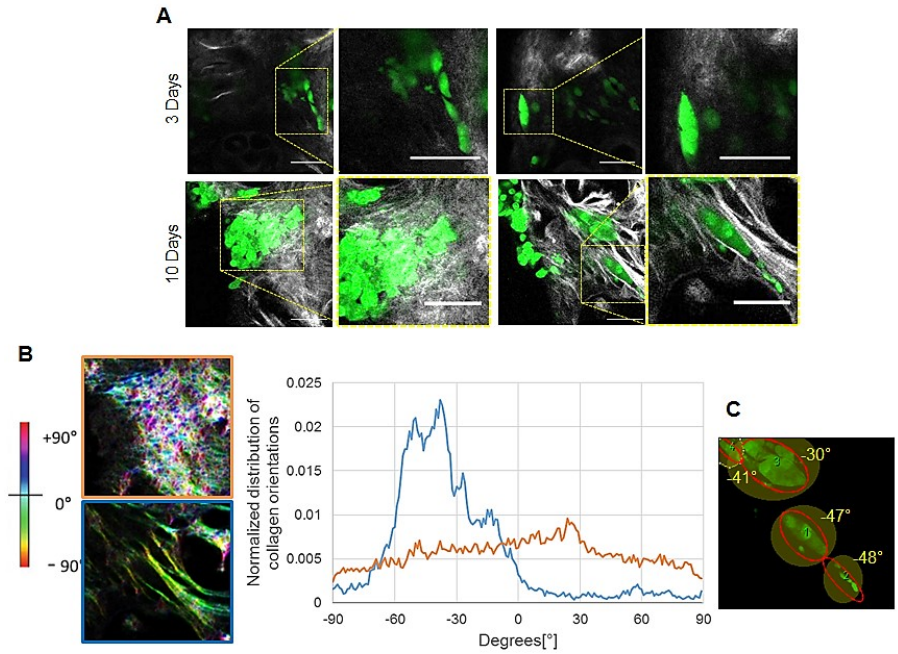

Fig. 11 Collagen heterogeneity: A) In green MCF7 ZsGreen1+ and in gray the SHG signal of collagen. Images of different parts of MCF7-µTPs 3 (up) and 10 days (down) after MCF7 seeding, at 2 different magnifications. Scale bar 75µm. B) *OrienationJ* analysis. On the left the color map related to images on the center, on the right the graphic of the normalized distribution of collagen orientations; C) Analysis of the orientations of 4 tumor clusters surrounded by preferentially oriented collagen fibers.

3.4 Discussion

In this work, we have developed a breast cancer model able to recapitulate spatiotemporal tumor heterogeneity into a dynamic microenvironment in which pro-angiogenic response and desmoplastic reaction occur.

We seeded human metastatic MCF7 on the surface of μTPs made up of HDFs embedded into a collagen rich ECM, produced by fibroblasts themselves, and HUVECs organized into a capillary-like network.

MCF7 cell line were derived from the pleural effusion of a 69-year-old female patient with a diagnosis of malignant adenocarcinoma of the breast [116]. These cells are well-documented in the literature and a suitable model cell line for breast cancer investigations worldwide [109].

Vascularized HDF-μTPs were used as CRTL in this work and they were characterized by a growing capillary network until 28 days (Fig.1) without signs of morphological regression which can occur in non-perfused vessels [6]. Thus, demonstrating that the dynamic culture condition into spinner flask could have important implication in the maintenance of angiogenesis even in absence of a perfusion flow through capillaries structures, probably because of the shear forces into the bioreactor [117] which are known to be correlated with vessel morphology and function [118].

Another control of our experiments was a healthy mammalian model obtained by seeding MCF10 cells on vascularized HDF-μTPs.

In the healthy model, MCF10, seeded on the surface of the sample, penetrated the interstitial space among micro-scaffolds and were able to form acinar structures in 10 days as typical of normal mammary epithelial cells. On the other hand, in the tumor model, MCF7, seeded in the same number and way of MCF10, formed disorganized cell masses and maintained higher proliferation rates (Fig.2). These

results are in agreement with previous literature data showing the behavior of normal and tumor cells in 3D environments [27] [119].

Our model is able to recapitulate how a healthy microenvironment can be perturbed by cancers cells. MCF7-μTPs represent a complex milieu in which tumor cells, endothelial cells and the ECM are in mutual interaction.

Firstly, we analyzed how MCF7 affect angiogenesis. We found that the CLS volume fraction and the number of junctions/μm^3 in tumor tissue were always higher than the controls and that they were increasing from 3 to 10 days leading major differences at the end of the culture time. Moreover, the average diameters length was always higher in tumor tissue with large standard deviations due to the cancer characteristic heterogeneities in capillary size. These data indicate that the tumor tissue was able to provide pro-angiogenic stimuli inducing the increase of the capillary extension, ramification and dimension (Fig.3 and Fig.4).

Endothelial and tumor cells grew in synergistic way into MCF7-μTPs and they were also physically very close. From the immunofluorescence, it is possible to see that tumor cells clusters were often aligned to capillary structures (Fig.5A). It's quite frequent to find single file of tumor cells parallel to the vascular network, assuming a conformation very similar to circulating tumor cells cluster migrating into capillaries [58] but outside these structure. We suppose that this particular conformation of tumor cells isn't only due to the physical confinement which capillaries impose on tumor clusters during circulation but also to paracrine signals which endothelial cells release affecting cancer cells behavior and that endothelial and tumor cells themselves deliver influencing the folding of the ECM.

The tumor model mirror the ability of tumor cells to attract endothelial cells from the environment [120]. In fact, images in Fig. 5C represent MCF7 and HUVECs in a very close contact and forming tumor masses crossed and surrounded by a discontinuous and intricate vascular network.

Furthermore, MCF7-µTPs model showed the presence of mosaic vessels with tumor cells becoming part of the capillary wall. The Fig.5 D/E show tumor cells cluster into the wall of leaky capillaries. The mosaic wall formation is a phenomenon which has profound implications for metastasis, drug delivery, and antivascular therapy. Munn et al calculate that half of the tumor cells exposed to the vessel lumen are shed into the circulation in a given day. [121] [60]. In line with this evidences our results demonstrate that MCF7 maintain their metastatic potential *in vitro*.

In 10 days, MCF7-µTPs were featured by the activation of the stromal desmoplastic reaction (Tab.1) with increase in collagen (Fig.6) and hyaluronic acid (Fig.7) amount. In invasive cancers, the collagen matrix is dense and the alignment degree is associated with poor prognosis. As *in vivo*, MCF7-µTPs had high level of dense and aligned collagen fibers as demonstrated by the quantitative analysis of the collagen fraction and assembly and by the GLCM analysis. Starting from SHG images, representing collagen fibers in gray, the correlation quantifies the dependence of gray levels between two pixels separated by distance *d*. The high correlation found in tumors indicates that one or several patterns repeat themselves inside the computational window and reveal a similar organization of the collagen fibers with certain periodicity [122]. The entropy measures the lack of tissue spatial organization [123]. The high correlation length and the low entropy values in MCF7-µTPs indicate that in 10 days the ECM acquires a certain degree of organization which features tumor tissues whereas normal interstitial matrix is comprised of cross-linked collagen fibers, generally arranged in non-isotropic orientations. This matrix organization can affect the diffusion pattern of molecules and drugs [124] and represents a troublesome point to investigate in order to develop new therapies for ‘inaccessible tumors’.

Moreover, the desmoplastic reaction, with increase in collagen density, is also linked to the heterogeneous organization of MCF7 in clusters. In fact, previous

works showed that epithelial cells within low-density matrix form well differentiated acini structures, while colonies that formed within high-density matrices are larger and less-organized [46]. The endogenous MCF7-µTPs environment, product by fibroblasts and altered by tumor cells, offer the opportunity to find different types of tumor cluster organizations which recapitulate different morphologies of invasive cancer cells during collective migration and metastasis (Fig.10). Cancer cell invasion is a heterogeneous and adaptive process in which tumor cells assume different migrations modes into the matrix in order to stay always motile and move toward vessels [51]. The various cluster conformation that we identified in the same tissue and at different time points are the mirror of different environmental conditions dictated by the ECM, fibroblasts and endothelial cells.

Among the different morphologies, when tumor cells were near to capillaries, they arranged parallel to them, as discussed before, or in cluster driven by leader cells which seemed to point the *endothelium*. This spiculated contour reminds that observed by mammography (Fig.10) and considered as positive predictive value of malignancy [125].

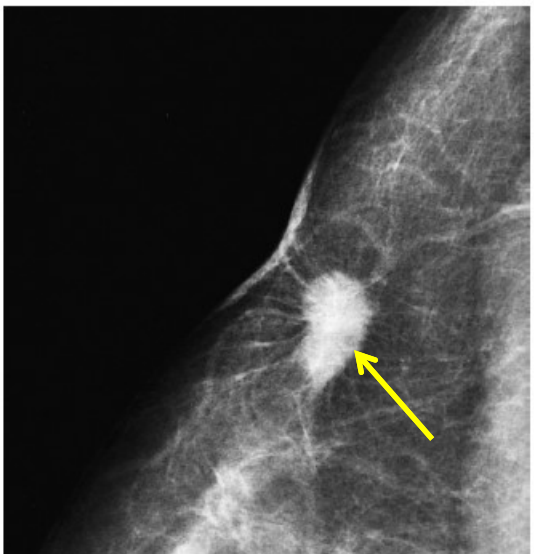

Fig. 10 Invasive ductal carcinoma, not otherwise specified (IDC, NOS). Close-up of mammogram with x-ray beam tangential to the area of skin retraction shows the underlying oval, spiculated, high density mass representing carcinoma [146].

MCF7-µTPs model uniquely recapitulates spatiotemporal heterogeneity of tumor cells organization and environment, as demonstrated by the morphological analysis of tumor cluster as well as collagen fibers orientation analysis. *In vivo*, tumor heterogeneity is associated with cancer resistance during therapy [51] and the

opportunity to have an *in vitro* model with this feature represents an intriguing chance for the study of these mechanisms and for the development and test of new drugs.

Taking together, our results show that MCF7, embedded into a dynamic matrix produced by human fibroblasts, have pro-angiogenic effect on the vascular network, are able to activate the desmoplastic reaction of the stroma and retain heterogeneous invasive properties into the matrix.

MCF7 were generally described in the literature as cells with low invasiveness, migration ability and pro-angiogenic effect *in vitro* [126] [72] [108] [109], although being metastatic breast cancer cells from pleural effusion *in vivo*. Our results highlight that the microenvironment has deep implications for cell behavior *in vitro* and demonstrate that MCF7-µTPs context is able to provide appropriate stimuli for the maintenance of tumor features *in vitro*.

We speculate that MCF7-µTPs can serve as unique multicomponent platform representative of fundamental aspects involved in tumor progression.

3.5 Conclusions and Future Perspectives

This work focus on the development of a new breast cancer model representative of the multiplicity of events occurring during tumor genesis and progression. The vascular response, the stromal desmoplastic reaction, cancer cell invasion and mosaic vessels formation have a central and active role in metastatic breast cancer and could be target of therapies.

We show that MCF7 cell line into a human ECM, rich in dense collagen product by mammary fibroblasts, retain their invasive phenotype and display higher pro-angiogenic properties than control and healthy tissues.

Here we present MCF7-µTPs as complex model for the study of tumor features and as platform for drug screening.

MCF7-µTP is an *in vitro* model for the study of the heterogeneity featuring *in vivo* tumors and molecular event associated with tumor growth and progression, into a microenvironment which converts from a normal to an activate/pathological condition and that is influenced and in turn influence cancer cells behavior.

About drug screening, at now, it could be possible study of the diffusion of active principles across the dense extracellular matrix and their effect on tumor vasculature, stroma and migration ability. We provide some benchmarks for the study of the vascular network and the stroma in healthy and pathological micro-tissues. In the future it might be interesting to examine other quantitative aspects of tumor heterogeneity in order to optimize the model for drug-screening.

Moreover, it will be very interesting to integrate MCF7-µTP into specific microfluidic systems in order to find a way to perfuse them and study the outcomes of systemic drugs.

Chapter 4

Development of vascularized dermis/skin equivalent model featured by endogenous extracellular matrix

4 Abstract

The presence of a pre-vascularized network into engineered tissue can accelerate the formation of functional anastomosis with host vasculature after *in vivo* graft, ensuring the sustenance of the implant, its integration and long term survival. This is fundamental for full thickness grafts for example after burns, surgery loss substance or injury leading tissue necrosis.

In the same time, *in vitro*, it can be a suitable model in view of fundamental research about angiogenesis and industrial applications like drugs screening.

Despite the improvements occurred in the issue of vascularized engineered tissues, actually there aren't skin or dermal pre-vascularized substitutes used in the clinic. One of the major challenges is to obtain a pervious and stable vascular network within a construct with good mechanical strength, poor deformability and controlled degradation of the scaffold.

Using a bottom-up approach, we have developed a dermis/skin equivalent model in which endothelial cells deeply penetrate and form mature capillary-like-structures branching within a collagen rich extracellular matrix produced by fibroblasts and able to offer pro-angiogenic signals leading the physiological development of the network itself.

Endothelial cells are able to migrate during wound heling assay and follow geometric control imposed by specific dermis shapes.

Keratinocytes seeded on the vascularized dermis equivalent develop a stratified, keratinized and differentiated *epithelium*.

We speculate that this model could be useful for *in vivo* applications in order to repair and restore damaged tissues. Furthermore, the construct could have interesting *in vitro* applications for the study of angiogenesis and drugs or molecules acting via topical administration.

4.1 Introduction

The main compartments of the skin are the *epithelium* and dermis. The *epithelium* is the top layer of the skin, which comprised mainly of keratinocytes. It provides the barrier against exogenous substances, chemicals, pathogens and prevents dehydration through the regulation of fluid loss. Beneath the epidermis, the dermis is a thicker layer of connective tissues that consists mainly of extracellular matrix (ECM) or structural components (predominantly collagen and elastin) which give mechanical strength and elasticity and a vascular plexus for skin nourishment. Cells interspersed within the ECM (Extracellular Cell Matrix) include fibroblasts, endothelial cells, smooth muscle cells and mast cells [87]. Skin model try to reproduce human skin structure and function and are mainly achieved seeding fibroblasts within 3D scaffold able to mimic the functions of the extracellular matrix in order to obtain the dermis compartment and following seeding of keratinocytes to develop the *epithelium* [93]. Typical 3D matrix used as scaffold are decellularized matrix, collagen type I, collagen-glycosaminoglycans, fibrin, fibroblasts derived matrix or synthetic polymers [22]. Several works used hydrogel as scaffold because of their similarity with the extracellular matrix but in the main time they have poor mechanical properties and are of animal origin [127].

Over the past 30 years Tissue Engineering has made numerous efforts to get substitutes that mimic the structure and function of human skin [93]. This is important for several reasons. Firstly, these substitutes can be used in the clinic in order to replace and restore damaged tissues e.g. after burns, surgery or pathology leading tissue necrosis, when it is not possible to perform an autograft because of the extension and thickness of the injured area [87] [95]. Besides their use as *in vivo* grafts other applications have emerged for skin substitutes as *in vitro* test systems. In this context, they enable not only the investigation of fundamental processes in the skin, but also the hazard assessment of various chemical

compounds that are topically applied on the skin without the need to use animal models [93].

At now, several epithelial/dermal/skin models are effectively used in the clinic and as platform for *in vitro* testing by pharmaceutical or cosmetic companies [93] [87] [128].

Despite the availability of these commercial products, they all suffer from the same problems of extremely high cost, sub-normal skin microstructure and inconsistent engraftment, especially in full thickness graft [87].

Furthermore, one of the major problems of full thickness skin graft is that it is slowly vascularized *in vivo*, so increasing time of tissue complete integration with host. About this issue, vascularization strategies in Tissue Engineering come in help with the aim to obtain a faster vascularization promoting graft invasion by host vessels or developing pre-vascularized models. Scaffolds can be functionalized using pro-angiogenic growth factors such as VEGF (Vascular Endothelial Growth Factor), PDGF (Platelet-derived Growth Factor) or heparin, but the effective use of these scaffolds is limited by the difficulty to adjust the release kinetics *in vivo* [2].

In several works pre-vascularization strategies are based on the co-culture of endothelial cells with other cell types. In fact when endothelial cells are cultured *in vitro* under permissive conditions, in particular when they are in 3D co-culture with other cell types and a relevant ECM, spontaneously are capable to form capillary networks [1]. Auger et al in 2006 have shown that fibroblasts promote the proliferation of endothelial cells, their migration and angiogenesis. This is due to their ability to produce an organized ECM and growth factors that represent the microenvironment suitable to promote the organization of endothelial cells in 3D and the formation of capillary-like tubular structures [9].

The first vascularized skin equivalent model is to Auger et al in 1998. They fabricated a collagen/Chitosan biopolymer in which three human cell types—

keratinocytes, dermal fibroblasts, and umbilical vein endothelial cells—were co-cultured. In this context endothelial cells develop a mature capillary network in 31 days [129].

It was demonstrated that the presence of a capillary network into an engineered skin model can quickly guarantee the formation of functional anastomosis with host vessels in 4 days whereas *de novo* vascularization of non-vascularized construct by host vessels is a longer process and require at least 14 days depending on the size of the implant [103].

Recent studies show the possibility of achieving engineered skin models pre-vascularized by an extensive network of both blood and lymphatic vessels. Reichmann et al used a co-culture of endothelial cells and fibroblasts in collagen I/fibrin hydrogel. In particular, they used HDMECs (Human Dermal Microvascular Endothelial Cells) extracted by foreskin and including a mixed endothelial cells population. After three weeks of *in vitro* culture cells organize themselves into blood and lymphatic structures which, interestingly, never anastomose between them *in vitro*. After implantation successful anastomosis were achieved between lymphatic vessels of the construct with the host ones as well as for blood vessels [4].

Despite the improvements occurred in the issue of vascularized engineered tissues, actually there aren't skin or dermal pre-vascularized substitutes used in the clinic.

The gold standard skin substitute should be physiologically vascularized, easily handled, poor deformable, able to withstand the shear forces *in vivo* and transplantable in one surgical intervention without scarring [130].[131]. The scaffold should be biodegradable in a controlled manner and non-immunogenic [132].

Here we show the development of a vascularized dermis/skin equivalent model obtained by bottom up approach. The model is strengthened by a collagenous matrix product by fibroblasts and able to offer pro-angiogenic stimuli for

endothelial cells sprouting and ramification. The vascular network recapitulates all the events of physiological angiogenesis with the formation of a capillary network and its following regression. VEGF and Ang-2 are together involved in vessel formation and remodeling whereas Ang-2 alone is linked with vessel regression. The vascular network gains structural maturity *in vitro*, being surrounded by collagen, laminin and pericytes-like cells.

We speculate that the vascularized dermis equivalent could be suitable for clinical applications for several reasons. Previous works showed that the dermis model exhibit increasing mechanical strength until 6 weeks of culture [23], it is easy to handle and has tunable shape and dimensions[21] [22] [23]. Moreover the scaffold degradation occurs *in vitro* with known timing [94] allowing the further synthesis of new tissue. Here we show that such environment allows the physiological evolution and maturation of the vascular network. Furthermore, endothelial cells are able to migrate during wound assay and to follow geometric controls imposed by modeling dermis shape, so placing increasing confidence in their ability and chance to form anastomosis *in vivo*.

Keratinocytes, seeded on a surface of the vascularized dermis model, develop a stratified and differentiated *epithelium* which could give barrier function in specific cases of graft.

Furthermore, a so representative vascularized model could be useful to study angiogenesis and as platform to examine the effect of topically administered compounds.

4.2 Materials and Methods

4.2.1 HDFs and Keratinocytes source

Cells were extracted from human tissue biopsies surplus obtained by "Azienda Ospedaliera di Rilievo Nazionale e di Alta Specializzazione (AORN) A. Cardarelli/Santobono/Pausillipon at Urology and Biotechnology Centre - AORN" according to the project "Realization of human skin equivalent *in vitro*" after approval of ethical committee.

4.2.2 HDFs and Keratinocytes extraction

All the solutions used during the extraction procedure were cool. Human biopsies were washed in PBS1X+antibiotics (1%penicillin/streptomycin- Microgem L0022-100- or 50µg/ml gentamicin- SIGMA G1397), PBS1X+antimycotic (1%Amphotericin-SIGMA A2942-) and PBS1X. Fat from the bottom side was removed as much as possible with a scalpel and the tissue was washed again in PBS1X. The skin biopsy was cut into strips of about 3mm width and incubated Dispase (GIBCO 0698) solution 1.8U/mL overnight for 14h.

Epidermis and dermis were separated with tweezers and then washed in PBS1X. The dermal pieces were cut in smaller pieces and put in 2,5mg/ml collagenase A solution (ROCHE 11088793001) for 40 minutes at 37°C. The collagenase was stopped with FBS and then removed. All the pieces were suspended in a little volume of complete MEM and arranged on a petri dish in order to allow the migration of fibroblasts on the surface of the petri.

Epidermal parts were washed with PBS1X and cut into smaller pieces and incubated with preheated Trypsin/EDTA (Microtech L0930-100) for 5 min at 37°C water bath. The enzyme reaction was stopped by adding FBS. The solution was pipetted vigorously for 5' in order to separate cell clumps and then centrifuged for

5’ at 1200 rpm. Cells were suspended in the culture media and seeded at high density (about 30.000 cells/cm²).

4.2.3 Cell culture

Human dermal fibroblasts (HDFs) were extracted from healthy foreskin or breast biopsies and cultured in enriched MEM: MEM (Microtech L0440-500) with 20% of FBS (Sigma Aldrich), 2% of Non-Essential Aminoacids (EuroClone ECB3054D), 1% of L-Glutamine (Lonza 17-605E) and 1% of penicillin/streptomycin (Microtech L0022-100), until passage 4/7.
HUVECs (GIBCO C0035C) were cultured in enriched M200: M200 (GIBCO Invitrogen Cell Culture M-200-500) supplemented with LSGS Kit (GIBCO Invitrogen Cell Culture S-003-K) until passage 3.
Human keratinocytes were grown KGM-2 culture media (PromoCeLL C-20111) and were used for the experiments at passage 1.

4.2.4 Micro-scaffold production

Gelatin porous microbeads (GPMs) were prepared according to a modified double emulsion protocol (O/W/O) [110]. GPMs were stabilized by crosslink reaction with glyceraldehyde (GAL) (SIGMA-G5001), in order to make them stable in aqueous environment at 37 °C, as previously described [94]. GAL at 4% w/w of the microbeads was used to perform all the experiments.

4.2.5 Micro-tissues (µTPs) production

About 11 HDFs P5/8 were seeded for bead. Cells were cultured into spinner flask bioreactor (Integra) in continuous agitation (30 rpm) after 6 hours of intermitting stirring regime in order to promote cell seeding (30 min at 0 rpm, 5 min at 30 rpm). The culture medium was enriched MEM plus Ascorbic Acid (2-O-α-D-

Glucopyranosiyl-L-Ascorbic-Acid TCI; Cf: 0.5mM). µTPs were cultured for 9 days before the phase of assembly in order to guarantee the initial collagen synthesis.

4.2.6 Dermis equivalent model production

As previously described [117] µTPs suspension was transferred from the spinner flask to a 50 ml Falcon centrifuge tube and, after settling, transferred by pipetting into the maturation chamber to allow their molding in disc-shaped construct (1 mm in thickness, 5 or 8 mm in diameter). During the filling procedure, the maturation chamber was accommodated on a device connected with a vacuum pump to make the process faster and to assure that any bubble was in the maturation space. The assembling chamber was a sandwich-like structure with in the middle a silicon mold with empty spaces (disc shape:1 mm in thickness, 5 or 8 mm in diameter; wire shape: 1 mm in thickness, 5cm length) for the µTPs housing. A particular conformation of the mold was used in order to obtain channeled biohybrids: a capillary with outside diameter of 364µm and inner diameter of 74µm (Polyimide Coated Fused Silica Capillary Tubing, Molex TSP075375) was inserted into the empties spaces (disc shape: 1 mm in thickness, 8 mm in diameter) of the mold, as stamp around which allow tissue assembly.

The silicon mold was delimited on both the top and bottom sides by two stainless steel rigid grids characterized by a porous mesh (18 µm) that was able to retain the µTPs and to guarantee the passage of nutrients and waste products. Two polytetrafluoroethylene (PTFE) rings were placed on the grids on both sides of the system and were fastened to each other by means of stainless steel screws, which close the system.

The assembling chamber was placed on the bottom of a spinner flask (Bellco biotechnology code 1967- 00050) and completely surrounded by culture medium.

The spinner was operated at 60 rpm. The culture medium was enriched MEM plus Ascorbic Acid. After 4-5 weeks of culture the assembling chamber was opened and biohybrids were collected.

4.2.7 Vascularized dermis equivalent model production

Endothelial cells seeding and culture was performed into multiwall low attach in order to avoid cells adhesion on the surface of the petri and to allow cells adhesion on the biohybrid dermis equivalent. HUVECs P4 were seeded as a drop on a surface of the sample, at high density of about 10.000/15.000 cells for mm^2. Cells were suspended in 5-10µl of medium, depending on the size and form of the biohybrid, in order to avoid drop falling. After the seeding, the sample was left at 37°C for 2 hours enabling endothelial cells adhesion and, afterwards, complete medium was added up to completely cover the sample. During the first 2 hours, the sample was monitored to avoid drying and eventually a drop of medium was added on the surface. M200 complete was used for cell seeding and adhesion, while from the following day complete MEM and M200 were used in 2:1 ratio. Samples were cultured for 3 weeks.

4.2.8 HUVECs injection into the channeled biohybrid dermis equivalent

After the maturation period the assembling chamber was opened and biohybrids assembled around the capillary structure were derived. The capillary was pulled out from the sample leading the channel structure. One extremity of the capillary was left inserted into the initial part of the channel whereas the other one was connected to another longer capillary (length 10cm), by a silicon connector hand made by us, in turn attached to a syringe pump. HUVECs P3 were detached and charged into a syringe at a density of 1.500 cells/µl within a final volume of 100µl. Cells were injected using a syringe pump at an initial flow rate of 50µl/min for few minutes in

order to release any bubbles from the channel and then at a flow rate of 1µl/min. Sample was rounded after the injection of 50µl of cell solution and cycles of injection and stop (less than 1 minute) were alternated during the entire procedure in order to allow cells seeding.

4.2.9 Vascularized skin equivalent model

1week after HUVECs seeding the sample was rounded and placed on a transwell insert (with pores of 3.0 µm) in order to seed on the opposite surface keratinocytes. The dermis equivalent surface was coated using 50µg/ml human fibronectin (Sigma Aldrich F0895). The coating was performed with a minimal volume of about 5-10 µl of fibronectin. Samples were left under hood, at RT, for 40' and into the incubator, at 37°C, for 10'. Meanwhile human keratinocytes were washed 3 or 4 times with PBS/EDTA 0.01 M (Invitrogen 15575-038) for few minutes. Cells colonies were detached by using trypsin/EDTA (Microtech L0930-100) for 5 min at 37 °C. Cells were counted and the appropriate number of cells was transferred into a Falcon tube and centrifuged at 1.200 rpm for 5'.

About 4.000 cells/mm^2 were seeded on the surface of the biohybrid, suspended in 5-10µl of medium, depending on the size of the sample, in order to avoid drop falling. After 3hours the sample was submerged with the medium: complete KGM-2+5%FBS and CaCl2 0.06 mM. The next day the medium was changed with complete KGM-2+ 3%FBS and CaCl2 0.06 mM2 days later with complete KGM-2+ 3%FBS and CaCl2 0.06 mM until the 6th day of submerged culture. During the following 2 weeks of culture the sample was elevated at the air liquid interface using a complete KGM-2 medium without EGF and BPE and with CaCl2 1.88 mM.

4.2.10 Immunofluorescence analysis

- **Immunofluorescence on the whole sample**

Sample were fixed in 4% Paraformaldehyde (P61148-500g Sigma Aldrich) for 30' at RT and washed in PBS1X. They were permeabilized using 0,1% Triton (Triton® X-100 T9284-100ML Sigma) in PBS1X for 5' at RT, washed in PBS1X and blocked in 1%BSA (A9418-100G Sigma) for 1h at RT. Samples were stained with Rhodamine Ulex Europaeus Agglutinin I (UEAI Vector Laboratories RL-1062) at a final concentration of 20µg/ml in blocking solution, in order to mark the *endothelium*, overnight (ON) at 4°C in the dark. The morning after, samples were washed with PBS1X. The nuclei of all the cells were stained with Sytox Green (Invitrogen S7020) for 20' at RT.

- **Samples clarification**

Samples were dehydrated by serial immersions, each of 30', in Methanol 50%, 70%, 80%, 90%, 100%, 100%. BABB solution was prepared containing Benzyl Alcohol (BA) and Benzyl Benzoate (BB) (SIGMA) in 1:2 ratio. Samples were moved into a glass bottle and treated with Methanol and BABB (1:1) for 4h and following with BABB for 24h at RT. Samples were investigated into fluorodish by Confocal Leica TCS SP5 II.

- **Immunofluorescence on frozen tissue sections**

Sample were fixed in 4% Paraformaldehyde (Sigma Aldrich P61148-500g) for 30' at RT, washed in PBS1X and soaked into a sucrose water solution (2 M). After 24h samples were included in OCT Killik (Bio Optica 05-9801) in a suitable mold (Peel-A, Ted Pella INC), submerged in liquid nitrogen vapors for 1 minute and

then stored at -80 °C. All samples were cut in slices 7 µm in thickness by using a criomicrotome (Leica CM 1850).

For immunofluorescences analyses, tissue slices were washed in PBS1X to remove the fixative and then permeabilized and blocked with 0.01% Triton X-100 in PBS/BSA 3% for 2h at RT. Subsequently, slices were incubated ON in presence of the primary antibodies: UEAI (Cf 20µg/ml), Mouse monoclonal Anti alpha-SMA (1:100, Abcam ab7817), Rabbit polyclonal anti Laminin (1:30, SIGMA L9393). The morning after samples were washed in PBS1X and the secondary antibodies Alexa Fluor 488 Goat anti-Mouse IgG (H+L) (1:500, Thermo Fisher Scientific A11001) and Alexa Fluor 488 Goat anti-Rabbit IgG (H+L) (1:500, Thermo Fisher Scientific A11008) in PBS1X BSA3% were added for 1h and half at RT. Nuclei were stained with DAPI (Sigma-Aldrich D9542) and samples were investigated by Confocal Leica TCS SP5 II.

- **Immunofluorescence on paraffin sections**

Samples were fixed in Formalin 10% (Sigma HT501320) for 1h at Room Temperature (RT) and washed in PBS1X (Sigma P4417-100TAB). They were dehydrated in Ethanol from 75% to 100% and treated with Xylene (A9982 ROMIL) before the inclusion in Paraffin. Tissue slices thick 7µm were cut using a microtome (Thermo Scientific HM 355S) and then deparaffinized using xylene. Sections were hydrated in ethanol from 100% to 75% and washed in water, Triton 0,2% and PBS1X. In order to release the epitopes from paraffin, heat mediated citrate buffer (pH=6, Thermo scientific TA-125-PM1X) unmasking was performed. Sections were washed in PBS1X, blocked using BSA6%, FBS 5%, $MgCl_2$ 20Mm and Tween20 0,02% in PBS1X for 2h at RT and incubated with the primary antibodies ON at 4°C in a wet environment: p63 Mouse anti-p63(1:50, Invitrogen 4B1E12), k10 (1:500, Covance PRB-159P-100), k14 (1:500, Covance PRB-155P-

100), involucrin (1:500, Covance PRB-140C), filaggrin (1:500, Covance PRB-417P).

The morning after samples were washed in PBS1X and the secondary antibodies Alexa Fluor 488 Goat anti-Mouse IgG (H+L) (1:500, Thermo Fisher Scientific A11001), and Goat Anti-Rabbit IgG (H+L) Secondary Antibody Alexa Fluor 488 (1:500, A11008) and Donkey Anti Rabbit IgG (H+L) Alexa Fluor 546 (A10040) in PBS1X were added for 1h and half at RT. Nuclei were stained with DAPI and samples were investigated by Confocal Leica TCS SP5 II.

4.2.11 Histology on paraffin sections

Samples were fixed in Formalin 10% (HT501320 Sigma) for 1h at Room Temperature (RT) and washed in PBS1X (P4417-100TAB Sigma). They were dehydrated in Ethanol from 75% to 100% and treated with Xylene (A9982 ROMIL) before the inclusion in Paraffin. Tissue slices thick 7µm were cut using a microtome (Thermo Scientific HM 355S) and then deparaffinized using xylene. Sections were hydrated in ethanol from 100% to 75%, washed in water and stained using Hematoxylin/Eosin (Bio Optica W01030708). The sections were mounted with Histomount Mounting Solution (Bio Mount HM 05-BMHM500 Bio-Optica) on coverslips and the morphological features of µTPs were observed with a light microscope (Olympus, BX53).

4.2.12 Second harmonic generation signal

For SHG imaging samples were investigated by confocal microscopy (TCS SP5 II Leica) combined with a MPM where the NIR femtosecond laser beam was derived from a tunable compact mode-locked titanium: sapphire laser (Chamaleon Compact OPO-Vis, Coherent). Two-photon excited fluorescence was used to induce second harmonic generation (SHG) and obtain high-resolution images of

unstained collagen structures. The samples were observed by using λex = 840 nm (two photons) and λem=415-425 nm. The SHG images were acquired with a resolution of 12 bit, 512x512 pixel by using a 25X water immersion objective (HCX IRAPO L 25.0X0.95 Water, n.a. 0.95).

4.2.13 Scanning electron microscopy (SEM)

SEM was performed to analyze the morphology of channeled biohybrids. Fixed samples were dehydrated in an incremental series of Ethanol (50%, 75%, 85%, 95% and 100% at room temperature) followed by critical point drying (CPD-300 Leica). Then they were mounted onto metal stubs and then coated with 100 A ultrathin platinum layer (thickness 7 nm) in a glow-discharge coater to minimize charging and increase the conductivity of the biological material (sputter coater Cressington_HR 208). Images were acquired using InLens and SE2 detectors (SEM, FEG_Ultrapluss by ZEISS).

4.2.14 Quantitative Capillary-like structures (CLS) analysis

Whole samples were investigated by Confocal Leica TCS SP5 II performing 5 z-stacks in different random points of different μTPs. Samples were observed using λex = 543 nm/ λem=550/560 nm to detect Rhodamine and λex=488 nm/ λem=500/530 nm to detect Sytox Green. The stacks were acquired with a resolution of 12 bit, 512x512 pixels by using a 25X water immersion objective (HCX IRAPO L 25.0X0.95 Water, n.a. 0.95). Each stack was composed by 16 sequential images with a z-slice-space of 1,98 μm.

- **CLS volume fraction**

The capillary like structures (CLS) volume fraction was calculated as percentage of the ratio between the thresholded red volume of the *endothelium* marked by

Rhodamine-UEAI and the total volume of the sample acquired for each stack. The volume values were obtained applying the *ImageJ* plugin *Measure Stack* to the red thresholded channel and to the total volume of tissue acquired.

$$\text{CLS Volume fraction} = \frac{\text{acquired CLS volume}}{\text{acquired sample volume}} * 100$$

- **Analysis of the junctions**

The number of junctions for each stack was calculated using the plugin *Skeletonize 3D* of *ImageJ*. Before the analysis, the red channel of each stack was thresholded and smoothed in order to avoid the identification of false positive junctions by the plugin. The number of junctions for μm^3 was calculated as ratio between the number of junctions for stack and the total acquired volume obtained by *Measure Stack*. Thanks to the plugin *Skeletonize 3D* of *ImageJ* we were able to distinguish triple and quadruple points of junction.

$$\text{Junctions}/\mu m^3 = \frac{\text{n° of junctions for stack}}{\text{acquired sample volume}}$$

- **CLS diameter analysis**

The diameter of the capillary like structures was calculated tracing at least 3 adjacent lines joining the opposite major sides of capillaries using *ImageJ*. For each sample the diameter was calculated at least three times on each image of the z stack and then the mean and the standard deviation were represented in the graphic.

4.2.15 Molecular analysis

Vascularized biohybrid dermis equivalent, 1, 2 and 3 weeks after HUVECs seeding, were weighed, cut and treated with 2,5mg/ml Collagenase A (ROCHE) for 30'. Samples in lysis buffer were placed into 2ml Eppendorf with a stainless-steel ball for mechanical digestion on a vortex. RNA extraction was performed by means of the High Pure RNA Tissue Kit (ROCHE 12033674001) according to manufacturer's protocol. Lysates were centrifuged into high pure filter tube. The flow through was discarded and samples were incubated in presence of DNase and DNase Incubation buffer for 15' at RT. Washing buffer 1 with Ethanol was added and samples were centrifuged for 10'' at 10.000 rpm and flow through was discarded, so for washing buffer 2. After a second wash in Buffer 2, samples were centrifuged for 2' at 13.000rpm. Finally, RNA was eluted in 50µl of elution Buffer after centrifugation for 1' at 10.000rpm. RNA was quantified by means of spectrophotometer (Eppendorf Bio Photometer). 100ng of RNA were retro-transcribed using iScript™ Reverse Transcription Supermix (Biorad 1708840). 4µl of super-mix and water were added to samples up to a final volume of 20µl. The complete reaction mix was incubated in a thermal cycler using the following protocol: 5' at 25°C, 30' at 42°C and 5' at 85°C.

Real Time PCR was performed using BIORAD CFX96 Real-time system C100 Touch Thermal cycler. 2,5µl of cDNA were mixed with iQ™ SYBR® Green Super-mix (Biorad 170-8880), 0.6µl of Forward and 0.6 µl Reverse Primers (from stock solutions 100µM) and water to a final volume of 10µl.

All quantifications were normalized with the GAPDH mRNA level, then the fold induction was calculated by the ΔΔCt method as described in the original paper [133].

Table 3 Oligonucleotides sequences

Gene	For 5→3'	Rev 3'→5'
VEGF	CGAGGCAGCTTGAGTTAAACG	AGATCTGGTTCCCGAAACCCT
ANGP2	GGTGGTTTGATGCATGTGGTCCTT	TCTGCTGGTCGGATCATCATGGTT
HIF1α	TTGGCAGCAACGACACAGAAACTG	TTGAGTGCAGGGTCAGCACTACTT
THBS1	TGACAAGGACAACTGCAGACTCGT	AGGAATCATCTGGAATCGGCGGAA
GAPDH	CCACCCATGGCAAATTCCATGGCA	TCTAGACTGGCAGGTCAGGTCCACC

4.2.16 Decellularization protocol

We used a protocol exploiting non-ionic detergent, adapted from [134]. Dermis pieces after 3 weeks of maturation were treated with 0.25% trypsin for 4 hours at RT, H2Od x 15' (3x), 70% EtOH x 10-12 h (1x), 3% H2O2, 15' (1x), H2Od x 15' (2x), 1% Triton X-100 in 0.26% EDTA/0.69% Tris (SIGMA) (ON), H2Od x 15' (3x), 4% EtOH x 2 h (1x), PBS x 15'(2x) and H2Od x 15' (2x).

4.2.17 Endothelial contribution during wound healing

After 5 weeks of maturation the assembling chamber was opened and HUVECs P4 were seeded on a surface of the biohybrid, made up of breast HDFs P7, and cultured in multiwell low attach in MEM:M200 (2:1). 10 days after seeding biohybrids were cut and the extremities of different samples with HUVECs or with and without HUVECs were placed in contact and closed again into the maturation chamber, similarly as previously described [135]. Samples were harvested 1 and 2 weeks after cut, they were stained with UEAI and Sytox and analyzed by Confocal Leica TCS SP5 II.

4.2.18 Statistics

Experiments were performed in triplicate. Data are expressed as mean ± SD. Differences between groups were determined using the statistic test ANOVA Tukey HSD test. Significance between groups was established for p value<0.01 or p value<0,05.

4.3 Results

4.3.1 Vascularized dermis equivalent model: characterization

- **HUVECs sprouting into the dermis equivalent model**

In this work HUVECs were seeded on the surface of a biohybrid dermis equivalent rich in collagen product by fibroblasts (Fig.1A). Endothelial cells deeply penetrated the ECM for about 700µm after 1week (Fig.1B) and formed capillary like structures observable from 1 to 3 weeks after HUVECs seeding (Fig.2A).

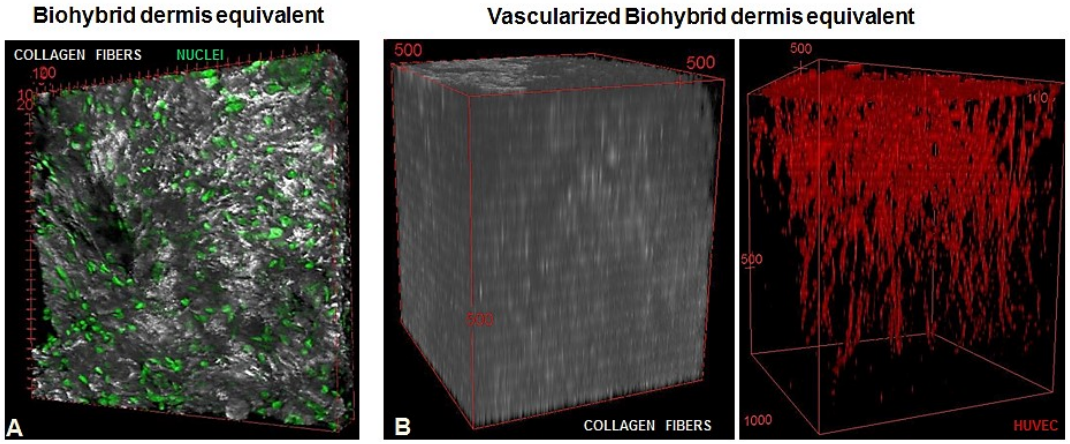

Fig. 1 3D views of the biohybrid dermis equivalent and vascularized dermis equivalent: A) In gray the SHG signal of collagen and in green the HDFs nuclei marked by Sytox; B) On the left the SHG signal of collagen and on the right in red the endothelial cells marked by UEAI.

- **CLS image analysis: volume fraction and n° of junctions/µm3**

The image analysis of the CLS volume fraction and of the number of junctions/μm^3 showed an increment from 1 to 2 weeks and a decrement from 2 to 3 weeks after HUVECs seeding (Fig.2B/C). Most of the analyzed junctions were triple, so among 3 structures (Fig.2C/D).

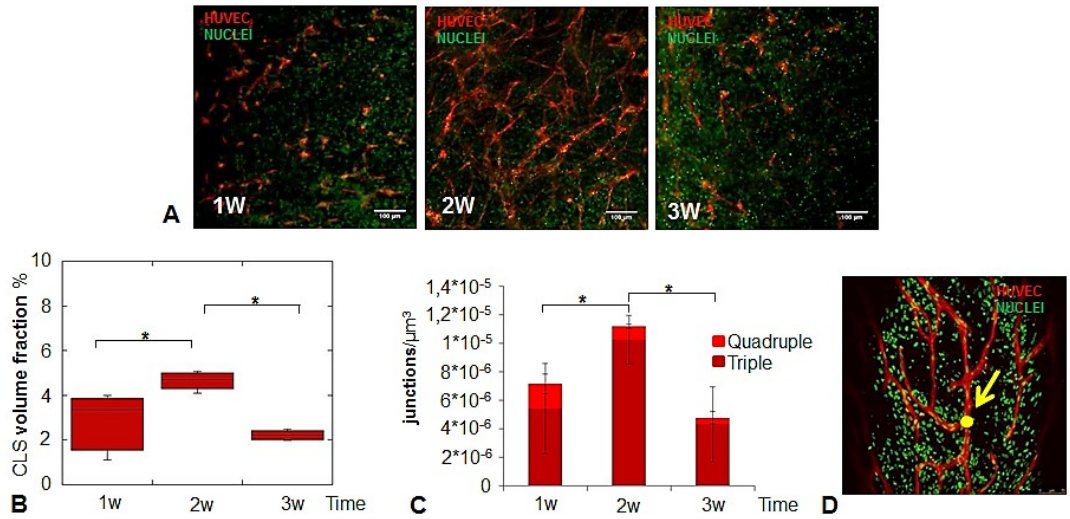

Fig. 2 CLS *in vitro* progression: A/D) in red the HUVECs marked by UEAI and in green the nuclei of all the cells marked by Sytox; A) Images of CLS 1, 2 and 3 weeks after HUVECs seeding. Scale bar 100µm; B) Graphic of the CLS volume fraction and C) Graphic of the number of junctions for μm^3; B/C) * p value<0.05 or p<0.01. D) Image of CLS, the yellow dot represents a triple junction among 3 structures. Scale bar 75µm.

The capillary network was embedded into the collagen rich ECM produced by fibroblasts. The orthogonal view (Fig.3) and images at great magnification (Fig.4) showed that these structures were hollow.

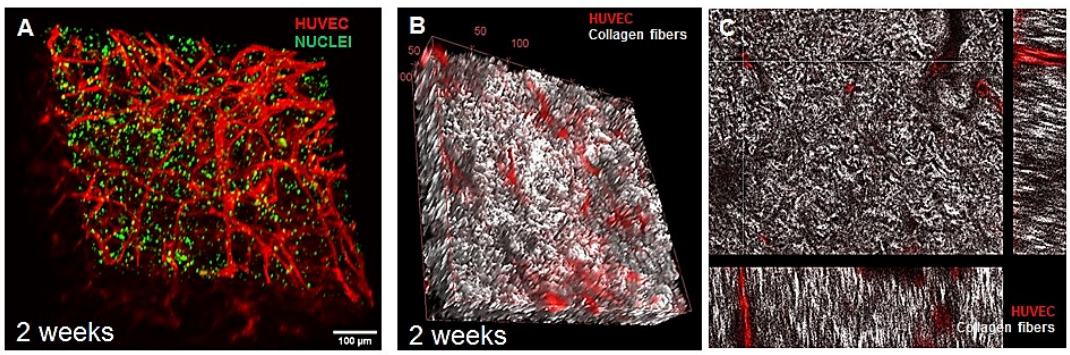

Fig. 3 CLS embedded into the ECM: A) 3D view of the vascularized dermis equivalent model, in red the HUVECs marked by UEAI and in green the nuclei of both HUVECs and HDFs. Scale bar 100µm; B)3D view showing the SHG signal of collagen in gray and CLS in red; C) Orthogonal view of CLS.

- **CLS diameters**

The diameter of the vessels, calculated from image analysis, was of about 9±3µm. The structures are showed at greater magnification in Fig. 4.

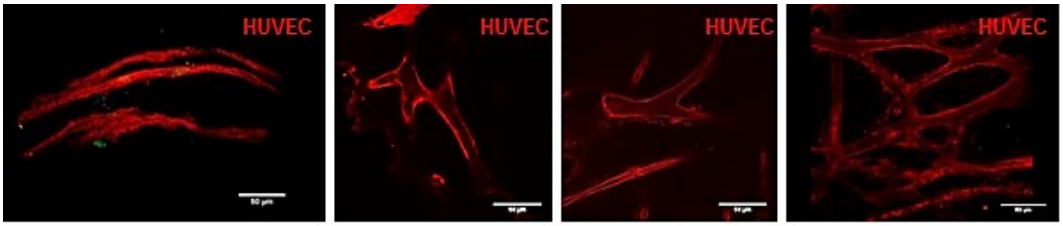

Fig. 4 CLS structures: In red the HUVECs marked by UEAI. Scale bar 50µm.

- **Molecular analysis**

The expression of the Vascular Endothelial Growth Factor (VEGF), Angiopoietin2 (ANGP2), Hypoxia inducible factor (HIF1α) and thrombospondin (THBS1) were evaluated by Real Time PCR. VEGF and ANGP2 were upregulated compared to the control (not vascularized dermis equivalent) 1 and 2 weeks after seeding and the upregulation was increasing from 1 to 2 weeks. Only ANGP2 was upregulated after 3 weeks whereas VEGF expression was similar to the control. The HIF1α was slightly upregulated in the vascularized dermis only 2 weeks after seeding. THBS1 didn't seem to be involved in this process because its expression level was always comparable with the control (Fig.5).

- **CLS structural maturity**

In 2 weeks of culture some of the cells surrounding capillaries acquired positivity for α Smooth muscle actin (αSMA) and the ECM develop a continuous layer of a Collagen and Laminin around vessels as shown by the immunofluorescence (Fig. 6)

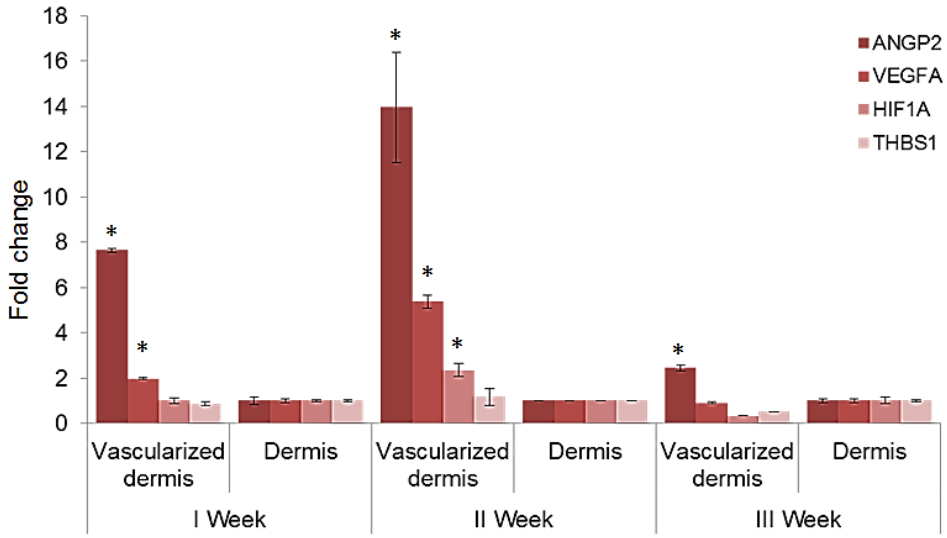

Fig. 5 Molecular analysis of factors involved in angiogenesis: The vascularized dermis was compared to the dermis without endothelial cells in the same culture conditions. *p<0.05.

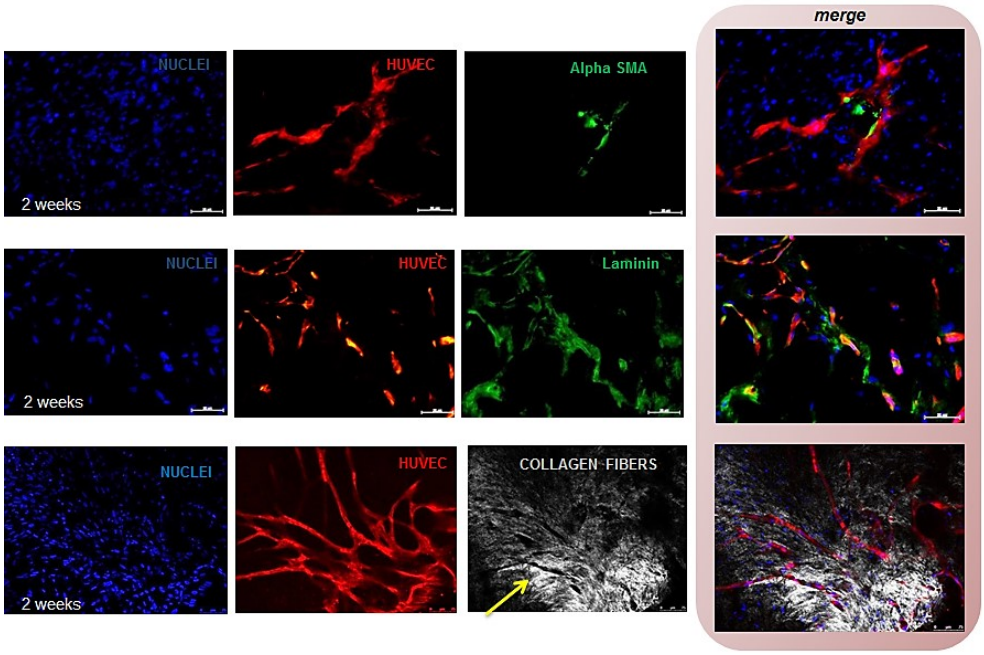

Fig. 6 Structural vessels maturity: In blue the nuclei of all the cells marked by DAPI, in red the HUVECs marked by UEAI, in green the αSMA and Laminin, in gray the SHG signal of collagen fibers, the arrow indicates thicker collagen bundle around capillaries. Merges of the images are on the right. Scale bar 50µm for the first 2 lines and 75µm in the last one.

4.3.2 Vascularized dermis equivalent model: Assessment of tissue function for *in vivo* application

We argue that the vascularized dermis model could be used for *in vivo* studies after 10 days of culture because in this time structures are still evolving *in vitro* and they have achieved a certain degree of structural maturity. For the *in vivo* study, we want to analyze the time of tissue integration comparing the vascularized dermis model with the dermis and the decellularized dermis model.

- **Dermis decellularization**

Using a decellularization protocol exploiting non-ionic detergent we were able to remove all the cells from the dermis model keeping intact the collagen structure as shown by the SHG signal image (Fig.7).

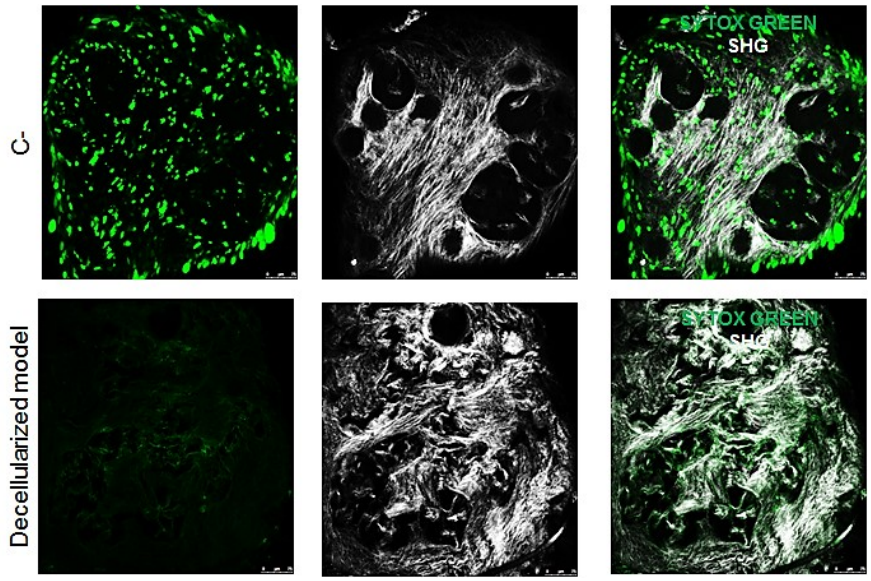

Fig. 7 Decellularized dermis model: Control and decellularized dermis model using non-ionic detergents. In green the nuclei marked in Sytox and in gray the second harmonic generation signal of collagen. Scale bar 75µm.

- **Endothelial behavior in wound healing**

In order to assess endothelial cells ability to migrate in the wound area between host and implant after graft we performed a wound healing assay [135]. Cut biohybrids were placed near into the maturation chamber in both the conformations of vascularized biohybrids or vascularized and not vascularized biohybrid. In both cases the HUVECs migrated in the wound area which narrows visibly from 1 to 2 weeks (Fig.8).

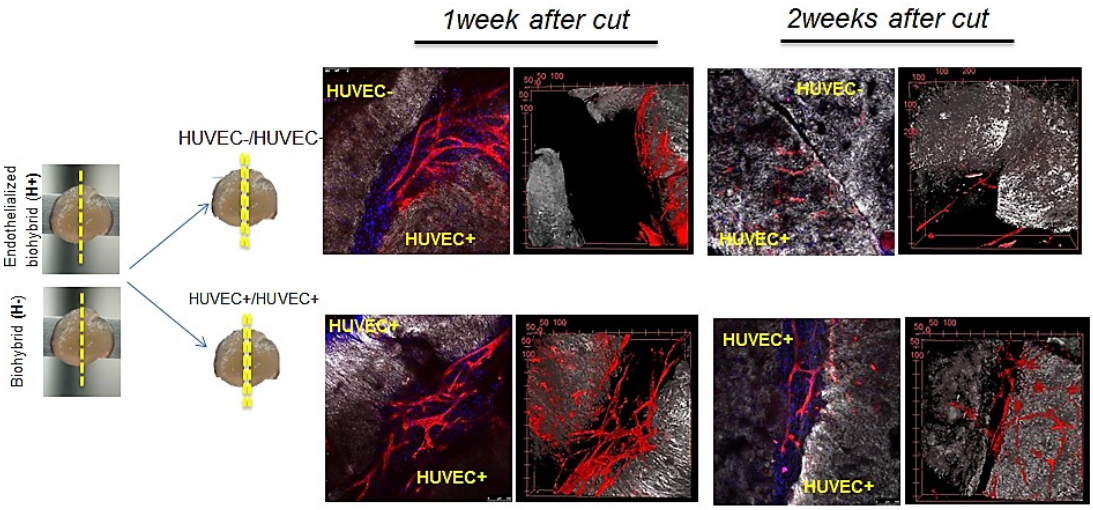

Fig. 8 HUVECs migration in the wound area: Images of the cut biohybrids on the left. On the right images and 3Dviews of endothelial cells in red marked by UEAI and collagen in gray marked by SHG. The nuclei of all the cells were marked in blue by DAPI. Scale bar 100µm.

- **Geometric control of the vascular network**

The dermis vascularization have a fine architecture and there are works in literature which show that recapitulating vascular architecture *in vitro* can accelerate the formation of functional anastomoses *in vivo* [16][136]. For these reasons, we have used 2 different approaches in order to obtain a vascular network geometrically oriented.

In the first approach, we have achieved channeled biohybrids assembling µTPs around a capillary as stamp (Fig.9 A). HUVECs were seeded into the channel using a syringe pump. The obtained channel was surrounded by collagen as shown by the SEM images (Fig.9B/C) but it undergoes shrinkage during the culture period in fact the initial diameter of the cannel was of about 364µm (Outside diameter of the capillary used as stamp) whereas 10 days after endothelial cells seeding it was of about 150µm. HUVECs seeded into the channel form a capillary network into the channel spreading into the surrounding matrix (Fig 9D).

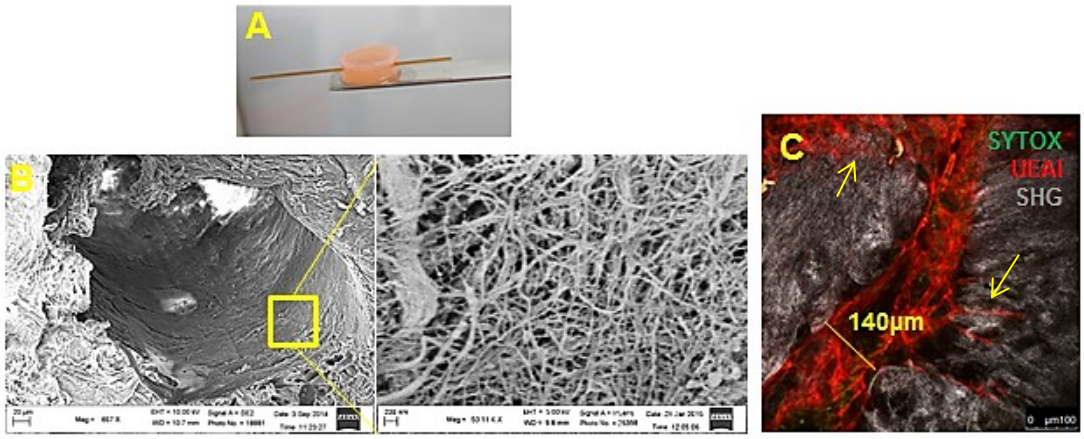

Fig. 9 Channeled/vascularized dermis equivalent: A) Picture of the channeled biohybrid before capillary extraction; B) SEM image of the channeled biohybrid and magnification of the collagen matrix into the channel. Scale bar on the left 20µn, on the right 200nm; C) Immunofluorescence of the vascularized biohybrid, in red the HUVECs marked by UEAI and in gray the SHG collagen signal. The yellow arrows indicate vascular sprouts into the collagen matrix. Scale bar 100µm.

The second approach consisted in the seeding of endothelial cells on a dermis equivalent in wire form kept in tension from the extremities. After 10 days of culture HUVECs developed a capillary network following the main direction of the wire (Fig.10).

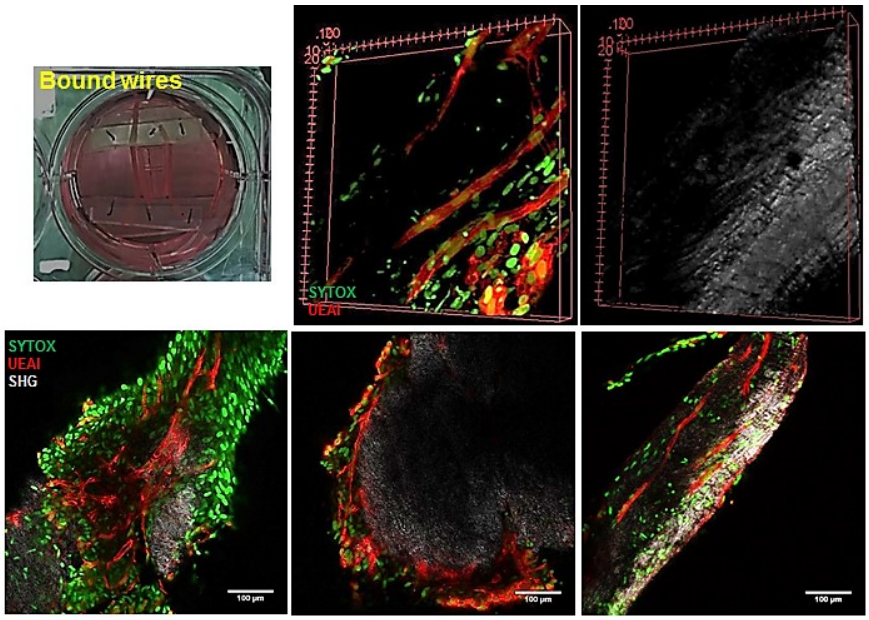

Fig. 10 The capillary network follows the mail direction of the wire: Up on the left a picture of the biohybrid dermis equivalent bound at the ends. Up on the right and down images of the capillary network marked by UEAI in red, the SHG collagen signal in gray and the nuclei of all the cells marked in green by Sytox. Scale bar 100µm.

4.3.3 Vascularized skin equivalent model

Keratinocytes, seeded on the surface of the vascularized biohybrid dermis equivalent, proliferated, differentiated and stratified during the culture period. Histological and immunofluorescence analysis were performed 3 weeks after epithelial cells seeding. The histology showed the development of a keratinized *epithelium* on a complete basal lamina (Fig.11A). The *epithelium* expressed keratin 14 in the basal layer and keratin 10 in the super basal layer. It was positive for p63, marker of the basal layer, and for involucrin and filaggrin, markers of the more external layer (Fig.11B). The 3d view showed the complete model featured by the presence of a stratified *epithelium* lying on the dermis compartment, which was strengthened by the endogenous ECM rich in collagen and in which the *endothelium* sprouted toward the *epithelium* (Fig.11C).

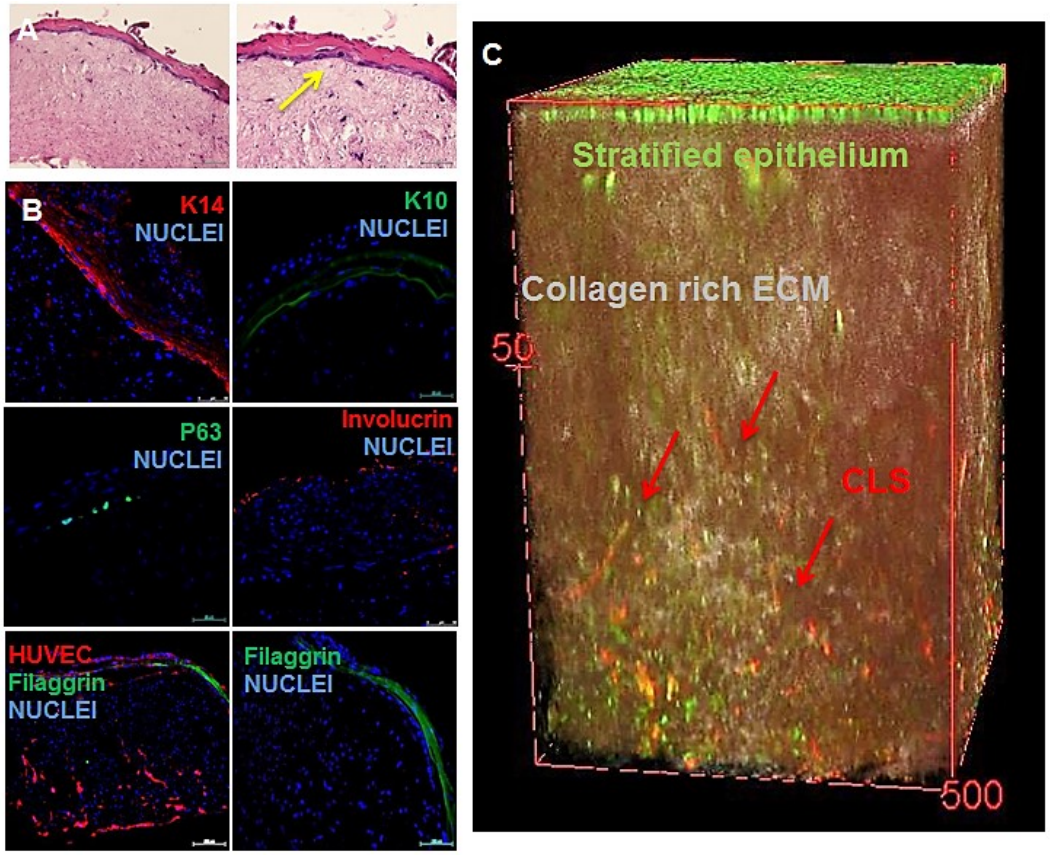

Fig. 11 Vascularized skin equivalent model: A) Hematoxylin eosin of a tissue section, the arrow indicates the basal lamina. Scale bar on the left 100µm, on the right 50µm. B) Immunofluorescence for K14 and Involucrin in red and for K10, p63, Filaggrin in green. In the images on the lower left the endothelial cells are marked in red by UEAI. Scale bar 50µm for all the images excluded the lower left which scale bar is 200µm. C) 3D View of the vascularized skin equivalent model with the *epithelium* marked in green by Sytox, the HUVECs in red by UEAI and the collagen matrix in gray by SHG. The red arrows indicate capillary like structures.

4.4 Discussion

In this work, we have developed a vascularized dermis and a vascularized skin model strengthened by endogenous ECM produced by fibroblasts.

We seeded HUVECs on the surface of a dermis equivalent biohybrid obtained by bottom up approach and rich in collagen [21] [113] which is one of the main component of the extracellular matrix responsible for tissue mechanical strength [87] [23]. This is a very important parameter considering that the gold standard skin substitutes should be slightly deformable, easily handled and able to withstand the shear forces *in vivo* [87] [130]. HUVECs, seeded on a surface of the sample, were able to deeply penetrate the collagen matrix for about 700µm (Fig.1), such as indicate by some endothelial cells migration assay in pro-angiogenic culture conditions [137] [138]. Endothelial cells formed a capillary-like network totally embedded into the stroma and evolving until 3 weeks of culture. These structures had a diameter of about 10µm, as most of the vessels in the human papillary dermis [91] and, from the orthogonal view (Fig.3C) and from the images of the structures at greater magnification, it is possible evaluate that they possess an inner lumen. CLS were growing up until 2 weeks and then regressing as demonstrated by the image analysis of the CLS volume fraction and n° of junctions/μm^3. Node points were mostly triple, so among 3 structures (Fig.2). We consider that these parameters indicate a physiological evolution of the endothelial network *in vitro*. In fact normal angiogenesis refers to a naturally existing process of blood vessel growth and regression, and it occurs as an integral component of tissue repair and regeneration [139]. Capillary tube regression is a well-known response during wound repair, developing retina, and the menstrual cycle in the ovary and uterus in humans [140], and it occurs as natural secure mechanism [6]. Moreover, the fact that we found mostly triple junctions indicate a capillary-network expansion by

bifurcation as it occurs physiologically, whereas trifurcation is most frequent in pathological angiogenesis [41].

The molecular analysis shows that the evolution of CLS in guided by VEGF and Angp-2. VEGF is the most well studied growth factors involved in ECs migration, mitogenesis, sprouting, and tube formation [141]. Angiopoietin-2 (Ang-2) is a biological antagonist of angiopoietin-1(Ang-1) and reduces vascular stability to block the stabilizing action of Ang-1. On the other hand, it was shown that in presence of VEGF, Ang-2 induces vascular sprouting and angiogenesis. Ang-2 is markedly expressed in organs that undergo vascular remodeling such as the ovaries and placenta [142]. In our experiment, the increasing overexpression of VEGF and Angp-2 leaded the expansion and remodeling of the vascular network until 2 weeks. From 2 to 3 weeks the expression of VEGF became comparable to the control whereas Angp-2 still remained upregulated, so inducing vascular regression [140] (Fig.5).

In 2 weeks capillaries gained a certain degree of structural maturity (Fig.6) being surrounded by laminin and collagen, which are key elements of the basal membrane around vessels, and by pericytes-like cells, positive for αSMA and mainly associated with blood vessel stabilization [143].

We speculate that the vascularized dermis equivalent model could be suitable for *in vivo* applications given its mechanical strength, easy handling and the presence of a physiological and mature endothelial network within the endogenous matrix. Our request for *in vivo* studies has been accepted by the Ethics Committee and next experiments will aim to evaluate the formation of functional anastomoses between the vascularized dermis equivalent and host vasculature after sub cutis graft into nu/nu athymic mice.

To this end, we have evaluated the ability of endothelial cells to migrate from the vascularized dermis equivalent to a wound area achieved cutting biohybrids and placing them in close contact into the maturation chamber. Results (Fig.8) indicate

that most of the endothelial cells were able to invade the wound area, as typical of the granulation tissue [140]. We argue that this feature, besides indicating the tissue ability to recapitulate a physiological event, could increase the chance to form functional anastomosis in the wound area between host tissue and implant after *in vivo* graft.

Moreover, we have evaluated that it is possible obtain a geometric control of the vascular network by seeding endothelial cells on a dermis equivalent model with specific form and features. In our experiment, after HUVECs injection into a channeled biohybrid, CLS preferentially developed into the channel and then sprouted into the surrounding matrix (Fig.9). Endothelial cells, seeded on a wire shaped dermis equivalent, followed the main geometric direction of the biohybrid (Fig.10). This is very interesting because *in vivo* human dermis vascular network has a fine architecture with 2 main parallel plexuses connected by capillaries and trying to reproduce this vessel organization *in vitro* could improve graft outcomes. In fact it was demonstrated that multicellular architecture in tissue is very important to guarantee tissue integration via the formation of functional anastomosis between the vascular network of the implant and that of the host having the same preferential direction[16].

Keratinocytes, seeded on the opposite surface of the vascularized dermis equivalent compared to endothelial cells, developed a stratified, keratinized and differentiated *epithelium* in 3 weeks of culture. Cells of the germinative layer expressed p63 which is important to initiate epithelial stratification and to maintain the proliferative potential of basal keratinocytes in mature epidermis [144] [22]. The basal layer of the *epithelium* was positive for K14, a fundamental keratin of all keratinocytes in stratified epithelia, whose expression is correlated with the mitotic activity and degree of potency of basal cells. Post-mitotic keratinizing cells in the supra basal layers of the epidermis expressed K10, a keratin which apparently prevents further cell divisions. The terminal differentiation of epidermis was

demonstrated by the expression involucrin and filaggrin in the stratum *corneum* [145] [22]. The presence of a mature *epithelium* could improve tissue functions acting as barrier and cross-talking with the dermis layer [130] [22]. From the 3D reconstruction in Fig.11C it is possible to see the complete vascularized skin model with a stratified *epithelium* lying on the dermis compartment strengthened by the endogenous ECM rich in collagen, in which the *endothelium* sprouts toward the *epithelium*. Capillaries do not enter in direct contact with epithelial cells as it happens in the *in vivo* condition in which they exchange substances by diffusion within the connective tissue [82].

4.5 Conclusions and Future Perspectives

This work focus on the development of a vascularized dermis/skin equivalent model for clinical applications. Despite the improvements occurred in the last year in the study of vascularized engineered models, none of the dermis/skin substitutes used in the clinic is actually pre-vascularized. The presence of a capillary network has a central role in determining the success of full-thickness graft.

We show that endothelial cells, seeded on a surface of a biohybrid dermis equivalent, are able to develop a capillary like network branching into the endogenous ECM, produced by fibroblasts and rich in collagen. These structures physiologically evolve and gain structural maturity in 2 weeks.

Endothelial cells migrate in the wound area during *in vitro* assay and can develop structures geometrically oriented under specific culture conditions. Thus, encouraging the chance to form functional anastomosis after *in vivo* graft and so the feeding of the entire tissue.

Next experiments will aim to *in vivo* trials but we speculate that the vascularized dermis/skin equivalent model could also be exploited as research platform and for drug screening.

The model could be suitable for fundamental research since it recapitulates both vascular progression and regression, *phenomena* characteristics of adult physiological angiogenesis and wound healing.

Moreover, the vascularized dermis/skin model could be used for the screening of molecules or principles acting via topical administration on the vascular network, such as vaso-constriction/dilatator, anti-inflammatory or pro- and antiangiogenic drugs.

In view of this kind of application it might be interesting evaluate other quantitative parameters related to vascular tissue function such as vasoconstriction or dilatation in response to thermal variations.

Since most of these drugs are systemically administrated, it could be very attractive find a way to perfuse CLS *in vitro*. The tissue could be integrated into a microfluidic device in order to promote the formation of anastomoses between the vascular network and channels acting as accessible vascular pedicles. Thanks to *in vitro* perfusion it would be possible characterize other fundamental vascular features such as permeability, leukocytes adhesion and vascular response to inflammatory stimuli.

References

[1] F. A. Auger, L. Gibot, and D. Lacroix, “The pivotal role of vascularization in tissue engineering.,” *Annu. Rev. Biomed. Eng.*, vol. 15, pp. 177–200, 2013.

[2] M. Lovett, K. Lee, A. Edwards, and D. L. Kaplan, “Vascularization strategies for tissue engineering.,” *Tissue Eng. Part B. Rev.*, vol. 15, no. 3, pp. 353–370, 2009.

[3] M. Snapyan, M. Lemasson, M. S. Brill, M. Blais, M. Massouh, J. Ninkovic, C. Gravel, F. Berthod, M. Götz, P. a Barker, A. Parent, and A. Saghatelyan, “Vasculature guides migrating neuronal precursors in the adult mammalian forebrain via brain-derived neurotrophic factor signaling.,” *J. Neurosci.*, vol. 29, no. 13, pp. 4172–4188, 2009.

[4] D. Marino, J. Luginbühl, S. Scola, M. Meuli, and E. Reichmann, “Bioengineering dermo-epidermal skin grafts with blood and lymphatic capillaries.,” *Sci. Transl. Med.*, vol. 6, p. 221ra14, 2014.

[5] B. Vailhé, D. Vittet, and J. J. Feige, “*In vitro* models of vasculogenesis and angiogenesis.,” *Lab. Invest.*, vol. 81, no. 4, pp. 439–452, 2001.

[6] C. Korn and H. G. Augustin, “Mechanisms of Vessel Pruning and Regression,” *Dev. Cell*, vol. 34, no. 1, pp. 5–17, 2015.

[7] G. S. E. Razavi, G. M.N.V, and T. Allen, “Role of Vascular Endothelial Growth Factor Receptor Inhibitors in Refractory Cervical Cancer,” *Jacobs J. Cell Mol. Biol.*, vol. 1, no. 1, 2015.

[8] Y. Ikada, “Challenges in tissue engineering.,” *J. R. Soc. Interface*, vol. 3, no. April, pp. 589–601, 2006.

[9] F. Berthod, L. Germain, N. Tremblay, F.A. Auger., “Extracellular matrix deposition by fibroblasts is necessary to promote capillary-like tube formation *in vitro*,” *J. Cell. Physiol.*, vol. 2, no. 2, pp. 491–498, 2006.

[10] A. Asti and L. Gioglio, “Natural and synthetic biodegradable polymers: different scaffolds for cell expansion and tissue formation.,” *Int. J. Artif. Organs*, vol. 37, no. 3, pp. 187–205, 2014.

[11] Dr. Pinar Zorlutuna, Dr. Nasim Annabi, Dr. Gulden Camci-Unal, Dr. Mehdi Nikkah, Dr. Jae Min Cha, Dr. Jason Nicho, Amir Manbachi, Dr. Hojae Bae, Prof. Shaochen Chen, “Microfabricated biomaterials for engineering 3D tissues,” *Adv Mater.*, vol. 29, no. 14, 2012.

[12] J. Y. Wong, J. B. Leach, and X. Q. Brown, “Balance of chemistry, topography, and mechanics at the cell-biomaterial interface: Issues and challenges for assessing the role of substrate mechanics on cell response,” *Surf. Sci.*, vol. 570, no. 1–2, pp. 119–133, 2004.

[13] K. M. Chrobak, D. R. Potter, and J. Tien, “Formation of perfused, functional microvascular tubes *in vitro*,” *Microvasc. Res.*, vol. 71, pp. 185–196, 2006.

[14] A. K. Luiz E. Bertassoni, Martina Cecconi, Vijayan Manoharan, Mehdi Nikkhah, Jesper Hjortnaes, Ana Luiza Cristino, Giada Barabaschi, Danilo Demarchi, Mehmet R. Dokmeci, Yunzhi Yange, “Hydrogel bioprinted microchannel networks for vascularization of tissue engineering constructs,” *Lab Chip*, no. 13, 2014.

[15] V. K. Lee, D. Y. Kim, H. Ngo, Y. Lee, L. Seo, S. S. Yoo, P. a. Vincent, and G. Dai, “Creating perfused functional vascular channels using 3D bio-printing technology,” *Biomaterials*, vol. 35, no. 28, pp. 8092–8102, 2014.

[16] J. D. Baranski, R. R. Chaturvedi, K. R. Stevens, J. Eyckmans, B. Carvalho, R. D. Solorzano, M. T. Yang, J. S. Miller, S. N. Bhatia, and C. S. Chen, “Geometric control of vascular networks to enhance engineered tissue integration and function.,” *Proc. Natl. Acad. Sci. U. S. A.*, vol. 110, pp. 7586–91, 2013.

[17] Y. Kim, H. Ko, I. K. Kwon, and K. Shin, “Extracellular matrix revisited: Roles in tissue engineering,” *Int. Neurourol. J.*, vol. 20, pp. S23–S29, 2016.

[18] F. Urciuolo, G. Imparato, A. Totaro, and P. A. Netti, “Building a tissue *in vitro* from the bottom up: Implications in regenerative medicine.,” *Methodist Debakey Cardiovasc. J.*, vol. 9, no. 4, pp. 213–217, 2013.

[19] A. Khademhosseini, R. Langer, J. Borenstein, and J. P. Vacanti, “Microscale technologies for tissue engineering and biology,” *Proc. Natl. Acad. Sci.*, vol. 103, no. 8, pp. 2480–2487, 2006.

[20] A. P. McGuigan and M. V. Sefton, “Vascularized organoid engineered by modular assembly enables blood perfusion,” *Proc. Natl. Acad. Sci.*, vol. 103, no. 31, pp. 11461–11466, 2006.

[21] C. Palmiero, G. Imparato, F. Urciuolo, and P. Netti, “Engineered dermal equivalent tissue *in vitro* by assembly of microtissue precursors,” *Acta Biomater.*, vol. 6, pp. 2548–2553, 2010.

[22] C. Casale, G. Imparato, F. Urciuolo, and P. A. Netti, “Endogenous human skin equivalent promotes *in vitro* morphogenesis of follicle-like structures,” *Biomaterials*, vol. 101, pp. 86–95, 2016.

[23] F. Martorina, C. Casale, F. Urciuolo, P. A. Netti, and G. Imparato, “*In vitro* activation of the neuro-transduction mechanism in sensitive organotypic human skin model,” *Biomaterials*, vol. 113, pp. 217–229, 2017.

[24] G. Imparato, F. Urciuolo, C. Casale, and P. a. Netti, “The role of microscaffold properties in controlling the collagen assembly in 3D dermis equivalent using modular tissue engineering,” *Biomaterials*, vol. 34, pp. 7851–7861, 2013.

[25] J. Ferlay, I. Soerjomataram, R. Dikshit, S. Eser, C. Mathers, M. Rebelo, D. M. Parkin, D. Forman, and F. Bray, “Cancer incidence and mortality worldwide: Sources, methods and major patterns in GLOBOCAN 2012,” *Int. J. Cancer*, vol. 136, no. 5, pp. E359–E386, 2015.

[26] Anonim, “Breast Cancer Overview What is breast cancer ?,” *Am. Cancer Soc.*, 2016.

[27] J. J. Campbell, R. D. Hume, and C. J. Watson, “Engineering Mammary Gland *in vitro* Models for Cancer Diagnostics and Therapy,” 2014.

[28] B. Weigelt, J. L. Peterse, and L. J. van ’t Veer, “Breast cancer metastasis: markers and models.,” *Nat. Rev. Cancer*, vol. 5, no. August, pp. 591–602, 2005.

[29] K. Guiro and T. L. Arinzeh, “Bioengineering Models for Breast Cancer Research,” *Breast CanCer BasiC Clin. Res.*, vol. 9, pp. 9–2, 2015.

[30] K. Polyak, “Review series introduction Heterogeneity in breast cancer,” *J.Clin.Invest.*, vol. 121, no. 10, pp. 2011–2013, 2011.

[31] S. D. Soysal, A. Tzankov, and S. E. Muenst, “Role of the Tumor Microenvironment in Breast Cancer,” *Pathobiology*, vol. 82, no. 3–4, pp. 142–152, 2015.

[32] Aranzazu Villasante, and Gordana Vunjak-Novakovic, “Tissue-engineered models of human tumors for cancer research,” *Expert Opin Drug Discov.*, vol. 10, no. 3, pp. 257–268, 2015.

[33] D. R. Pattabiraman and R. A. Weinberg, “Tackling the cancer stem cells - what challenges do they pose?,” *Nat Rev Drug Discov*, vol. 13, no. 7, pp. 497–512, 2014.

[34] G. Bergers and L. E. Benjamin, “Tumorigenesis and the angiogenic switch.,” *Nat. Rev. Cancer*, vol. 3, no. 6, pp. 401–410, 2003.

[35] B. R. Seo, P. DelNero, and C. Fischbach, “*In vitro* models of tumor vessels and matrix: Engineering approaches to investigate transport limitations and drug delivery in cancer,” *Adv. Drug Deliv. Rev.*, vol. 69–70, pp. 205–216, 2014.

[36] P. Carmeliet and R. K. Jain, “Angiogenesis in cancer and other diseases,” *Nat. 2000 Macmillan Mag. Ltd*, vol. 407, pp. 249–257, 2000.

[37] L. Gelao, C. Criscitiello, L. Fumagalli, M. Locatelli, S. Manunta, A. Esposito, I. Minchella, A. Goldhirsch, and G. Curigliano, “Tumour

dormancy and clinical implications in breast cancer," *Ecancermedicalscience*, vol. 7, no. 1, pp. 1–15, 2013.

[38] T. B. Kristensen, M. L. T. Knutsson, M. Wehland, B. E. Laursen, D. Grimm, E. Warnke, and N. E. Magnusson, "Anti-Vascular Endothelial Growth Factor Therapy in Breast Cancer," *Int. J. Mol. Sci.*, vol. 15, no. 12, pp. 23024–23041, 2014.

[39] J. a Nagy, S.-H. Chang, a M. Dvorak, and H. F. Dvorak, "Why are tumour blood vessels abnormal and why is it important to know?," *Br. J. Cancer*, vol. 100, no. 6, pp. 865–869, 2009.

[40] M. Papetti and I. M. Herman, "Mechanisms of normal and tumor-derived angiogenesis.," *Am. J. Physiol. Cell Physiol.*, vol. 282, no. 5, pp. C947–C970, 2002.

[41] J. Less, "Microvascular architecture in a mammary carcinoma: Branching patterns and vessel dimensions.," *Cancer Res.*, vol. 51, no. 265, pp. 265–273, 1991.

[42] W. W. Choi, M. M. Lewis, D. Lawson, Q. Yin-Goen, G. G. Birdsong, G. A. Cotsonis, C. Cohen, and A. N. Young, "Angiogenic and lymphangiogenic microvessel density in breast carcinoma: correlation with clinicopathologic parameters and VEGF-family gene expression," *Mod Pathol*, vol. 18, no. 1, pp. 143–152, 2005.

[43] J. W. Baish and R. K. Jain, "Perspectives in Cancer Research Fractals and Cancer 1," *Cancer Res.*, vol. 60, no. 7, pp. 3683–3688, 2000.

[44] K. Hori, M. Suzuki S. Tanda and S.Saito"*in vivo* Analysis of Tumor Vascularization in the Rat." Jpn. J Cancer Res 1990.

[45] M. W. Conklin, J. C. Eickhoff, K. M. Riching, C. A. Pehlke, K. W. Eliceiri, P. P. Provenzano, A. Friedl, and P. J. Keely, "Aligned collagen is a prognostic signature for survival in human breast carcinoma," *Am. J. Pathol.*, vol. 178, no. 3, pp. 1221–1232, 2011.

[46] P. P. Provenzano, D. R. Inman, K. W. Eliceiri, J. G. Knittel, L. Yan, C. T. Rueden, J. G. White, and P. J. Keely, “Collagen density promotes mammary tumor initiation and progression,” *BMC Med*, vol. 6, no. 1, p. 11, 2008.

[47] Z. M. Shao, M. Nguyen, and S. H. Barsky, “Human breast carcinoma desmoplasia is PDGF initiated.,” *Oncogene*, vol. 19, no. 38, pp. 4337–4345, 2000.

[48] A. Sainio, “Extracellular Matrix Macromolecules in Tumour Microenvironment with Special Reference to Desmoplastic Reaction and the Role of Matrix Proteoglycans and Hyaluronan,” *J. Carcinog. Mutagen.*, vol. S13, 2013.

[49] A. G. Clark and D. M. Vignjevic, “Modes of cancer cell invasion and the role of the microenvironment,” *Curr. Opin. Cell Biol.*, vol. 36, pp. 13–22, 2015.

[50] P. Friedl and K. Wolf, “Tumour-cell invasion and migration: diversity and escape mechanisms.,” *Nat. Rev. Cancer*, vol. 3, no. 5, pp. 362–74, 2003.

[51] P. Friedl and S. Alexander, “Cancer invasion and the microenvironment: Plasticity and reciprocity,” *Cell*, vol. 147, no. 5, pp. 992–1009, 2011.

[52] M. A. Huber, N. Kraut, and H. Beug, “Molecular requirements for epithelial-mesenchymal transition during tumor progression,” *Curr. Opin. Cell Biol.*, vol. 17, no. 5 SPEC. ISS., pp. 548–558, 2005.

[53] G. W. Prager and M. Poettler, “Angiogenesis in cancer,” *Hamostaseologie*, vol. 32, no. 2, pp. 105–114, 2011.

[54] N. Reymond, B. B. D’Água, and A. J. Ridley, “Crossing the endothelial barrier during metastasis.,” *Nat. Rev. Cancer*, vol. 13, no. 12, pp. 858–70, 2013.

[55] N. Weidner, “New paradigm for vessel intravasation by tumor cells.,” *Am. J. Pathol.*, vol. 160, no. 6, pp. 1937–1939, 2002.

[56] D. A. Haber, “Dissecting Metastasis Through Circulating Tumor Cells,” pp.

2015–2016, 2016.

[57] N. Aceto, A. Bardia, D. Miyamoto, M. Donaldson, B. Wittner, J. Spencer, M. Yu, A. Pely, A. Engstrom, H. Zhu, B. Brannigan, R. Kapur, S. Stott, T. Shioda, S. Ramaswamy, D. Ting, C. Lin, M. Toner, D. a Haber, and S. Maheswaran, "Circulating tumor cell clusters are oligoclonal precursors of breast cancer metastasis," *Cell*, vol. 158, no. 5, pp. 1110–22, 2014.

[58] S. H. Au, B. D. Storey, J. C. Moore, Q. Tang, Y.-L. Chen, S. Javaid, A. F. Sarioglu, R. Sullivan, M. W. Madden, R. O'Keefe, D. A. Haber, S. Maheswaran, D. M. Langenau, S. L. Stott, and M. Toner, "Clusters of circulating tumor cells traverse capillary-sized vessels," *Proc. Natl. Acad. Sci.*, vol. 113, no. 18, pp. 4947–4952, 2016.

[59] N. Aceto, M. Toner, S. Maheswaran, and D. A. Haber, "En Route to Metastasis: Circulating Tumor Cell Clusters and Epithelial-to-Mesenchymal Transition," *Trends in Cancer*, vol. 1, no. 1, pp. 44–52, 2015.

[60] J. Folkman, "Can mosaic tumor vessels facilitate molecular diagnosis of cancer?," *Proc. Natl. Acad. Sci. U. S. A.*, vol. 98, no. 2, pp. 398–400, 2001.

[61] L. C. Kimlin, G. Casagrande, and V. M. Virador, "*In vitro* three-dimensional (3D) models in cancer research: An update," *Mol. Carcinog.*, vol. 52, no. 3, pp. 167–182, 2013.

[62] D. Herrmann, J.R.W.Conway , C. Vennin, A. Magenau, W. E.Hughes, J. P.Morton and P. Timpson "Three-dimensional cancer models mimic cell-matrix interactions in the tumour microenvironment," *Carcinogenesis*, 2014.

[63] C. M. Nelson and M. J. Bissell, "Modeling dynamic reciprocity: Engineering three-dimensional culture models of breast architecture, function, and neoplastic transformation," *Semin. Cancer Biol.*, vol. 15, no. 5, pp. 342–352, 2010.

[64] A. Nyga, U. Cheema, and M. Loizidou, "3D tumour models: Novel *in vitro* approaches to cancer studies," *J. Cell Commun. Signal.*, vol. 5, no. 3, pp.

239–248, 2011.

[65] G. Imparato, F. Urciuolo, and P. A. Netti, "*In vitro* three-dimensional models in cancer research: a review," *Int. Mater. Rev.*, vol. 60, no. 6, pp. 297–311, 2015.

[66] K. J. Cheung, E. Gabrielson, Z. Werb, and A. J. Ewald, "Collective invasion in breast cancer requires a conserved basal epithelial program," *Cell*, vol. 155, no. 7, pp. 1639–1651, 2013.

[67] S. Krause, M. V Maffini, A. M. Soto, and C. Sonnenschein, "The microenvironment determines the breast cancer cells' phenotype: organization of MCF7 cells in 3D cultures.," *BMC Cancer*, vol. 10, p. 263, 2010.

[68] K. E. Sung, X. Su, E. Berthier, C. Pehlke, A. Friedl, and D. J. Beebe, "Understanding the Impact of 2D and 3D Fibroblast Cultures on *In vitro* Breast Cancer Models," *PLoS One*, vol. 8, no. 10, pp. 1–13, 2013.

[69] L. Chen, Z. Xiao, Y. Meng, Y. Zhao, J. Han, G. Su, B. Chen, and J. Dai, "The enhancement of cancer stem cell properties of MCF-7 cells in 3D collagen scaffolds for modeling of cancer and anti-cancer drugs," *Biomaterials*, vol. 33, no. 5, pp. 1437–1444, 2012.

[70] Prof. Seok Chung. C. Yoojin Shin, Hyunju Kim, Sewoon Han, Jihee Won, Prof. Eun-Sook Lee, Prof. Roger D. Kamm, Prof. Jae-Hong Kim, "Extracellular matrix heterogeneity regulates three-dimensional morphologies of breast adenocarcinoma cell invasion," *Adv Heal. Mater.*, 2013.

[71] X. J. Xian Xua, Mary C. Farach-Carsonb, "Three-Dimensional *In vitro* Tumor Models for Cancer Research and Drug Evaluation," *Biotechnol Adv.*, vol. 32, no. 7, pp. 1256–1268, 2014.

[72] C. S. Szot, C. F. Buchanan, J. W. Freeman, and M. N. Rylander, "*In vitro* angiogenesis induced by tumor-endothelial cell co-culture in bilayered,

collagen I hydrogel bioengineered tumors.," *Tissue Eng. Part C. Methods*, vol. 19, no. 11, pp. 864–74, 2013.

[73] S. M. Ehsan, K. M. Welch-reardon, M. L. Waterman, C. W. Christopher, S. C. George, and M. Genetics, "A three-dimensional *in vitro* model of tumor cell intravasation," *Integr. Biol.*, vol. 6, no. 6, pp. 603–610, 2015.

[74] F. Gioiella, F. Urciuolo, G. Imparato, V. Brancato, and P. A. Netti, "An Engineered Breast Cancer Model on a Chip to Replicate ECM-Activation *In vitro* during Tumor Progression," *Adv. Healthc. Mater.*, 2016.

[75] I. K. Zervantonakis, S. K. Hughes-Alford, J. L. Charest, J. S. Condeelis, F. B. Gertler, and R. D. Kamm, "Three-dimensional microfluidic model for tumor cell intravasation and endothelial barrier function.," *Proc. Natl. Acad. Sci. U. S. A.*, vol. 109, no. 34, pp. 13515–20, 2012.

[76] A. Sobrino, D. T. T. Phan, R. Datta, X. Wang, S. J. Hachey, M. Romero-López, E. Gratton, A. P. Lee, S. C. George, and C. C. W. Hughes, "3D microtumors *in vitro* supported by perfused vascular networks.," *Sci. Rep.*, vol. 6, no. July, p. 31589, 2016.

[77] M. L. Moya, Y.-H. Hsu, A. P. Lee, C. C. W. Hughes, and S. C. George, "*In vitro* Perfused Human Capillary Networks," *Tissue Eng. Part C Methods*, vol. 19, no. 9, pp. 730–737, 2013.

[78] L. F. Alonzo, M. L. Moya, V. S. Shirure, and S. C. George, "Microfluidic device to control interstitial flow-mediated homotypic and heterotypic cellular communication," *Lab Chip*, vol. 15, pp. 3521–3529, 2015.

[79] E. C. Ilya Serebriiskii, Remedios Castelló-Cros, Acacia Lamb, Erica A. Golemis, "Fibroblast-derived 3D matrix differentially regulates the growth and drug-responsiveness of human cancer cells," *Matrix Biol.*, vol. 27, no. 6, pp. 573–585, 2008.

[80] M. D. Amatangelo, D. E. Bassi, A. J. P. Klein-Szanto, and E. Cukierman, "Stroma-derived three-dimensional matrices are necessary and sufficient to

promote desmoplastic differentiation of normal fibroblasts.," *Am. J. Pathol.*, vol. 167, no. 2, pp. 475–488, 2005.

[81] R. Castelló-Cros, D. R. Khan, J. Simons, M. Valianou, and E. Cukierman, "Staged stromal extracellular 3D matrices differentially regulate breast cancer cell responses through PI3K and beta1-integrins.," *BMC Cancer*, vol. 9, no. 1, p. 94, 2009.

[82] S. V. Giuseppe Micali, Daniele Innocenzi, Gabriella Fabbrocini, Giuseppe Monfrecola, Antonella Tosti, "Le basi della dermatologia."

[83] V. P. Montagnini, Tazzi, Arcucci, Bareggi, Di mEGLIO, Gaeta, Gioglio, Guerra, Valenza, Varzè, *Anatomia unama normale*. 2007.

[84] F. Hom, Hebda, Gosain, *Essential Tissue Healing of the face and neck*. 2009.

[85] C. S. Harbor and W. King, "Cell-Extracellular Matrix Interactions in Normal and Diseased Skin Cell-Extracellular Matrix Interactions in Normal and Diseased Skin," no. December, pp. 1–15, 2014.

[86] V. S. LeBleu, B. Macdonald, and R. Kalluri, "Structure and function of basement membranes.," *Exp. Biol. Med. (Maywood).*, vol. 232, no. 9, pp. 1121–9, 2007.

[87] A. W. C. Chua, Y. C. Khoo, B. K. Tan, K. C. Tan, C. L. Foo, and S. J. Chong, "Skin tissue engineering advances in severe burns: review and therapeutic applications," *Burn. Trauma*, vol. 4, no. 1, p. 3, 2016.

[88] M. J. Bissel and D. Radisky, "Putting tumors in context," *Nat. Rev. Cancer*, vol. 1, no. 1, pp. 46–54, 2001.

[89] MacNeil S., "What role does the extracellular matrix serve in skin grafting and wound healing," *Burns*, vol. 20, 1994.

[90] P. Olczyk, Ł. Mencner, K. Komosinska-Vassev, P. Olczyk, Łukasz Mencner, K. Komosinska-Vassev, ukasz, and K. Komosinska-Vassev, "The Role of the Extracellular Matrix Components in Cutaneous Wound

Healing," *Biomed Res. Int.*, vol. 2014, pp. 1–8, 2014.

[91] I. M. Braverman, "The cutaneous microcirculation," *J. Investig. Dermatology Symp. Proc.*, vol. 5, no. 1, pp. 3–9, 2000.

[92] H. Lenasi, "Assessment of Human Skin Microcirculation and Its Endothelial Function Using Laser Doppler Flowmetry," 2008.

[93] F. Groeber, M. Holeiter, M. Hampel, S. Hinderer, and K. Schenke-Layland, "Skin tissue engineering - *In vivo* and *in vitro* applications," *Adv. Drug Deliv. Rev.*, vol. 63, no. 4, pp. 352–366, 2011.

[94] G. Imparato, F. Urciuolo, C. Casale, and P. a. Netti, "The role of microscaffold properties in controlling the collagen assembly in 3D dermis equivalent using modular tissue engineering," *Biomaterials*, vol. 34, no. 32, pp. 7851–7861, 2013.

[95] E. R. Sophie Bottcher-Haberzeth, Thomas Biedermann, "Tissue engineering of skin," *BURNS*, vol. 36, pp. 450–460, 2010.

[96] M. A. Karasek, "*In vitro* Culture of Human Skin Epithelial Cells," *J. Invest. Dermatol.*, vol. 47, no. 6, pp. 533–540, 1966.

[97] Rheinwald JG, Green H., "Serial Cultivation of Strains of Human Epidermal Keratinocytes: the Formation Keratinizin Colonies from Single Cells," *Cell*, 1975.

[98] S. Böttcher-Haberzeth, T. Biedermann, C. Schiestl, F. Hartmann-Fritsch, J. Schneider, E. Reichmann, and M. Meuli, "Matriderm® 1 mm versus Integra® Single Layer 1.3 mm for one-step closure of full thickness skin defects: A comparative experimental study in rats," *Pediatr. Surg. Int.*, vol. 28, no. 2, pp. 171–177, 2012.

[99] R. Zaulyanov, L, Kirsner, "A review of a bi-layered living cell treatment (Apligraf) in the traetment of venous leg ulcers and diabetic foot ulcers," *Clin Interv Aging*, vol. 2, no. 1, pp. 93–98, 2007.

[100] M. Ponec, "Skin constructs for replacement of skin tissues for *in vitro*

testing," *Adv. Drug Deliv. Rev.*, vol. 54, no. SUPPL., pp. 19–30, 2002.

[101] S. G. Hyun-Ho Greco Song, Kyung Min Park, "Hydrogels to Model 3D *in vitro* Microenvironment of Tumor Vascularization," *Adv Drug Deliv Rev*, 2014.

[102] B. D. Wever, D. Petersohn, and K. R. Mewes, "Overview of human three-dimensional (3D) skin models used for dermal toxicity assessment Part 1" *H& PC Today - Househ. Pers. Care Today*, vol. 8, no. 1, pp. 18–23, 2013.

[103] P. L. Tremblay, V. Hudon, F. Berthod, L. Germain, and F. a. Auger, "Inosculation of tissue-engineered capillaries with the host's vasculature in a reconstructed skin transplanted on mice," *Am. J. Transplant.*, vol. 5, pp. 1002–1010, 2005.

[104] I. Montaño, C. Schiestl, J. Schneider, L. Pontiggia, J. Luginbühl, T. Biedermann, S. Böttcher-Haberzeth, E. Braziulis, M. Meuli, and E. Reichmann, "Formation of human capillaries *in vitro*: the engineering of prevascularized matrices.," *Tissue Eng. Part A*, vol. 16, no. 1, pp. 269–282, 2010.

[105] R. E. Ayata, S. Chabaud, M. Auger, and R. Pouliot, "Behaviour of Endothelial Cells in a Tridimensional *In vitro* Environment," vol. 2015, no. 2010, 2015.

[106] H. Sekine, T. Shimizu, K. Sakaguchi, I. Dobashi, M. Wada, M. Yamato, E. Kobayashi, M. Umezu, and T. Okano, "*In vitro* fabrication of functional three-dimensional tissues with perfusable blood vessels.," *Nat. Commun.*, vol. 4, p. 1399, 2013.

[107] M. Wu and M. A. Swartz, "Modeling tumor microenvironments *in vitro*.," *J. Biomech. Eng.*, vol. 136, no. 2, p. 21011, 2014.

[108] M. M. Vantangoli, S. J. Madnick, S. M. Huse, P. Weston, and K. Boekelheide, "MCF-7 human breast cancer cells form differentiated microtissues in scaffold-free hydrogels," *PLoS One*, vol. 10, no. 8, pp. 1–20,

2015.

[109] S. Comsa, A.M. Cimpean, M. Raica“The Story of MCF-7 Breast Cancer cell line: 40 years of experience in Research,” *Anticancer Res.*, vol. 35, no. 6, 2015.

[110] K. Nilsson, F. Buzsaky1 & K. Mosbach, “Growth of anchorage-dependent cells on macroporous microcarriers,” *Nature Biotechnology. Gr,* 1986.

[111] R. F. Walker, P. T. Jackway and D. Longstaff, “Genetic algorithm optimization of adaptive multi-scale glcm features,” *World Sci.*, vol. 17, no. 1, pp. 17–39, 2003.

[112] S. Wu, Y. Peng, L. Hu, X. Zhang, and H. Li, “Classification and recognition of texture collagen obtaining by multiphoton microscope with neural network analysis,” *J. Phys. Conf. Ser.*, vol. 680, p. 12014, 2016.

[113] F. Urciuolo, G. Imparato, C. Casale, S. Scamardella, and P. Netti, “Fabrication of 3D tissue equivalent: An *in vitro* platform for understanding collagen evolution in healthy and diseased models,” *Proc. SPIE - Int. Soc. Opt. Eng.*, vol. 8792, pp. 1–6, 2013.

[114] R. Cicchi, D. Kapsokalyvas, V. De Giorgi, V. Maio, A. Van Wiechen, D. Massi, T. Lotti, and F. S. Pavone, “Scoring of collagen organization in healthy and diseased human dermis by multiphoton microscopy,” *J. Biophotonics*, vol. 3, no. 1–2, pp. 34–43, 2010.

[115] R. Rezakhaniha, A. Agianniotis, J. T. C. Schrauwen, A. Griffa, D. Sage, C. V. C. Bouten, F. N. Van De Vosse, M. Unser, and N. Stergiopulos, “Experimental investigation of collagen waviness and orientation in the arterial adventitia using confocal laser scanning microscopy,” *Biomech. Model. Mechanobiol.*, vol. 11, no. 3–4, pp. 461–473, 2012.

[116] E. E. Sweeney, R. E. Mcdaniel, P. Y. Maximov, P. Fan, and V. Craig, “Models and Mechanisms of Acquired Antihormone Resistance in Breast Cancer: Significant Clinical Progress Despite Limitations,” *Horm Mol Biol*

Clin Investig, vol. 9, no. 2, pp. 143–163, 2013.

[117] F. Urciuolo, G. Imparato, C. Palmiero, A. Trilli, and P. a Netti, "Effect of process conditions on the growth of three-dimensional dermal-equivalent tissue obtained by microtissue precursor assembly.," *Tissue Eng. Part C. Methods*, vol. 17, no. 0, pp. 155–164, 2011.

[118] J. Ando and K. Yamamoto, "Vascular Mechanobiology," *Circ. J.*, vol. 73, no. 11, pp. 1983–1992, 2009.

[119] E. H. L. & M. J. B. Genee Y Lee, Paraic A Kenny, "Three-dimensional culture models of normal and malignant breast epithelial cells," *Nat.Methods*, vol. 4, no. 1548–7091 (Print), pp. 359–365, 2007.

[120] M. A. J. Chaplain and A. M. Stuart, "A model mechanism for the chemotactic response of endotheliai cells to tumour angiogenesis factor," *IMA J. Math. Appl. Med. Biol.*, vol. 10, pp. 149–168, 1993.

[121] Y. S. Chang, E. di Tomaso, D. M. McDonald, R. Jones, R. K. Jain, and L. L. Munn, "Mosaic blood vessels in tumors: frequency of cancer cells in contact with flowing blood," *Proc Natl Acad Sci U S A*, vol. 97, no. 26, pp. 14608–14613, 2000.

[122] J. Adur, L. DSouza-Li, M. V. Pedroni, C. E. Steiner, V. B. Pelegati, A. A. de Thomaz, H. F. Carvalho, and C. L. Cesar, "The Severity of Osteogenesis Imperfecta and Type I Collagen Pattern in Human Skin as Determined by Nonlinear Microscopy: Proof of Principle of a Diagnostic Method," *PLoS One*, vol. 8, no. 7, 2013.

[123] L. B. Mostaço-Guidolin, A. C.-T. Ko, F. Wang, B. Xiang, M. Hewko, G. Tian, A. Major, M. Shiomi, and M. G. Sowa, "Collagen morphology and texture analysis: from statistics to classification.," *Sci. Rep.*, vol. 3, p. 2190, 2013.

[124] T. Stylianopoulos, B. Diop-Frimpong, L. L. Munn, and R. K. Jain, "Diffusion anisotropy in collagen gels and tumors: The effect of fiber

network orientation," *Biophys. J.*, vol. 99, no. 10, pp. 3119–3128, 2010.

[125] H. Berment, V. Becette, M. Mohallem, F. Ferreira, and P. Chérel, "Masses in mammography: What are the underlying anatomopathological lesions?," *Diagn. Interv. Imaging*, vol. 95, no. 2, pp. 124–133, 2014.

[126] M. Perrot-Applanat and M. Di Benedetto, "Autocrine functions of VEGF in breast tumor cells," *Cell Adh. Migr.*, vol. 6, no. 6, pp. 547–553, 2014.

[127] M. L. Oyen, "Mechanical characterisation of hydrogel materials," *Int. Mater. Rev.*, vol. 59, no. 1, pp. 44–59, 2014.

[128] S. MacNeil, "Progress and opportunities for tissue-engineered skin.," *Nature*, vol. 445, no. 7130, pp. 874–80, 2007.

[129] A F. Black, F. Berthod, N. L'heureux, L. Germain, and F. a Auger, "*In vitro* reconstruction of a human capillary-like network in a tissue-engineered skin equivalent.," *FASEB J.*, vol. 12, no. 1, pp. 1331–1340, 1998.

[130] S. Bottcher-Haberzeth, T. Biedermann, E. Reichmann "Tissue engineering of skin," *BURNS*, vol. 36, pp. 450–460, 2010.

[131] A. Halim, T. Khoo, and J. Y. Shah, "Biologic and synthetic skin substitutes: An overview," *Indian J. Plast. Surg.*, vol. 43, no. 3, p. 23, 2010.

[132] S. F. Badylak and T. W. Gilbert, "Immune Response to Biologic Scaffold Materials," *Semin Immunol.*, vol. 20, no. 2, pp. 109–116, 2008.

[133] K. J. Livak and T. D. Schmittgen, "Analysis of relative gene expression data using real-time quantitative PCR and the 2(-Delta Delta C(T)) Method.," *Methods*, vol. 25, no. 4, pp. 402–8, Dec. 2001.

[134] Janet E. Reing, Bryan N. Brown, Kerry A. Daly, John M. Freund, Thomas W. Gilbert, Susan Hsiong, Alexander Huber, Karen E. Kullas, Stephen Tottey, Matthew Wolf, Stephen F. Badylak "The Effects of Processing Methods upon Mechanical and Biologic Properties of Porcine Dermal Extracellular Matrix Scaffolds," *Biomaterials*, vol. 31, no. 33, pp. 8626–8633, 2010.

[135] B. Lombardi and C. Casale, G. Imparato, F. Urciuolo, and P.A Netti, “Spatio-temporal evolution of the wound repairing process in a 3D human dermis equivalent,” *Adv Heal. Mater* accepted march 2017, doi 10.1002/adhm.201601422.

[136] S. Raghavan, C. M. Nelson, J. D. Baranski, E. Lim, and C. S. Chen, “Geometrically controlled endothelial tubulogenesis in micropatterned gels.,” *Tissue Eng. Part A*, vol. 16, no. 7, pp. 2255–2263, 2010.

[137] R. B. Vernon and E. H. Sage, “A Novel, Quantitative Model for Study of Endothelial Cell Migration and Sprout Formation within Three-Dimensional Collagen Matrices,” *Microvasc. Res.*, vol. 57, no. 2, pp. 118–133, 1999.

[138] H. Kang, K. Bayless, and R. Kaunas, “Fluid shear stress modulates endothelial cell invasion into three-dimensional collagen matrices,” ... *Physiol. ...*, vol. 3120, pp. 2087–2097, 2008.

[139] W. L. C. and L. A. D. Mateusz S. Wietecha and Abstract, “Mechanisms of Vessel Regression: Toward an Understanding of the Resolution of Angiogenesis,” *Curr. Top. Microbiol. Immunol.*, 2013.

[140] G. E. Davis and W. B. Saunders, “Molecular balance of capillary tube formation versus regression in wound repair: role of matrix metalloproteinases and their inhibitors.,” *J. Investig. dermatology Symp. Proc. Soc. Investig. Dermatology Inc Eur. Soc. Dermatological Res.*, vol. 11, no. 1, pp. 44–56, 2006.

[141] A. A. Ucuzian, A. A. Gassman, A. T. East, and P. Greisler, “Molecular Mediators of Angiogenesis,” *J Burn Care Res.*, vol. 31, no. 1, pp. 1–28, 2010.

[142] B. K. Sharma, R. Srinivasan, S. Kapil, B. Singla, Y. K. Chawla, A. Chakraborti, N. Saini, A. Duseja, A. Das, N. Kalra, and R. K. Dhiman, “Angiogenic and anti-Angiogenic factor gene transcript level quantitation by quantitative real time PCR in patients with hepatocellular carcinoma,” *Mol.*

Biol. Rep., vol. 40, no. 10, pp. 5843–5852, 2013.

[143] G. Bergers and S. Song, “The role of pericytes in blood-vessel formation and maintenance.,” *Neuro. Oncol.*, vol. 7, no. 4, pp. 452–464, 2005.

[144] M. I. Koster and D. R. Roop, “The role of p63 in development and differentiation of the epidermis,” *J. Dermatol. Sci.*, vol. 34, no. 1, pp. 3–9, 2004.

[145] H. H. Bragulla and D. G. Homberger, “Structure and functions of keratin proteins in simple, stratified, keratinized and cornified epithelia,” *J. Anat.*, vol. 214, no. 4, pp. 516–559, 2009.

[146] F. Lawrence W. Bassett, MD, FACR, Mary Catherine Mahoney, MD, FACR, Sophia Kim Apple, MD, Carl J. D’Orsi, MD, *Breast Imaging*. 2011.